NATIONAL CENTER FOR EARTHQUAKE
ENGINEERING RESEARCH
State University of New York at Buffalo

SCATTERING OF WAVES BY INCLUSIONS IN A NONHOMOGENEOUS ELASTIC HALF SPACE SOLVED BY BOUNDARY ELEMENT METHODS

by

P.K. Hadley, A. Askar and A.S. Cakmak
Department of Civil Engineering and Operations Research
School of Engineering and Applied Science
Princeton University
Princeton, New Jersey 08544

Technical Report NCEER-89-0027

June 15, 1989

This research was conducted at Princeton University and was partially supported by the National Science Foundation under Grant No. ECE 86-07591.

NOTICE

This report was prepared by Princeton University, Northeastern University, and Bogazici University as a result of research sponsored by the National Center for Earthquake Engineering Research (NCEER). Neither NCEER, associates of NCEER, its sponsors, Princeton University, Northeastern University, Bogazici University, nor any person acting on their behalf:

a. makes any warranty, express or implied, with respect to the use of any information, apparatus, method, or process disclosed in this report or that such use may not infringe upon privately owned rights; or

b. assumes any liabilities of whatsoever kind with respect to the use of, or the damage resulting from the use of, any information, apparatus, method or process disclosed in this report.

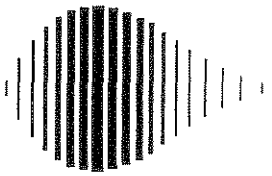

SCATTERING OF WAVES BY INCLUSIONS IN A NONHOMOGENEOUS ELASTIC HALF SPACE SOLVED BY BOUNDARY ELEMENT METHODS

by

P.K. Hadley[1], A. Askar[2] and A.S. Cakmak[3]

June 15, 1989

Technical Report NCEER-89-0027

NCEER Contract Number 88-3002

NSF Master Contract Number ECE 86-07591

1 Assistant Professor, Department of Civil Engineering, Northeastern University
2 Professor, Department of Mathematics, Bogazici University
3 Professor, Department of Civil Engineering and Operations Research, Princeton University

NATIONAL CENTER FOR EARTHQUAKE ENGINEERING RESEARCH
State University of New York at Buffalo
Red Jacket Quadrangle, Buffalo, NY 14261

PREFACE

The National Center for Earthquake Engineering Research (NCEER) is devoted to the expansion and dissemination of knowledge about earthquakes, the improvement of earthquake-resistant design, and the implementation of seismic hazard mitigation procedures to minimize loss of lives and property. The emphasis is on structures and lifelines that are found in zones of moderate to high seismicity throughout the United States.

NCEER's research is being carried out in an integrated and coordinated manner following a structured program. The current research program comprises four main areas:

- Existing and New Structures
- Secondary and Protective Systems
- Lifeline Systems
- Disaster Research and Planning

This technical report pertains to Program 3, Lifeline Systems, and more specifically to the study of dams, bridges and infrastructures.

The safe and serviceable operation of lifeline systems such as gas, electricity, oil, water, communication and transportation networks, immediately after a severe earthquake, is of crucial importance to the welfare of the general public, and to the mitigation of seismic hazards upon society at large. The long-term goals of the lifeline study are to evaluate the seismic performance of lifeline systems in general, and to recommend measures for mitigating the societal risk arising from their failures.

In addition to the study of specific lifeline systems, such as water delivery and crude oil transmission systems, effort is directed toward the study of the behavior of dams, bridges and infrastructures under seismic conditions. Seismological and geotechnical issues, such as variation in seismic intensity from attenuation effects, faulting, liquefaction and spatial variability of soil properties are topics under investigation. These topics are shown in the figure below.

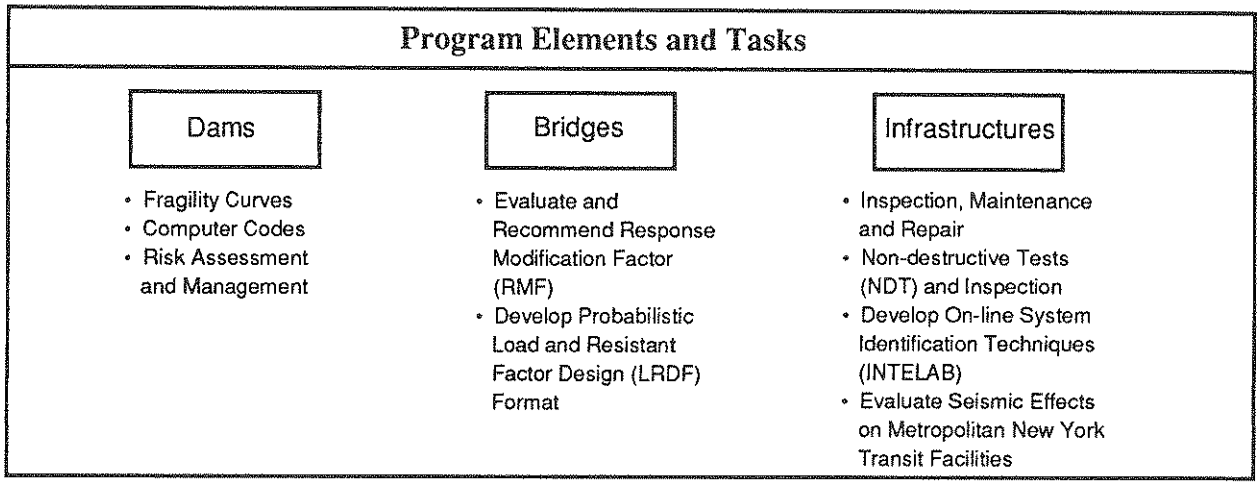

When the surface or subsurface topography of a site is irregular (canyon or basin structure), strains and stresses experienced by ground and underground structures may reach much higher values locally than predicted by the layered half-space model due to horizontal interferences and focusing of seismic energy originating from the irregular boundary. For the safer design of important lifeline systems, such local site effects must be investigated carefully and must be taken into account. This report describes how the Boundary Element Method can be used to solve this kind of problem, and presents various important applications.

ABSTRACT

In order to make structures safe from earthquake damage, a designing engineer needs to have some information about the waves to which it will be subjected and the structure's response to them. While a precise prediction of all seismic activity during the life of a structure is virtually impossible, earthquakes do occur within predictable limits with often repeated qualitative characteristics. We can, accordingly, choose a representative earthquake for a given site.

However, while we can guess well as to the nature of an earthquake in bedrock, we must also have some idea as to how the excitation is modified by the local conditions at the site. Some of the things influencing wave propagation would be soil material properties, layering of the soil, and the behaviour of structures embedded in and resting on the soil profile.

The present work presents a technique for examining the interaction of soil layers and structures in a two-dimensional profile subjected to incident SH waves. The analysis is carried out in the frequency domain where the response at any frequency in the spectrum is computed by the boundary element method. This enables the efficient solution of complex geometries, including lenses, tunnels, foundations, and cavities.

Results are presented which show that the method gives good agreement with known results and that the interaction of closely spaced structures is significant.

ACKNOWLEDGMENTS

This research was partially supported by the National Center of Earthquake Engineering under grant No. SUNYRF 88-3002. The support is gratefully acknowledged.

We should also like to thank Prof. Prevost of Princeton University and Prof. Ellis of Clarkeson University for the assistance they provided in sorting out and providing the accelerograms used in comparing our results to the behaviour of real earthquakes as presented in section 5.

TABLE OF CONTENTS

TABLE OF CONTENTS (Cont'd)

LIST OF ILLUSTRATIONS

LIST OF ILLUSTRATIONS (Cont'd)

LIST OF ILLUSTRATIONS (Cont'd)

LIST OF TABLES

SECTION 1
INTRODUCTION

An important part of the study of earthquake analysis is the propagation of stress waves through soil. The free-field behaviour of waves is fairly easily examined but when the waves come into contact with surfaces, cavities, and inhomogeneities, the behavior becomes more complicated. Wave energy reflects from these surfaces or refracts through the different media to form a more complicated pattern. There are very few geometries which possess closed-form solutions. Therefore, approximate methods are necessary for dealing with many different profiles.

One popular method of computing wave scattering is expansion in terms of matched functions as presented by Sanchez-Sesma *et al* [1]. Another group of methods is the discretization of the domain such as finite element methods and boundary element methods like those reported by Altay [2]. Other investigators who have worked on this problem with boundary methods are Banaugh and Goldsmith [3] who apparently applied the boundary element method to the problem before the method was recognized as an analytical tool and Beskos and Karabalis [4] who have developed three-dimensional time-domain elements where all inhomogeneity is finite.

This report presents a solution technique for wave propagation in two-dimensional, elastic, isotropic, heterogeneous problems. The problem is solved in the frequency domain for individual frequencies by the boundary element method and the resulting admittance function is convoluted with the Fourier series of an incident earthquake record and the results are rendered into the time domain.

It is an extension of the work done by Altay [2,5]. Altay's work solved the propagation problem for SH, SV, and P waves for homogeneous profiles. The current work presents the convolution into the time domain and the methodology for solving SH wave propagation in heterogeneous

media.

This approach seems capable of addressing a wide variety of problems over a large range of frequencies and is, therefore, a promising tool for research and analysis.

1.1 Organization of this report

The basic methodology is set forth in sections 2, 3, and 4. Section 2 sets forth the theory for homogeneous profiles and gives examples of some simple applications. Section 3 extends this theory to simple nonhomogeneous profiles (layers, inclusions, *etc.*) and shows examples of this extension for a few simple geometries. Finally, section 4 gives the theory for points where three or more media meet. Section 5 presents a brief study of a real profile, the Santa Felicia earth dam, subjected to the San Fernando earthquake of 1971.

More detailed mathematical derivations are reserved for the appendices. Appendix A holds the basic mathematical development for a single medium. Appendix B describes how the equations developed in appendix A are adapted to the numerical procedures and appendices C and D relate the extension to nonhomogeneous profiles. Appendix E gives a small example of the entire process of deriving the time response of a point in a profile to a given input.

SECTION 2
HOMOGENEOUS MEDIA

The purpose of this section is to present the methodology of the project for the case of a single homogeneous medium. The mathematics is presented more fully in appendix A but a brief description of the development is reproduced in the first section of this chapter. Following the analytical development is a section on the numerical methods described in detail in appendix B. The chapter closes with examples of the use of the methods described.

2.1 Mathematical theory of wave scattering

Figure 2-1 shows a bounded homogeneous medium subjected to an incident SH wave, $u^i(t)$. The purpose of this project is to find the response of the profile to this incident wave. When the incident wave strikes a surface, the energy is reflected as another wave field, the scattered field, $u^s(t)$. The incident and scattered field then undergo constructive and destructive interference. The response of the system is the sum of these two fields—the total field,

$$u^t = u^i + u^s \tag{2.1}$$

In order to obtain an equation of motion, we apply Newton's second law which is most succinctly expressed as

$$F = ma \tag{2.2}$$

where: F = force,

m = mass, and

a = acceleration.

Applying this to an element of linear elastic isotropic material in the homogeneous medium of figure 2-1 yields

$$(\lambda+\mu)u_{i,ji} + \mu u_{j,ii} + \rho u_j = \rho \ddot{u}_j \tag{2.3}$$

where: λ,μ = the Lame constants,

$\mathbf{u}$ = the vector displacement, and

ρ = density.

Subscripts are to be interpreted according to indicial notation. Because the scope of this project is limited to SH waves, $\frac{\partial}{\partial x_3}=0$ and $u_1=u_2=0$. Also, we can neglect body forces. Therefore, equation (2.3) becomes

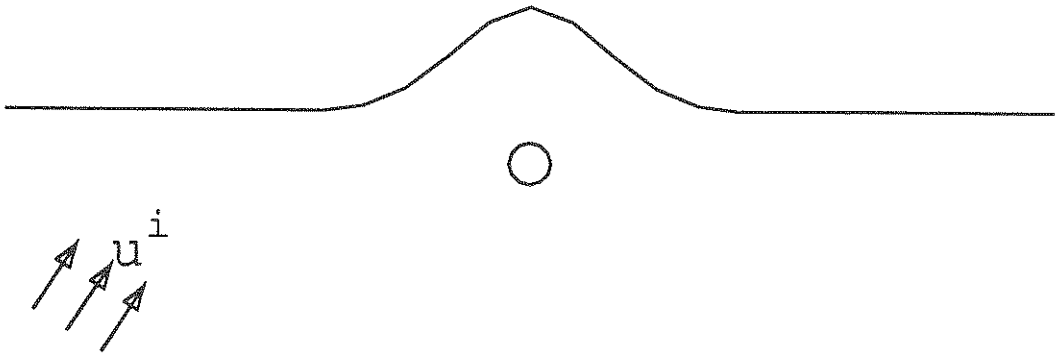

FIGURE 2-1 A bounded homogeneous medium

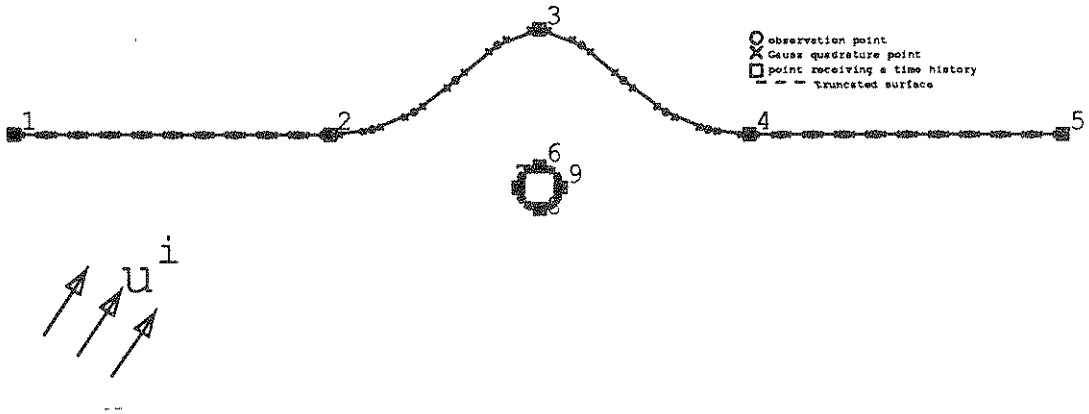

FIGURE 2-2 Discretization of the domain

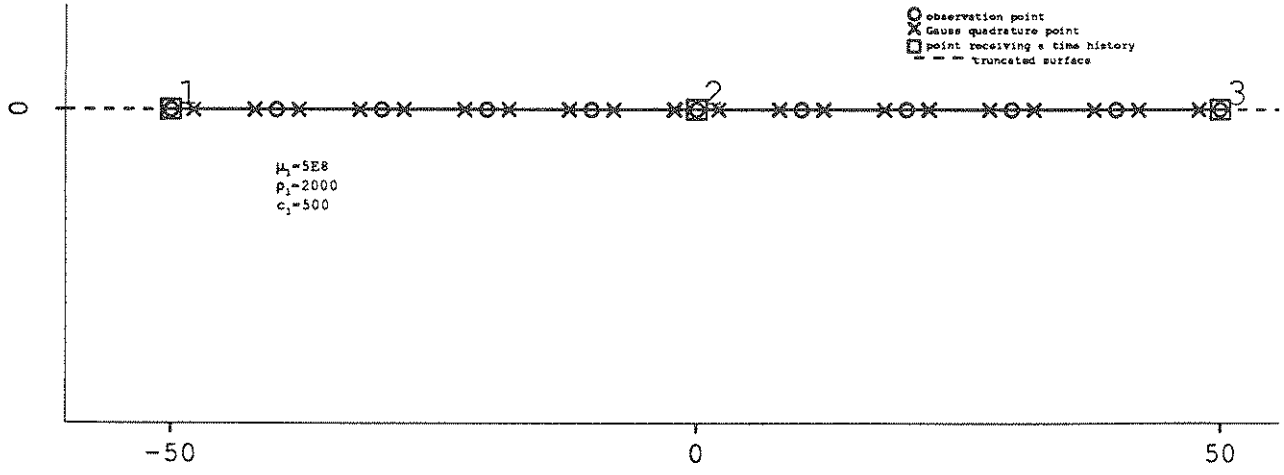

FIGURE 2-3 Homogeneous half space

$$\mu u_{3,11}+\mu u_{3,22}=\rho u_{3,tt} \tag{2.4}$$

or

$$\nabla^2 w=\frac{1}{c_s^2}\ddot{w} \tag{2.5}$$

where: w = displacement in the z–direction and

$c = \sqrt{\frac{\mu}{\rho}}$=shear wave velocity in the medium.

This equation governs the behaviour of transient SH waves in an homogeneous medium.

In order to simplify the equation further, a Fourier transform is applied. This procedure transforms the equation into an equation for steady-state wave propagation

$$\nabla^2\overline{w}=-\frac{\rho\omega^2}{\mu}\overline{w}=-\xi^2\overline{w} \tag{2.6}$$

where: $\overline{w}$ = the steady–state displacement amplitude,

ω = the frequency of the steady–state response, and

$\xi = \frac{\omega}{c}=\omega\sqrt{\frac{\rho}{\mu}}$=the wave number.

This equation can be rearranged to

$$\nabla^2\overline{w}+\xi^2\overline{w}=0 \tag{2.7}$$

The Green's function approach is now used to convert this differential equation into an integral equation

$$\iint_{A'}(g\,\nabla^2\overline{w}-\overline{w}\,\nabla^2 g)\,dA'=\begin{cases}\overline{w} \text{ for } \mathbf{r}\in A' \\ 0 \text{ for } \mathbf{r}\notin A'\end{cases} \tag{2.8}$$

where: A' = the two–dimensional profile,

$g = g(\mathbf{r},\mathbf{r}')$=the two–dimensional Green's function, and

$\frac{\partial g}{\partial n'}$ = its normal derivative.

This equation is written for an observation point, $\mathbf{r}$, and the integration is done across the integration points, $\mathbf{r}'$. By using Green's theorem, the integral is transformed from an

integral over the profile, A', to an integral around its boundary, S'.

$$\int_{S'}(g\frac{\partial \bar{w}}{\partial n'}-\bar{w}\frac{\partial g}{\partial n'})dS'=\begin{cases}\bar{w} \text{ for } r\in A' \\ 0 \text{ for } r\notin A'\end{cases} \tag{2.9}$$

There is a singularity in the normal derivative of the Green's function at the points where the integration crosses the observation point, (r=r'). This can be extracted and the integral interpreted in the Cauchy principal value sense to yield

$$\alpha\bar{w}+P\int_{S'}(g\frac{\partial \bar{w}}{\partial n'}-\bar{w}\frac{\partial g}{\partial n'})dS'=\begin{cases}\bar{w} \text{ for } r\in A' \\ 0 \text{ for } r\notin A'\end{cases} \tag{2.10}$$

where: α = the singularity in $\frac{\partial g}{\partial n'}$.

This equation applies to both the incident and the scattered fields. However, the incident wave, $\bar{w}^i$, originating at infinity, is not singular within the domain while the scattered wave, $\bar{w}^s$, is. Combining these two waves yields the equation

$$(1-\alpha)\,\bar{w}+P\int_{S'}(\bar{w}\frac{\partial g}{\partial n'}-g\frac{\partial \bar{w}}{\partial n'})dS'=\bar{w}^i \tag{2.11}$$

Solving this equation for $\bar{w}$ gives the response along the boundary for the given incident field at the given frequency, ω. If the incident field is a unit field, then the result is the admittance function. The admittance function for each point can be computed for a whole range of frequencies and the results convoluted back into the time domain by an inverse Fourier transform. Thus, the response in time of a point in the profile to a transient incident wave can be computed.

2.2 Numerical formulation

Because equation (2.11) is soluble in closed form for only a few geometries, a numerical method must be used to obtain a general solution. Equation (2.11) is an equation around the boundary of the medium and therefore lends itself directly to boundary element methods. Figure 2-2 shows the geometry of figure 2-1 discretized into segments. The endpoints of the segments are marked with circles. In the numerical method, we accept as unknowns the displacement, $\bar{w}$, and the normal derivative, $\frac{\partial \bar{w}}{\partial n'}$, at the endpoints of the segments. The behaviour of these functions is assumed to be linear between the endpoints. Therefore, the integral of equation (2.11) can be expressed numerically in terms of these unknowns. Using this scheme, we generate a matrix equation

$$H_{ij} w_j = f_i \tag{2.12}$$

where: H_{ij} = the matrix of coefficients from the integration,

w_j = the vector of unknowns (displacements and derivatives), and

f_i = the incident wave field at the observation point.

In the above equation the subscript j is the subscript of the integration point and the subscript i is the subscript of the observation point.

For each of the endpoints in figure 2-2, equation (2.12) can be written thereby generating N_{points} equations. At each of these points there are potentially two unknown quantities, $\bar{w}_i$ and $\frac{\partial \bar{w}}{\partial n'}_i$. There is also a boundary condition at each of the points. Therefore, while there are $2N_{points}$ unknowns, there are also $N_{points}+N_{points}$ equations and the problem is well posed.

Typically, the boundary condition is that the surface is a free surface. This means that $\frac{\partial \bar{w}}{\partial n'}=0$ and the unknown vector, w_j, of equation (2.12) contains only displacements. Solving

this equation for w gives the total field response to the steady-state incident wave within the limits of the numerical method.

The original goal of this derivation was to find the time history response of the profile. To do this the admittance is computed for a range of frequencies and reserved to build an admittance function. In figure 2-2 the points marked by squares and numbers have been chosen as points for which the admittance function is collected. By computing the admittance function for the range of frequencies and collecting them for the points shown, a complete admittance function for those points in that profile is generated. This admittance function can then be convoluted with the Fourier transform of the time series of the incident wave to generate the response of the point to the incident wave. A complete example of this procedure is shown in appendix E.

2.3 Examples

The remainder of this section is devoted to examples of the use of this method on several different geometries. First, results are obtained for problems which have been solved previously. This enables comparison of the results of this method. Then, there are examples of problems which are not easily solved by other methods. Finally, there are examples of time histories obtained by the methodology. Where possible, the accuracy and reasonableness of these results is explained.

2.3.1 Examples of problems possessing analytical solutions

In this section, we examine two homogeneous profiles for which analytical solutions exist—a circle in an infinite space and a halfspace. Plots of both geometries are shown with the numerical and analytical solutions.

Half space Figure 2-3 shows the surface of a homogeneous elastic halfspace. The reflected wave from the free surface is equal to the incident wave at the surface. Therefore, the total field is twice the incident field. Figure 2-4 shows the results for the numerical method (dashed line) and the exact results (dotted line). The fact that the agreement is exact is not surprising in light of the fact that for a flat free surface the stress terms all vanish and the Green's function ($\frac{\partial g}{\partial n'}$) from one point to another on a straight line is also zero. This leaves just the singularity, α=0.5, equal to the incident field at the point ($0.5\bar{w}=\bar{w}^i$). This means that the total field is twice the incident.

Cylindrical cavity in an infinite space Figure 2-5 shows a circle in an infinite space. The circle is centered at the origin and has a radius of 10. The material constants of the surrounding space are shear modulus, $\mu=10^6$, density, ρ=4, and shear velocity, c_s=500. This problem has been solved as a convergent series of Hankel functions in Eringen and Suhubi [6].

Figure 2-6 shows the response of this cavity at ω=50 rad/s. This gives a dimensionless frequency of ξr=1. As can be seen from the figure, the numerical solution, represented by the long dashes, gives a very good approximation of the analytical solution represented by the dotted line. Figure 2-7 shows the response at ω=150 rad/s. As can be seen, the approximation is still good though it has strayed somewhat. The results for these two frequencies are shown in tables 2-I and 2-II.

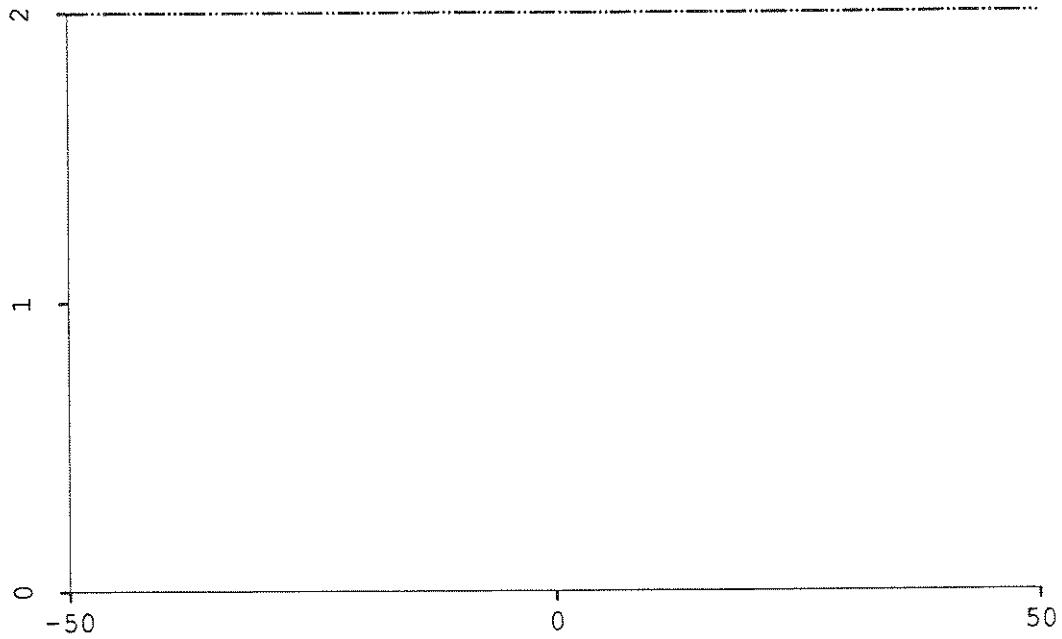

FIGURE 2-4 Admittance for half space at ω=50 rad/s

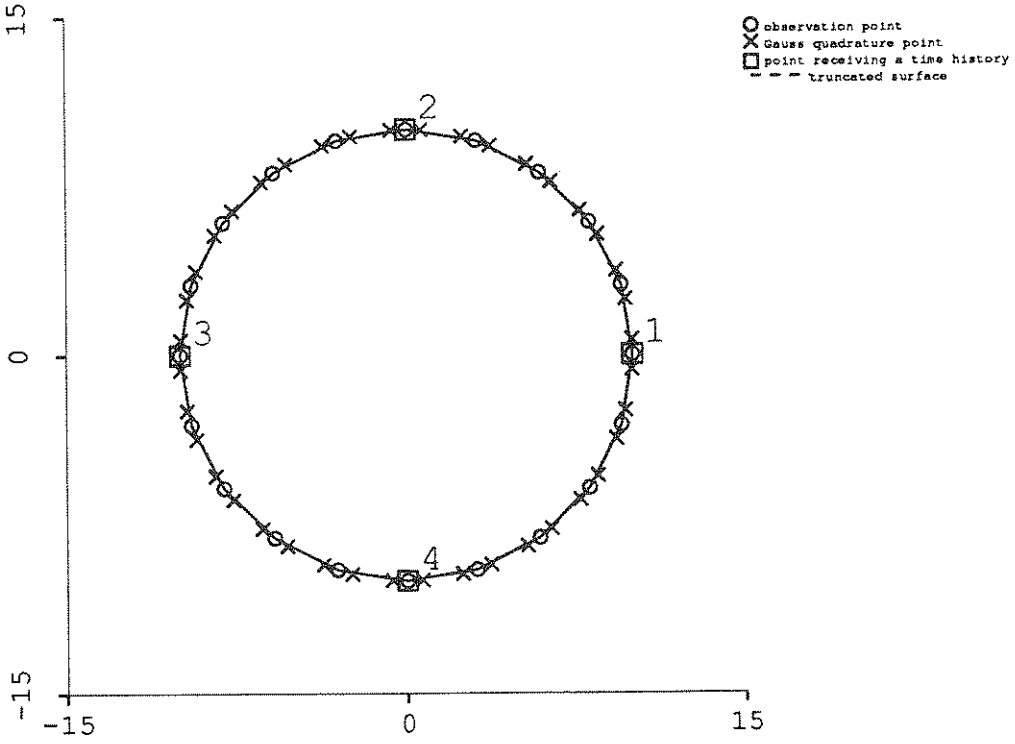

FIGURE 2-5 Cavity in an infinite space

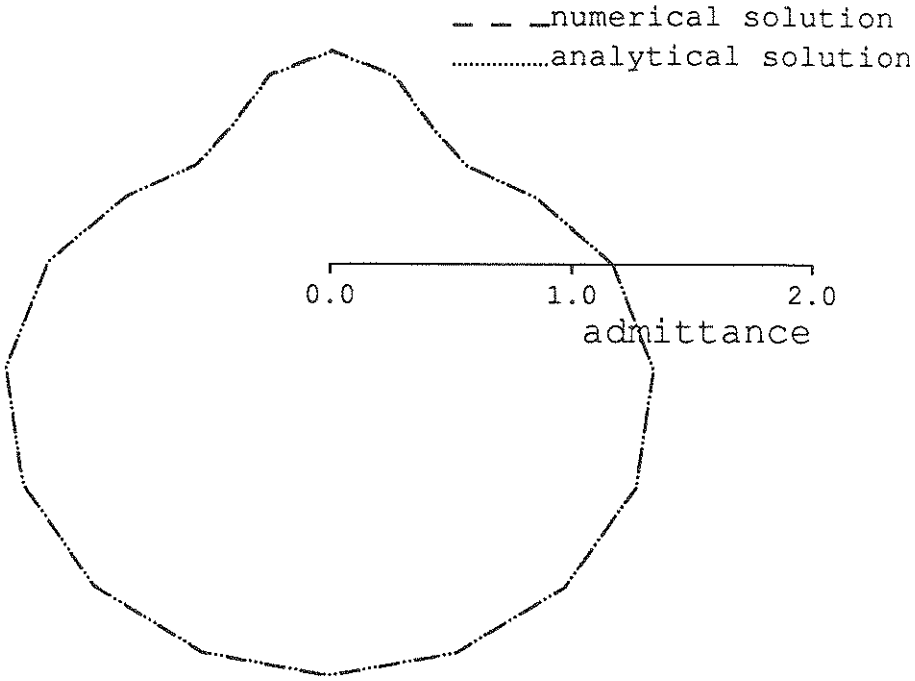

FIGURE 2-6 Response of cylindrical cavity at ω= 50 rad/s

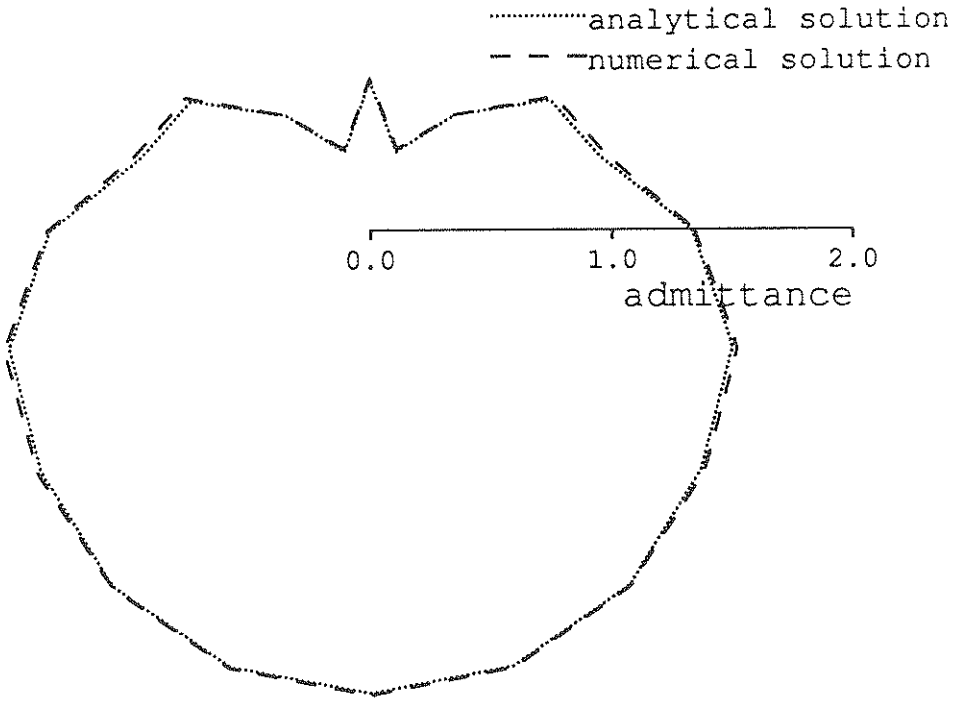

FIGURE 2-7 Response of cylindrical cavity at ω=150 rad/s

TABLE 2-I Results for the cylinder at ω=50 rad/s

	angle	exact solution		numerical solution		error	
point	(radians)	complex coefficient	magnitude	complex coefficient	magnitude	complex coefficient	magnitude
1	0.	(0.1130e+01,-.3066e+00)	1.1713	(0.1129e+01,-.3082e+00)	1.1704	(0.1363e-02,0.1595e-02)	0.0021
2	0.314	(0.8789e+00,0.1485e+00)	0.8914	(0.8784e+00,0.1483e+00)	0.8908	(0.5200e-03,0.2096e-03)	0.0006
3	0.628	(0.4828e+00,0.4962e+00)	0.6923	(0.4835e+00,0.4978e+00)	0.6940	(-.6781e-03,-.1658e-02)	0.0018
4	0.942	(0.6679e-01,0.7018e+00)	0.7050	(0.6869e-01,0.7055e+00)	0.7088	(-.1901e-02,-.3618e-02)	0.0041
5	1.257	(-.2409e+00,0.7922e+00)	0.8280	(-.2381e+00,0.7973e+00)	0.8321	(-.2803e-02,-.5115e-02)	0.0058
6	1.571	(-.3533e+00,0.8149e+00)	0.8882	(-.3502e+00,0.8206e+00)	0.8922	(-.3134e-02,-.5678e-02)	0.0065
7	1.885	(-.2409e+00,0.7922e+00)	0.8280	(-.2381e+00,0.7973e+00)	0.8321	(-.2803e-02,-.5115e-02)	0.0058
8	2.199	(0.6679e-01,0.7018e+00)	0.7050	(0.6869e-01,0.7055e+00)	0.7088	(-.1901e-02,-.3619e-02)	0.0041
9	2.513	(0.4828e+00,0.4962e+00)	0.6923	(0.4835e+00,0.4978e+00)	0.6940	(-.6774e-03,-.1657e-02)	0.0018
10	2.827	(0.8789e+00,0.1485e+00)	0.8914	(0.8784e+00,0.1483e+00)	0.8908	(0.5196e-03,0.2098e-03)	0.0006
11	3.142	(0.1130e+01,-.3066e+00)	1.1713	(0.1129e+01,-.3082e+00)	1.1704	(0.1366e-02,0.1595e-02)	0.0021
12	3.456	(0.1176e+01,-.7777e+00)	1.4102	(0.1175e+01,-.7801e+00)	1.4101	(0.1673e-02,0.2373e-02)	0.0029
13	3.770	(0.1048e+01,-.1167e+01)	1.5688	(0.1047e+01,-.1170e+01)	1.5698	(0.1490e-02,0.2648e-02)	0.0030
14	4.084	(0.8443e+00,-.1425e+01)	1.6560	(0.8433e+00,-.1427e+01)	1.6578	(0.1040e-02,0.2643e-02)	0.0028
15	4.398	(0.6726e+00,-.1557e+01)	1.6959	(0.6720e+00,-.1559e+01)	1.6980	(0.6136e-03,0.2548e-02)	0.0026
16	4.712	(0.6070e+00,-.1596e+01)	1.7071	(0.6065e+00,-.1598e+01)	1.7093	(0.4418e-03,0.2508e-02)	0.0025
17	5.027	(0.6726e+00,-.1557e+01)	1.6959	(0.6720e+00,-.1559e+01)	1.6980	(0.6145e-03,0.2546e-02)	0.0026
18	5.341	(0.8443e+00,-.1425e+01)	1.6560	(0.8433e+00,-.1427e+01)	1.6578	(0.1040e-02,0.2642e-02)	0.0028
19	5.655	(0.1048e+01,-.1167e+01)	1.5688	(0.1047e+01,-.1170e+01)	1.5698	(0.1491e-02,0.2648e-02)	0.0030
20	5.969	(0.1176e+01,-.7777e+00)	1.4102	(0.1175e+01,-.7801e+00)	1.4101	(0.1674e-02,0.2372e-02)	0.0029
1	6.283	(0.1130e+01,-.3066e+00)	1.1713	(0.1129e+01,-.3082e+00)	1.1704	(0.1363e-02,0.1595e-02)	0.0021

Table 2-II Results for the cylinder at ω=150 rad/s

	angle	exact solution		numerical solution		error	
point	(radians)	complex coefficient	magnitude	complex coefficient	magnitude	complex coefficient	magnitude
1	0.	(0.1317e+01,-.1759e+00)	1.3287	(0.1326e+01,-.1936e+00)	1.3399	(-.8798e-02,0.1769e-01)	0.0198
2	0.314	(0.5283e+00,0.8447e+00)	0.9963	(0.5537e+00,0.8604e+00)	1.0231	(-.2536e-01,-.1569e-01)	0.0298
3	0.628	(-.5002e+00,0.7724e+00)	0.9202	(-.4734e+00,0.8165e+00)	0.9438	(-.2673e-01,-.4412e-01)	0.0516
4	0.942	(-.5832e+00,0.1056e+00)	0.5927	(-.5781e+00,0.1362e+00)	0.5939	(-.5118e-02,-.3059e-01)	0.0310
5	1.257	(0.5653e-01,-.3404e+00)	0.3451	(0.3321e-01,-.3564e+00)	0.3580	(0.2332e-01,0.1603e-01)	0.0283
6	1.571	(0.4331e+00,-.4479e+00)	0.6231	(0.3972e+00,-.4901e+00)	0.6308	(0.3596e-01,0.4217e-01)	0.0554
7	1.885	(0.5653e-01,-.3404e+00)	0.3451	(0.3321e-01,-.3564e+00)	0.3580	(0.2332e-01,0.1603e-01)	0.0283
8	2.199	(-.5832e+00,0.1056e+00)	0.5927	(-.5781e+00,0.1362e+00)	0.5939	(-.5118e-02,-.3060e-01)	0.0310
9	2.513	(-.5002e+00,0.7724e+00)	0.9202	(-.4734e+00,0.8165e+00)	0.9438	(-.2673e-01,-.4411e-01)	0.0516
10	2.827	(0.5283e+00,0.8447e+00)	0.9963	(0.5537e+00,0.8604e+00)	1.0231	(-.2536e-01,-.1569e-01)	0.0298
11	3.142	(0.1317e+01,-.1759e+00)	1.3287	(0.1326e+01,-.1936e+00)	1.3399	(-.8795e-02,0.1769e-01)	0.0198
12	3.456	(0.7726e+00,-.1371e+01)	1.5734	(0.7693e+00,-.1397e+01)	1.5951	(0.3287e-02,0.2668e-01)	0.0269
13	3.770	(-.5611e+00,-.1593e+01)	1.6887	(-.5662e+00,-.1608e+01)	1.7052	(0.5045e-02,0.1573e-01)	0.0165
14	4.084	(-.1539e+01,-.9678e+00)	1.8181	(-.1544e+01,-.9701e+00)	1.8233	(0.4721e-02,0.2284e-02)	0.0052
15	4.398	(-.1875e+01,-.2958e+00)	1.8984	(-.1882e+01,-.2908e+00)	1.9047	(0.7151e-02,-.5048e-02)	0.0088
16	4.712	(-.1917e+01,-.4082e-01)	1.9177	(-.1926e+01,-.3386e-01)	1.9265	(0.8946e-02,-.6960e-02)	0.0113
17	5.027	(-.1875e+01,-.2958e+00)	1.8984	(-.1882e+01,-.2908e+00)	1.9047	(0.7149e-02,-.5048e-02)	0.0088
18	5.341	(-.1539e+01,-.9678e+00)	1.8181	(-.1544e+01,-.9701e+00)	1.8233	(0.4722e-02,0.2283e-02)	0.0052
19	5.655	(-.5611e+00,-.1593e+01)	1.6887	(-.5662e+00,-.1608e+01)	1.7052	(0.5046e-02,0.1573e-01)	0.0165
20	5.969	(0.7726e+00,-.1371e+01)	1.5734	(0.7693e+00,-.1397e+01)	1.5951	(0.3288e-02,0.2668e-01)	0.0269
1	6.283	(0.1317e+01,-.1759e+00)	1.3287	(0.1326e+01,-.1936e+00)	1.3399	(-.8798e-02,0.1769e-01)	0.0198

2.3.2 A problem which others have solved numerically

In this section we present the results of a problem which has been solved numerically and compare these results to the results of the boundary element method. Figure 2-8 shows the profile of a hill on a homogeneous halfspace of the type solved by Sanchez-Sesma, *et al* [1]. The shape of the hill is defined by the equation $y=h(1-(\frac{x}{b})^2)e^{-3(\frac{x}{b})^2}$ and the solution in reference [1] is obtained by an expansion. The results for the hill are shown in figure 2-9 for a frequency of 7.85 rad/s. This number was chosen in order to match dimensionless parameters to those for which Sanchez-Sesma *et al* give results. For dimensionless parameters of h/b= the ratio of height to half the width of the hill and $\eta=\frac{\xi b}{\pi}$= a dimensionless frequency,

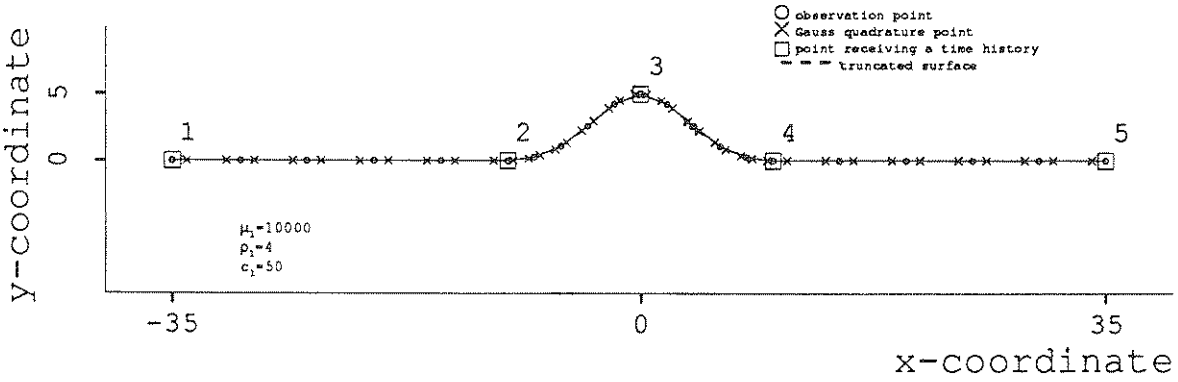

FIGURE 2-8 Hill of the shape solved by Sanchez-Sesma, *et al.*

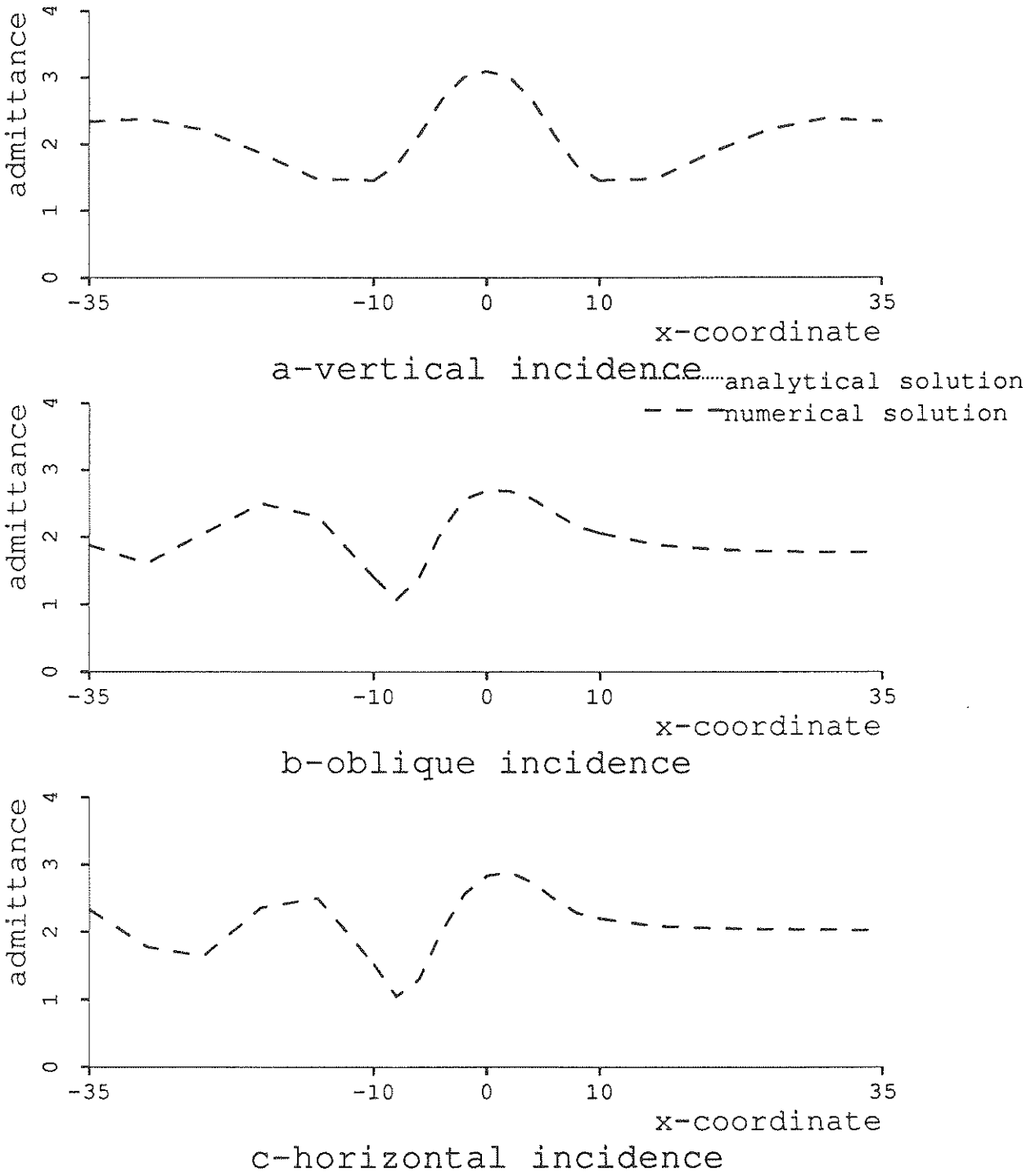

FIGURE 2-9 Admittance of the free surface

the admittances are shown by the dotted lines of figure 2-9. It should be noted that the boundary method used in this project can be applied for much higher (and lower) frequencies as well.

2.3.3 Time histories

In this section we present the completion of the solution method. For the geometries presented above, response in time is presented. The profiles are all solved over a range of frequencies by the methods given above and convoluted with the forward transforms of two earthquakes—a Gaussian pulse of energy (figure 2-10) and the east-west trace of the San Fernando earthquake of 1971 as recorded in the basement of 3360 Lomiskey Boulevard (figure 2-11).

Time response of a half space Figure 2-12 shows the response of point 2 in the half space of figure 2-3 to the incident Gaussian pulse shown in figure 2-10 at horizontal incidence. As can be seen, the response of the half space is twice the incident wave which is what theory predicts. Figure 2-13 shows the response of the same point to the San Fernando earthquake shown in figure 2-11. Again the input is doubled in the response.

Time response of a cavity Figure 2-14 shows the time response of the four points shown on the cylinder of figure 2-5 as response to the Gaussian pulse of figure 2-10. Figure 2-15 shows the time response of the four points as response to the San Fernando earthquake of figure 2-11.

Time response of a hill Figure 2-16 shows the time response of the five points shown on the hill profile of figure 2-8 as response to the Gaussian pulse for vertical, 45°, and horizontal incidence. Note that in the first column, corresponding to vertical incidence, symmetry is

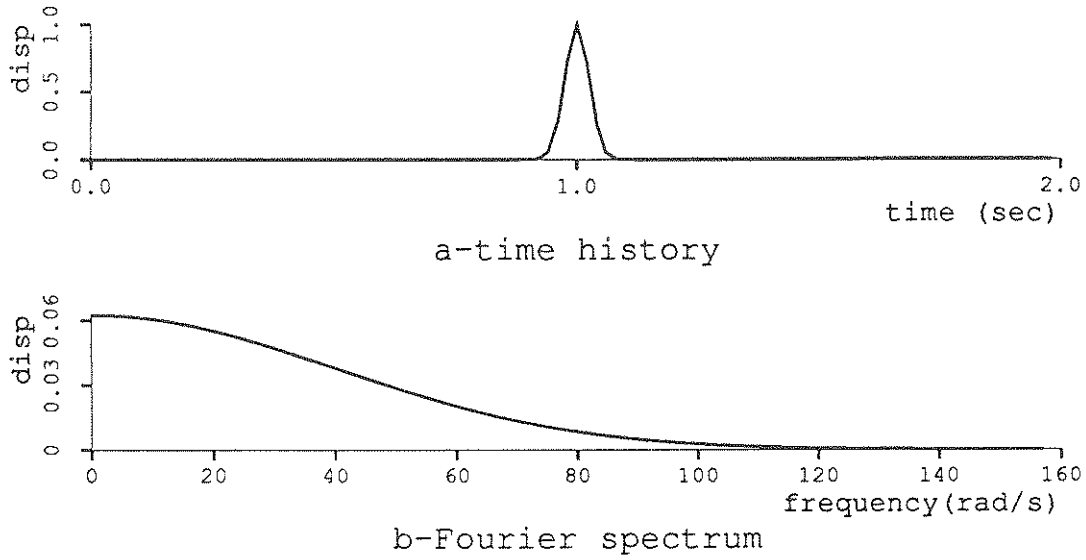

FIGURE 2-10 Record of Gaussian spike

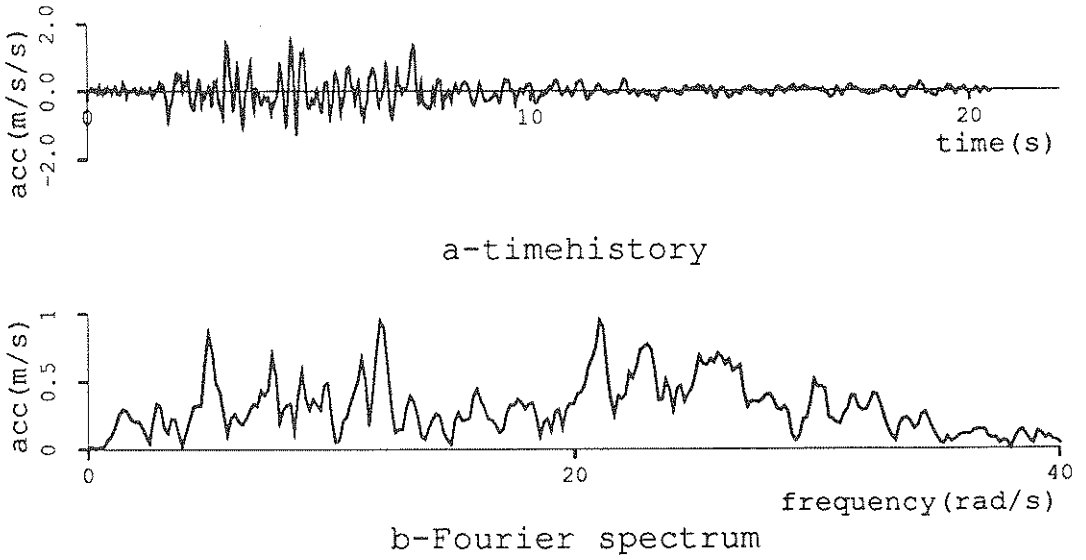

FIGURE 2-11 Record of the San Fernando earthquake

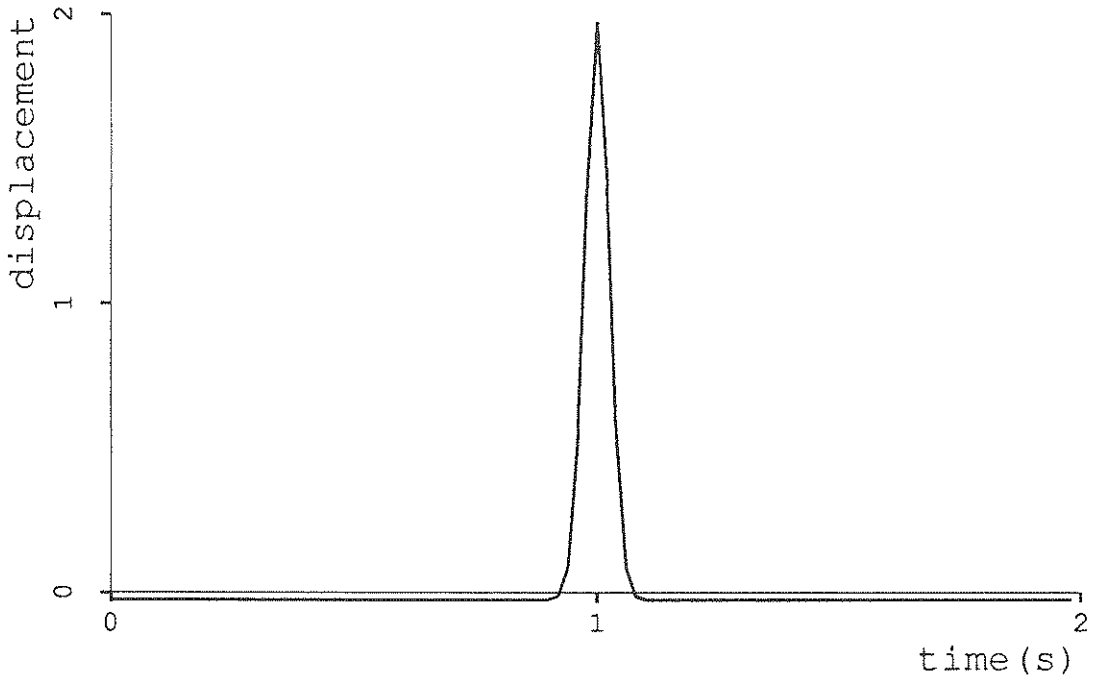

FIGURE 2-12 Time response of the half space to the Gaussian pulse

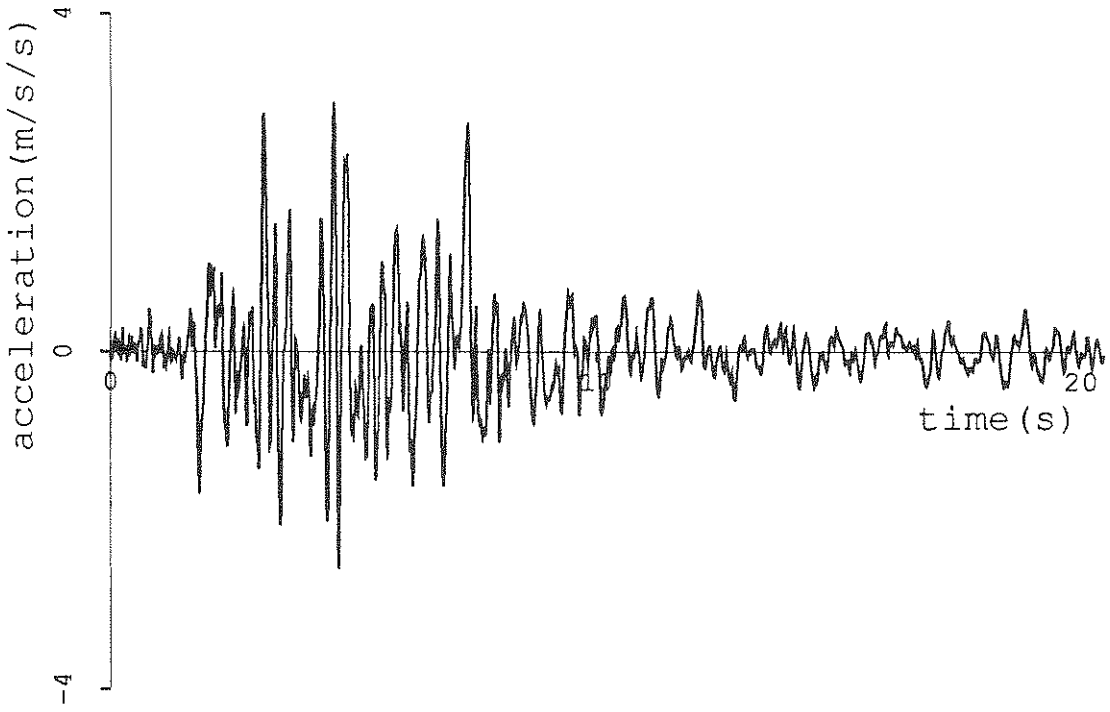

FIGURE 2-13 Response of the half space to the San Fernando earthquake

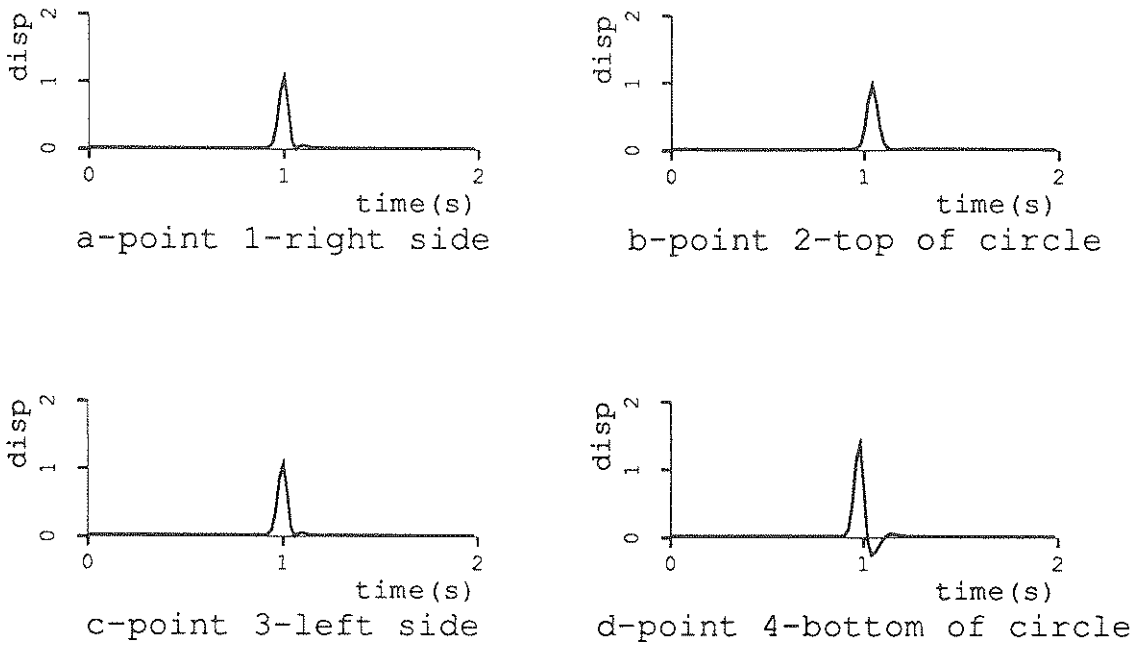

FIGURE 2-14 Time histories of four points on the cylinder

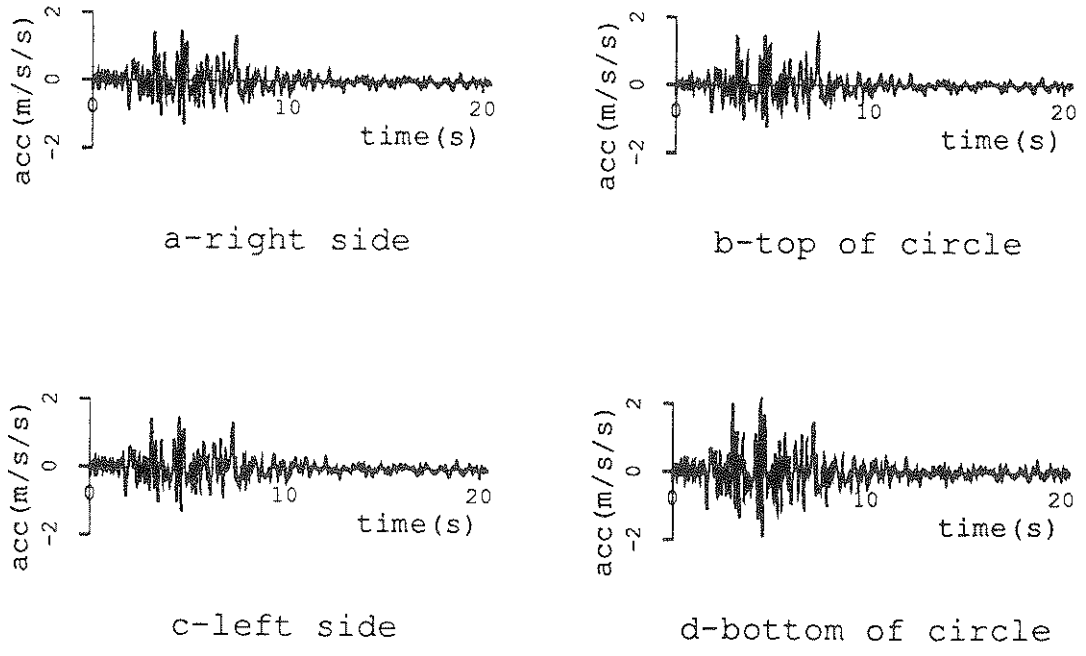

FIGURE 2-15 Time histories of four points on the cylinder

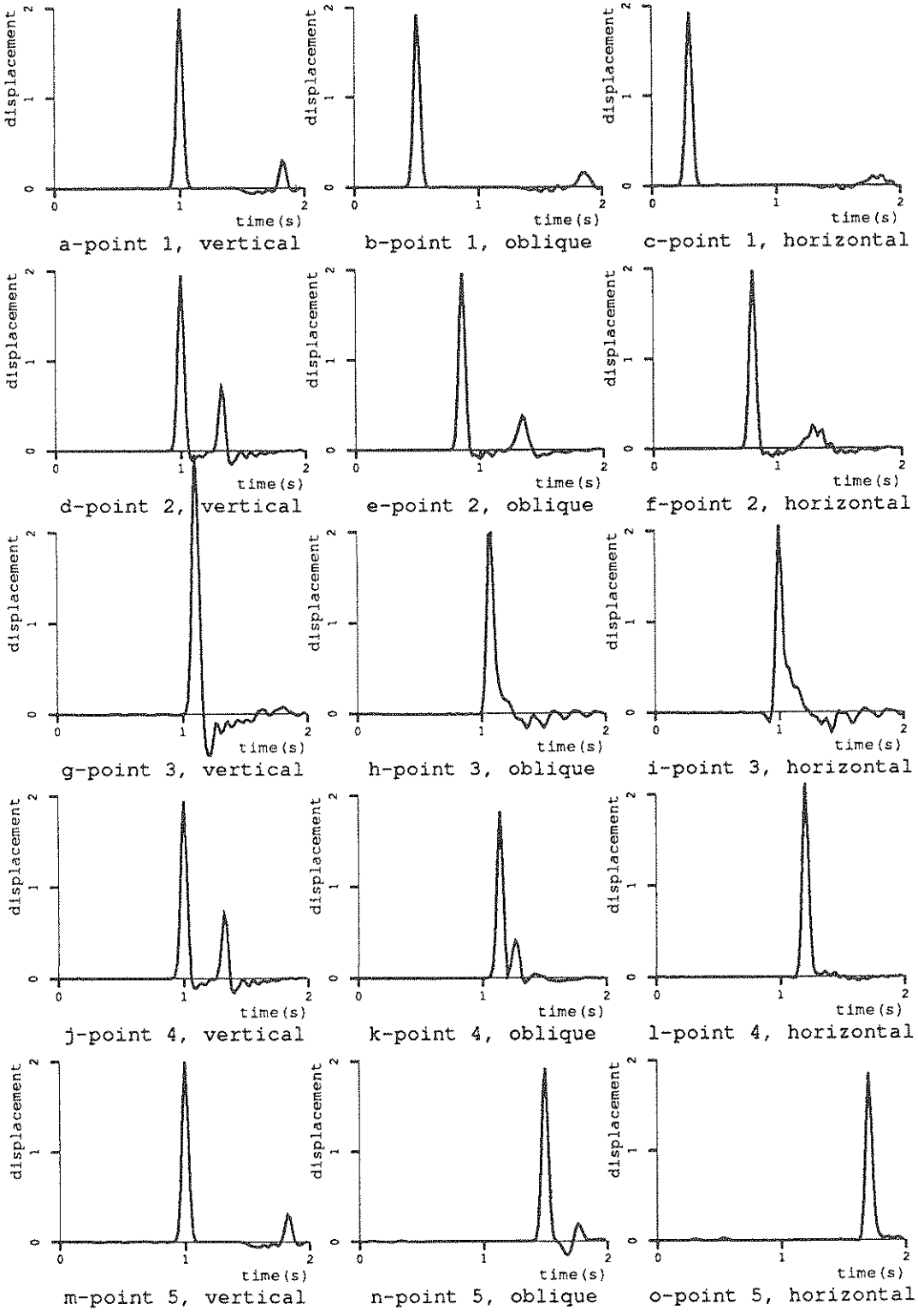

FIGURE 2-16 Time histories of five points on the hill profile

preserved. Parts a and m and parts d and j have identical responses in time. Part g shows an amplification in response above that expected for an ordinary half space. This could be due to a channeling of the energy by the hill. The second column, corresponding to 45° angle of incidence, and the third column, corresponding to horizontal incidence, show the lag in time for the wave to propagate across the profile. Figure 2-17 shows the time response of the five points to the San Fernando earthquake.

2.4 Conclusions

The results of section 2.3 show that the numerical scheme presented at the beginning of the chapter yields accurate, reasonable results. The present method can, therefore, be considered to be a reliable method for predicting the response of points in a homogeneous isotropic two-dimensional linear elastic halfspace to transient antiplane incident waves.

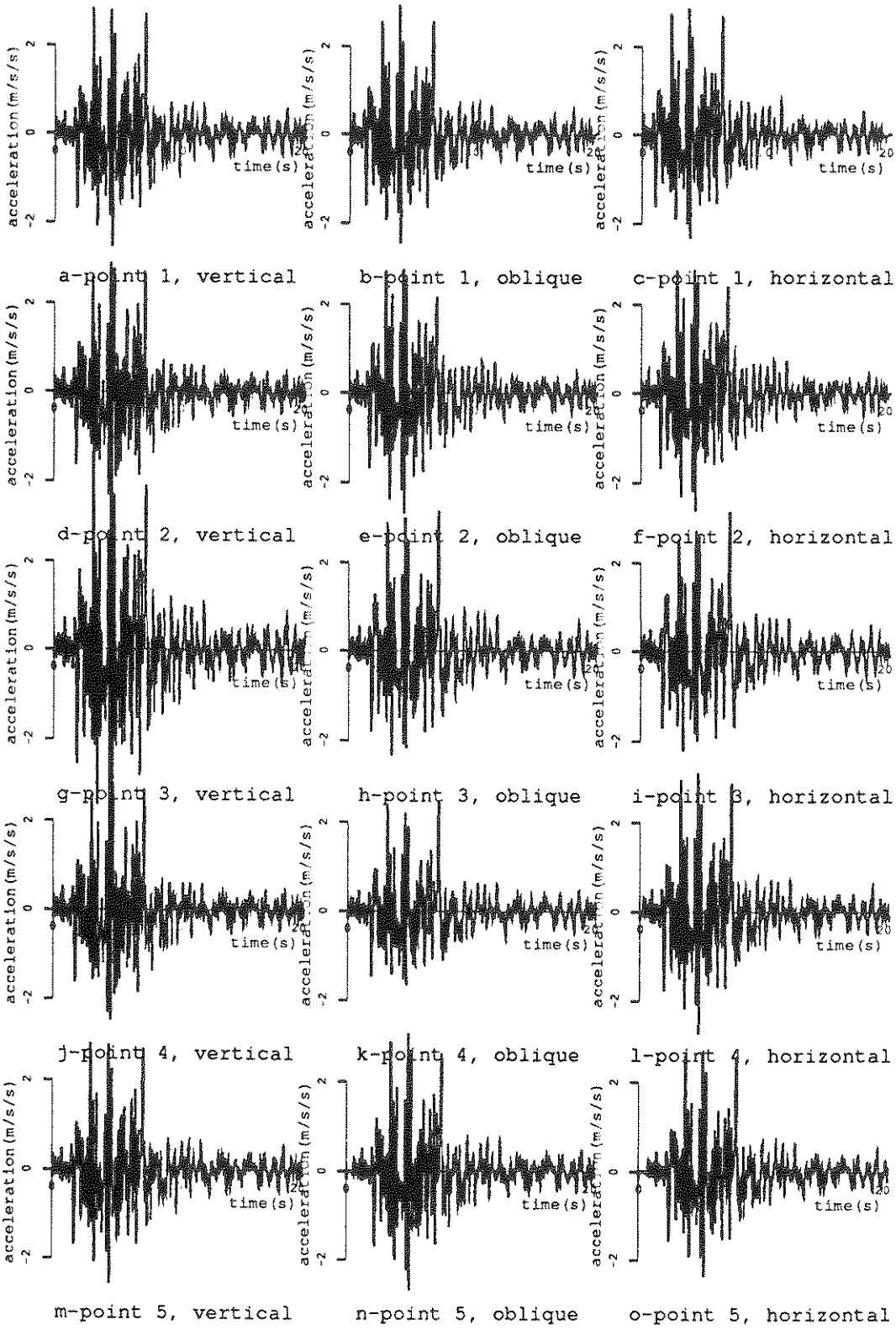

FIGURE 2-17 Time histories of five points on the hill profile

SECTION 3
NONHOMOGENEOUS PROFILES

In section 2 the application of the boundary integral method to the solution of wave scattering problems in an homogeneous medium is presented. In this section the technique is extended to profiles containing several different media. Each of the media is homogeneous but their interface permits the analysis of nonhomogeneous profiles.

This section contains a brief extension of the underlying mathematics of the problem for multiple media, then examples of its application. These examples show a high amount of agreement between the solution by the approximate method and several exact solutions which do exist.

The section closes with examples of complete problems convoluted back into the time domain.

3.1 Theory of wave scattering in nonhomogeneous profiles

In section 2, the equations governing a homogeneous medium were presented. The purpose of this section is to extend those equations to a nonhomogeneous profile. The profile will be considered to be made up of several different media with different material properties as shown in figure 3-1. The material within each medium is assumed to be homogeneous.

Because the material within each medium is homogeneous, the equations of section 2 apply. Therefore, the only extension required is the handling of the continuity conditions at the interfaces between media. For this project these conditions are assumed to be continuity of displacement and stress, that is

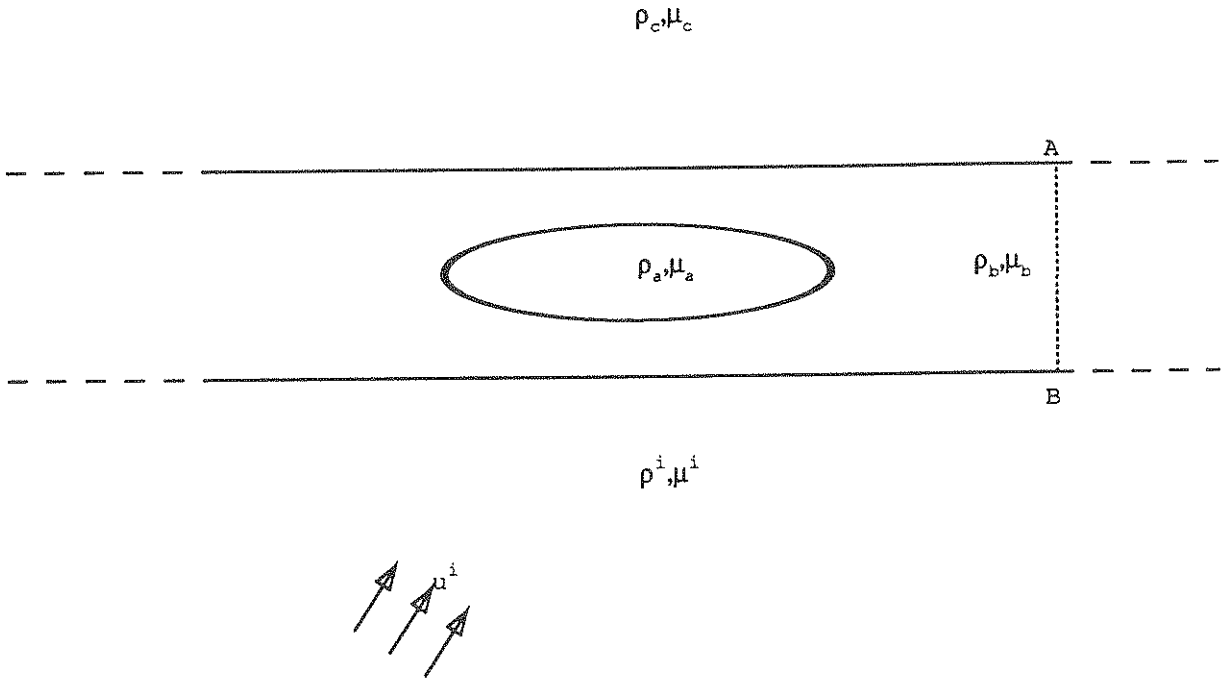

FIGURE 3-1 Heterogeneous profile

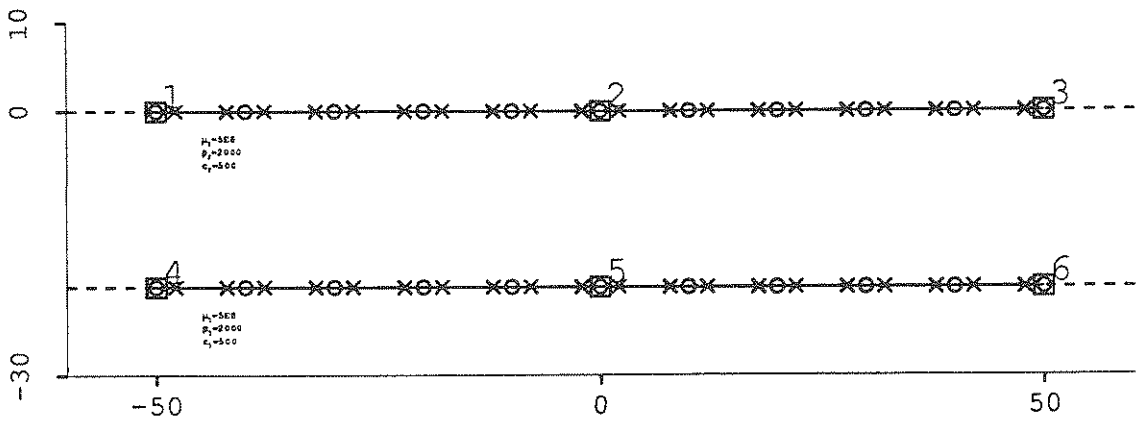

FIGURE 3-2 Half space with homogeneous layers

$$\bar{w}_b = \bar{w}_c \quad \text{and} \quad \bar{\tau}_b = \bar{\tau}_c \tag{3.1}$$

on either side of the interface.

Thus, the integral equation for a point on a surface or an interface bordering medium b is similar to that given in equation (2.11), to wit:

$$(1-\alpha)\bar{w} + P\int_{S_b} (\bar{w}\frac{\partial g}{\partial n'} - g\frac{\partial \bar{w}}{\partial n'})dS' = \bar{w}^i \tag{3.2}$$

where: S_b = the surface bounding medium b.

For the points on free surfaces this equation is written around the medium as it is done for the homogeneous medium in section 2. For the points on an interface there are two equations, one written around each medium. Accordingly, one can see that the problem is still well formed because while the interfaces have two unknowns (stress and displacement), they also have two equations.

3.2 Numerical formulation

The conversion of the continuous equation to the numerical system is the same as it is for the homogeneous case and the resulting equation can again be represented as

$$H_{ij} w_j = f_i \tag{3.3}$$

However, it is no longer possible to eliminate one of the unknowns. Therefore, while the equation has the same summary form, there are many more equations and many more unknowns. Also, more bookkeeping is necessary to keep the signs of the outward normals (direction of integration) straight. The $\bar{w}$'s are the displacements in the $z-$ or x_3-direction and are the same for both media. However, the stresses, $\bar{\tau}$, are the stress on the outer face of the medium of integration. Therefore, there is a sign difference between the stresses depending on which medium is being integrated.

3.3 Truncation

The discretization of the problem domain requires truncation of the surfaces and interfaces which extend to infinity as shown by the dashed lines of figure 3-1. By integrating just over the discretized part of the domain and ignoring the truncated portions, the equations have no contribution from those portions. This is equivalent to assuming that the displacement and stress along these lines is zero. In most cases this is a bad assumption.

The details of the method for handling these truncated portions is given in appendix D. Essentially, it involves the assumption that beyond the points of truncation the layers are infinite, horizontal, and parallel. Given this assumption, the wave field in the truncated portion is assumed to approach the free field solution for infinite parallel layers. That is

$$\bar{w}^t \sim \bar{w}^{ff} \tag{3.4}$$

where: $\bar{w}^{ff} = \bar{w}^i + \bar{w}^r$ =the free–field response in infinite parallel layers

$\bar{w}^r$ = the reflected wave in infinite parallel layers.

This is equivalent to the assumption that any scattering done by objects within the numerical portion of the problem is not transmitted beyond the truncation point. The shape of the Green's function, if not common sense, indicates that this must eventually be so at a point sufficiently removed from any scatterer.

3.4 Examples

In the following sections results are presented of the application of this method to profiles comprised of multiple layers. First, there is a section demonstrating the application to problems with known solutions, then some more general problems, and finally, several results of

convolutions back into the time domain.

3.4.1 Examples of problems possessing analytical solutions

There are several problems for which analytical solutions have been found. We first present the case of a homogeneous half space solved as a layered system. Then we proceed to the case of a heterogeneous layered half space. These results are compared to the analytical solutions.

Half space Figure 3-2 shows the geometry used for the solution of an homogeneous elastic half space solved as if it were layered. The solutions for this profile are presented in figure 3-3. Solutions for the half space at ω=50 rad/s are presented in table 3-I. The agreement between the approximate methods and the analytical solution is quite good.

Heterogeneous layered half space Figure 3-4 shows the profile of a layered half space in which the layers have different material properties—a soft layer overlies a stiffer layer. The method for obtaining the analytical solution for the layered system is presented in section D.1.1. Figure 3-5 and table 3-I show the solutions for it. Figure 3-6 shows the response of this profile to a field incident at a 45° angle at ω=50 rad/s. It can be seen that the method yields good results for oblique angles as well.

3.4.2 Examples of problems which do not possess analytical solutions

Figure 3-7 shows the geometry and discretization for a cylindrical cavity in a heterogeneous layered half space with modified surface topography. The admittance of this geometry for the three surfaces for vertical and oblique angles of incidence are shown in figures 3-8 and

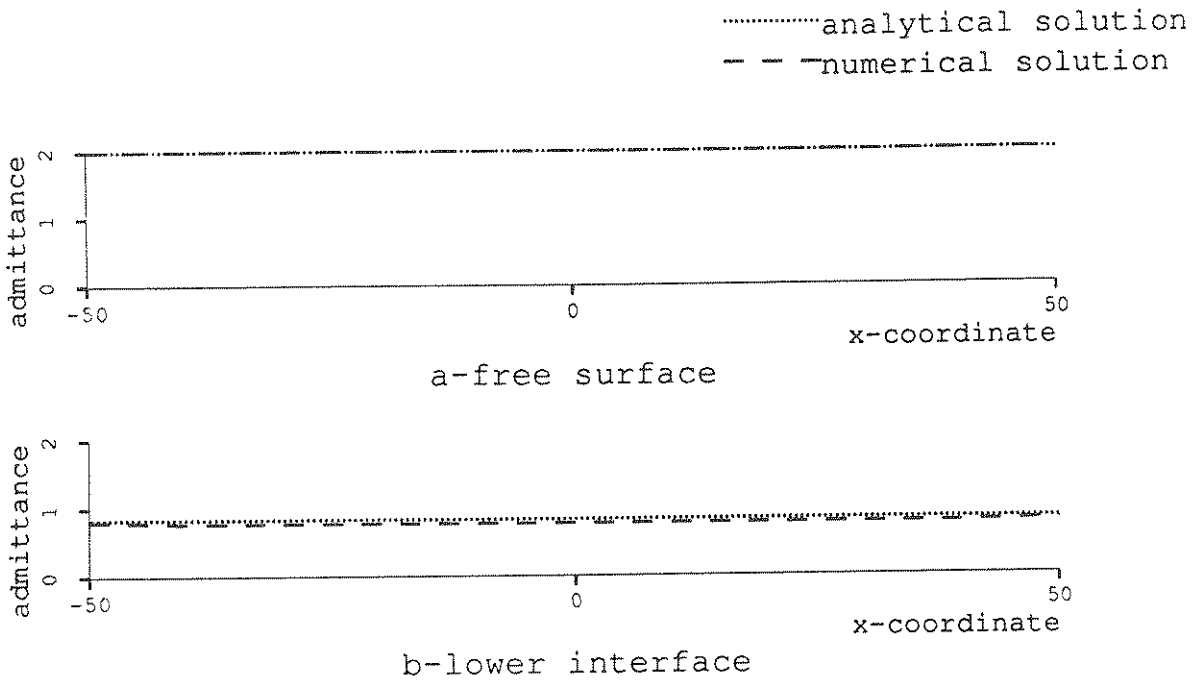

FIGURE 3-3 Solutions for the half space at ω=50 rad/s

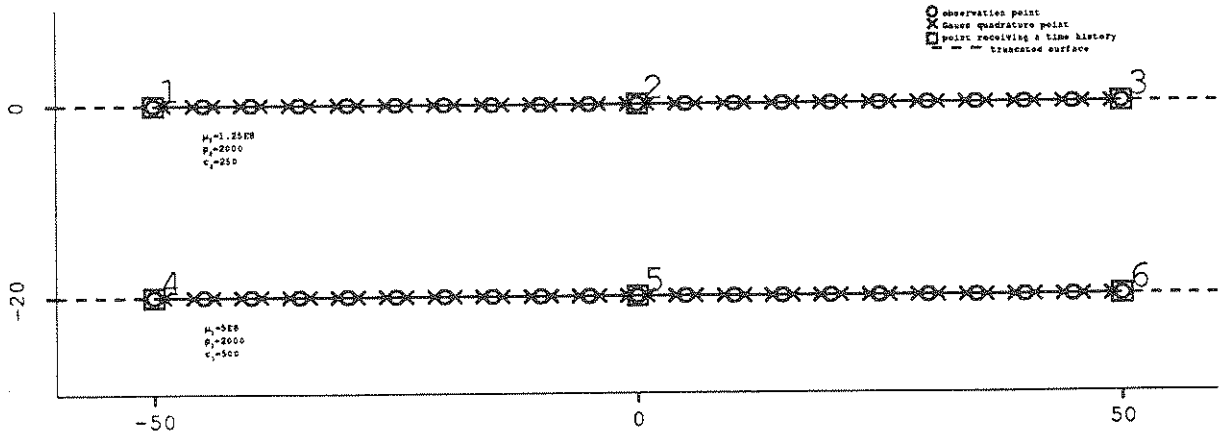

FIGURE 3-4 Heterogeneous layered half space

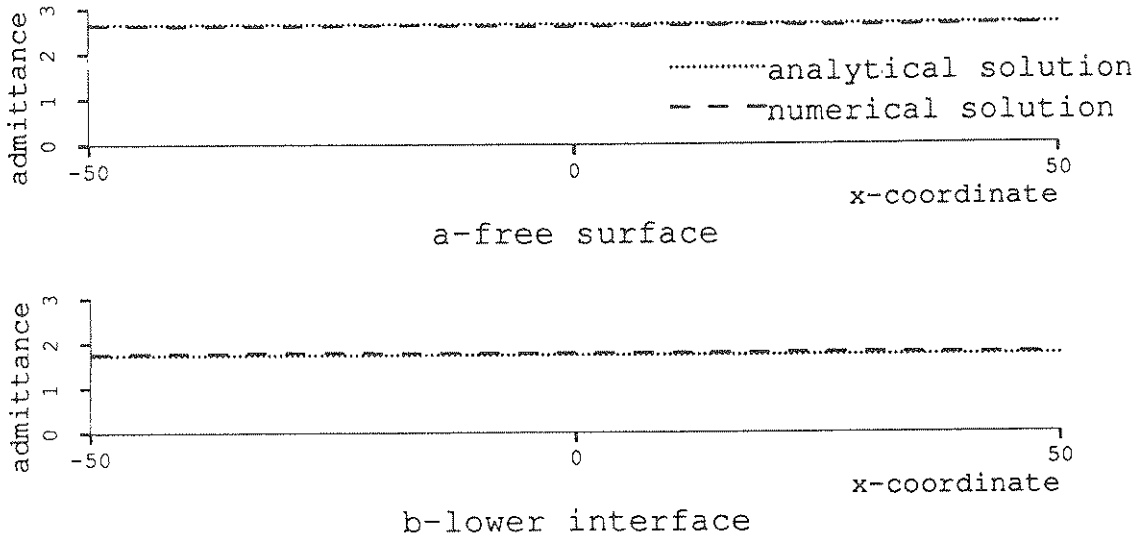

FIGURE 3-5 Solutions for the heterogeneous layered half space

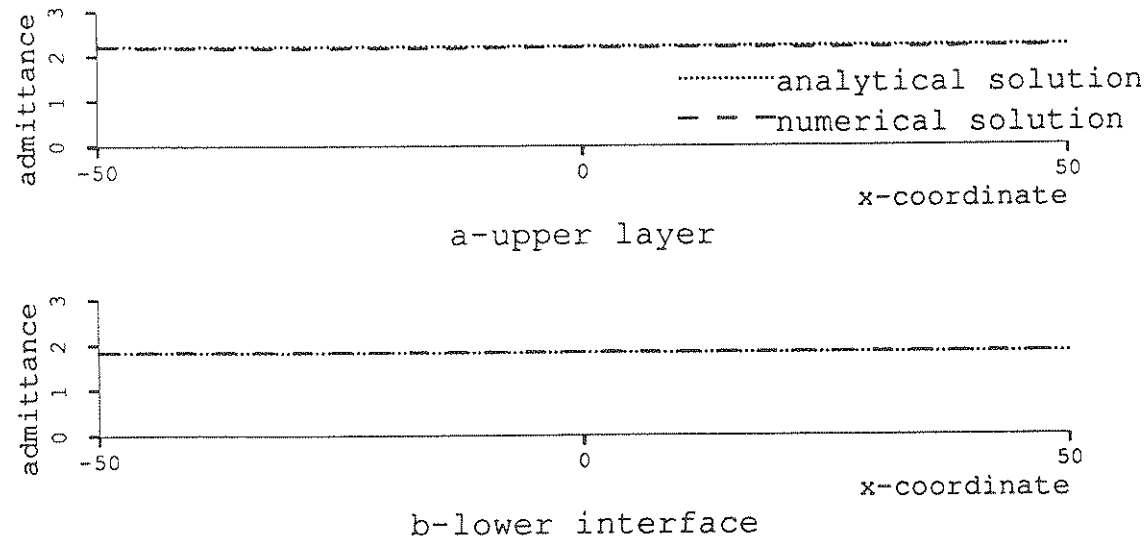

FIGURE 3-6 Response of heterogeneous layered profile to an oblique wave

TABLE 3-I Solutions for the layered half space at ω=50 rad/s

		analytical solution		numerical solution	
point	coordinates	complex coefficient	magnitude	complex coefficient	magnitude
1	(50,0)	(-0.254,2.636)	2.648	(-0.2351,2.625)	2.63518
2	(45,0)	(-0.254,2.636)	2.648	(-0.2321,2.615)	2.62513
3	(40,0)	(-0.254,2.636)	2.648	(-0.2299,2.605)	2.61541
4	(35,0)	(-0.254,2.636)	2.648	(-0.2284,2.600)	2.61018
5	(30,0)	(-0.254,2.636)	2.648	(-0.2271,2.602)	2.61158
6	(25,0)	(-0.254,2.636)	2.648	(-0.2263,2.607)	2.61718
7	(20,0)	(-0.254,2.636)	2.648	(-0.2270,2.611)	2.62112
8	(15,0)	(-0.254,2.636)	2.648	(-0.2298,2.608)	2.61847
9	(10,0)	(-0.254,2.636)	2.648	(-0.2340,2.599)	2.60936
10	(5,0)	(-0.254,2.636)	2.648	(-0.2379,2.588)	2.59920
11	(0,0)	(-0.254,2.636)	2.648	(-0.2395,2.584)	2.59480
12	(-5,0)	(-0.254,2.636)	2.648	(-0.2379,2.588)	2.59920
13	(-10,0)	(-0.254,2.636)	2.648	(-0.2340,2.599)	2.60936
14	(-15,0)	(-0.254,2.636)	2.648	(-0.2298,2.608)	2.61847
15	(-20,0)	(-0.254,2.636)	2.648	(-0.2270,2.611)	2.62112
16	(-25,0)	(-0.254,2.636)	2.648	(-0.2263,2.607)	2.61718
17	(-30,0)	(-0.254,2.636)	2.648	(-0.2271,2.602)	2.61158
18	(-35,0)	(-0.254,2.636)	2.648	(-0.2284,2.600)	2.61018
19	(-40,0)	(-0.254,2.636)	2.648	(-0.2299,2.605)	2.61541
20	(-45,0)	(-0.254,2.636)	2.648	(-0.2321,2.615)	2.62513
21	(-50,0)	(-0.254,2.636)	2.648	(-0.2351,2.625)	2.63518
22	(50,-20)	(0.166,-1.732)	1.740	(0.1659,-1.747)	1.75447
23	(45,-20)	(0.166,-1.732)	1.740	(0.1602,-1.761)	1.76832
24	(40,-20)	(0.166,-1.732)	1.740	(0.1534,-1.765)	1.77124
25	(35,-20)	(0.166,-1.732)	1.740	(0.1489,-1.769)	1.77480
26	(30,-20)	(0.166,-1.732)	1.740	(0.1475,-1.771)	1.77688
27	(25,-20)	(0.166,-1.732)	1.740	(0.1490,-1.770)	1.77651
28	(20,-20)	(0.166,-1.732)	1.740	(0.1522,-1.767)	1.77400
29	(15,-20)	(0.166,-1.732)	1.740	(0.1556,-1.764)	1.77057
30	(10,-20)	(0.166,-1.732)	1.740	(0.1583,-1.760)	1.76745
31	(5,-20)	(0.166,-1.732)	1.740	(0.1599,-1.758)	1.76541
32	(0,-20)	(0.166,-1.732)	1.740	(0.1604,-1.757)	1.76472
33	(-5,-20)	(0.166,-1.732)	1.740	(0.1599,-1.758)	1.76541
34	(-10,-20)	(0.166,-1.732)	1.740	(0.1583,-1.760)	1.76745
35	(-15,-20)	(0.166,-1.732)	1.740	(0.1556,-1.764)	1.77057
36	(-20,-20)	(0.166,-1.732)	1.740	(0.1522,-1.767)	1.77400
37	(-25,-20)	(0.166,-1.732)	1.740	(0.1490,-1.770)	1.77651
38	(-30,-20)	(0.166,-1.732)	1.740	(0.1475,-1.771)	1.77688
39	(-35,-20)	(0.166,-1.732)	1.740	(0.1489,-1.769)	1.77480
40	(-40,-20)	(0.166,-1.732)	1.740	(0.1534,-1.765)	1.77124
41	(-45,-20)	(0.166,-1.732)	1.740	(0.1602,-1.761)	1.76832
42	(-50,-20)	(0.166,-1.732)	1.740	(0.1659,-1.747)	1.75447

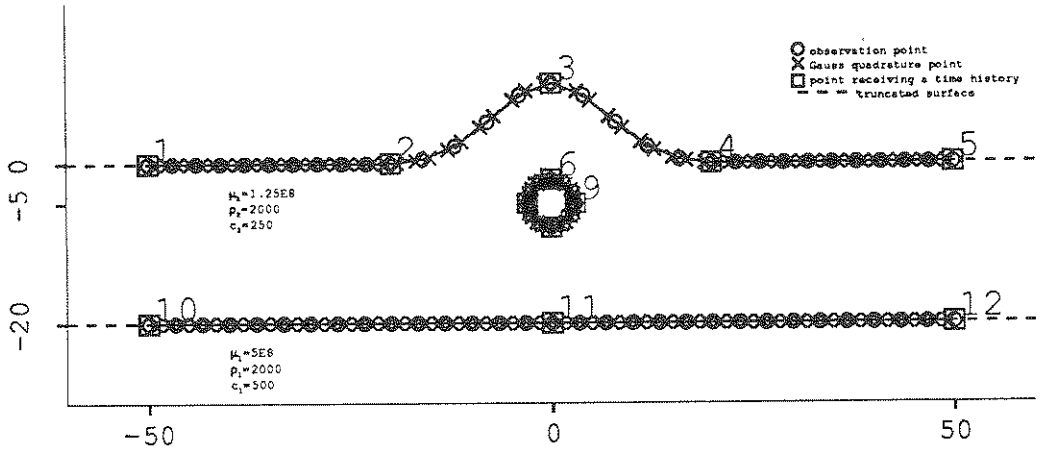

FIGURE 3-7 Profile geometry for a tunnel in a layered half space

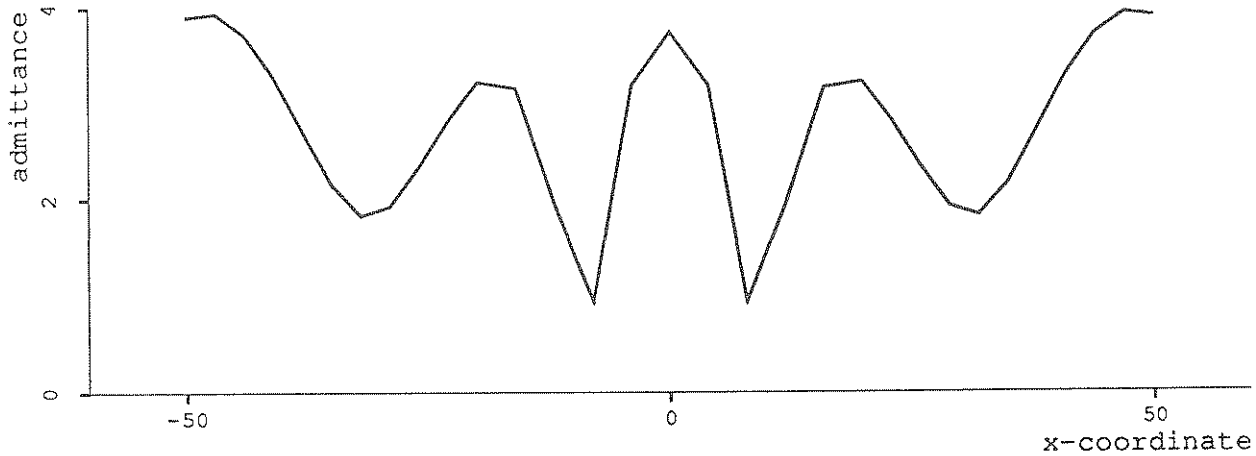

a-admittance of the free surface

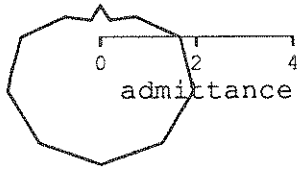

b-admittance of the cylinder

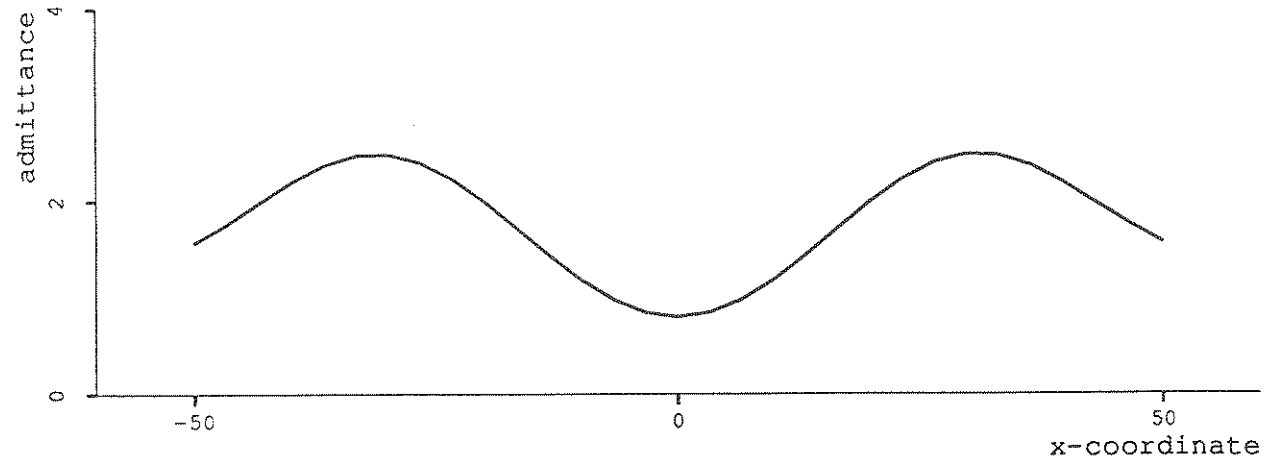

c-admittance of the lower interface

FIGURE 3-8 Admittance for tunnel in a layered half space with a hill—vertical incidence

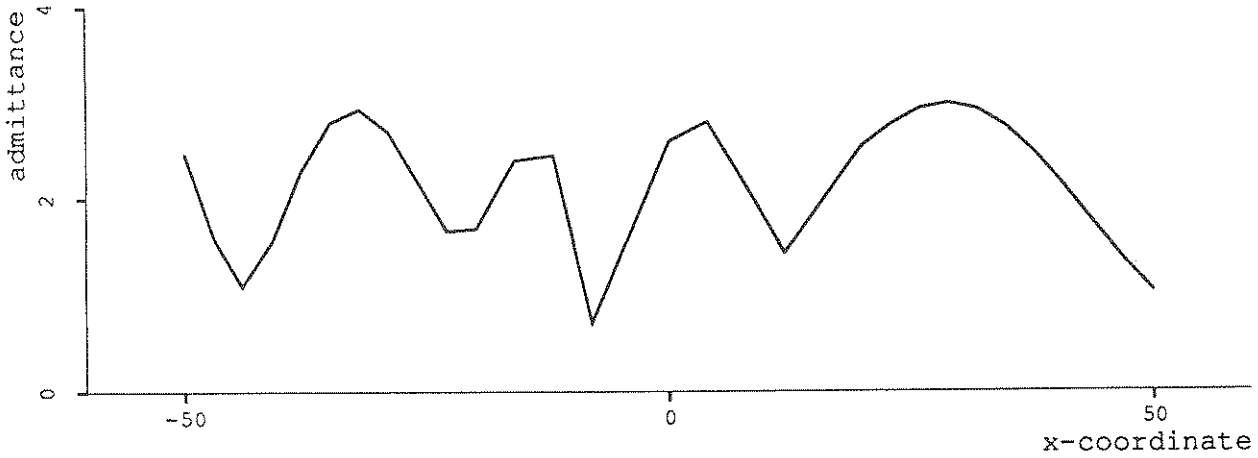

a-admittance of the free surface

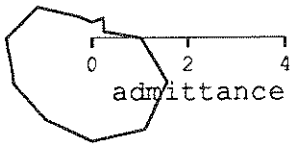

b-admittance of the cylinder

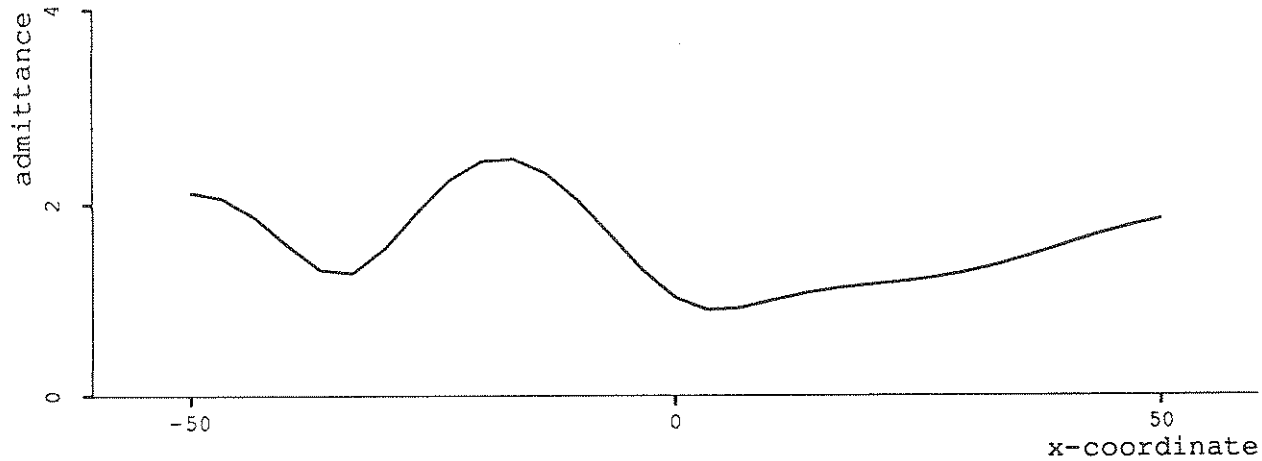

c-admittance of the lower interface

FIGURE 3-9 Admittance for tunnel in a layered half space with a hill—45° incidence

3-9. As can be seen by comparing these figures to others, the hill and the tunnel have an effect on each other. The response of the hill is somewhat deflected by the tunnel beneath it and the response of the tunnel is modified by the reflections from the hill.

Figure 3-10 shows the geometry and discretization for three cylindrical cavities in a heterogeneous layered half space with modified surface topography. The admittance of this geometry for the three surfaces for vertical and oblique angles of incidence are shown in figures 3-11 and 3-12. Again, there are effects of interaction. In fact, the presence of the two extra tunnels modifies the behaviour of the original tunnel of figure 3-7 as shown for the case of vertical incidence in figure 3-13. We can thus see that the interaction of buried objects can be a significant consideration in the response of the system.

The construction of other profiles is straightforward.

3.4.3 Time histories

This section contains examples of time histories convoluted back from the frequency domain. Results for several of the profiles introduced above have been convoluted with the Gaussian pulse and San Fernando earthquakes introduced in section 2. These are reproduced here as figures 3-14 and 3-15.

Figure 3-16 shows the response of the homogeneous half space treated as a layered system of figure 3-2 to the Gaussian pulse. The responses shown are for the points labeled 1, 2, 4, and 5 of figure 3-2. These responses correspond to the rows. The columns contain the results for vertical, 45°, and horizontal angles of incidence. If one looks at plots a-f, one sees the doubling of the incident function which is to be expected at the free surface of a half space. Furthermore, plots b and c show the earlier arrival of the pulse at the left side of

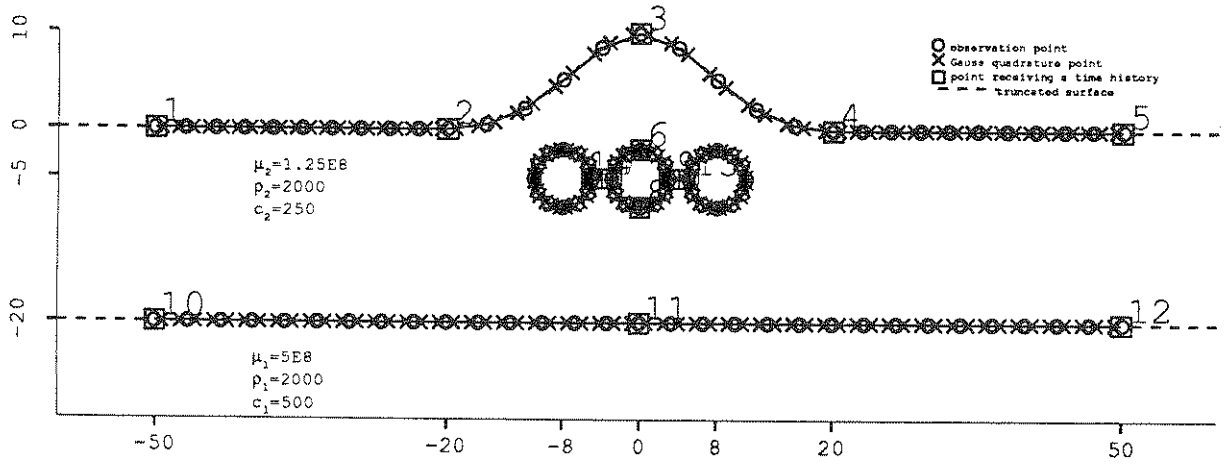

FIGURE 3-10 Profile geometry for three parallel tunnels in a layered half space

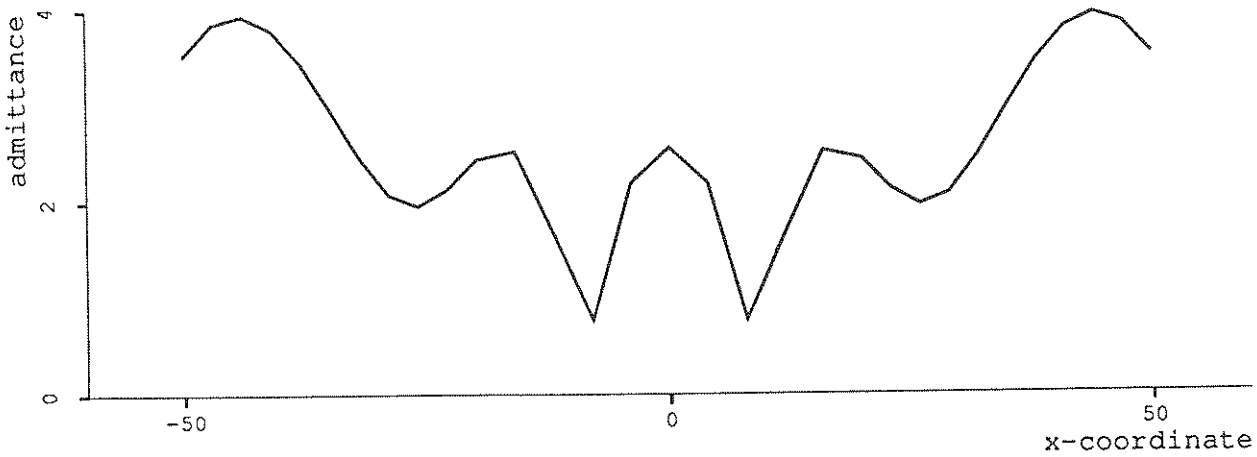

a-admittance of the free surface

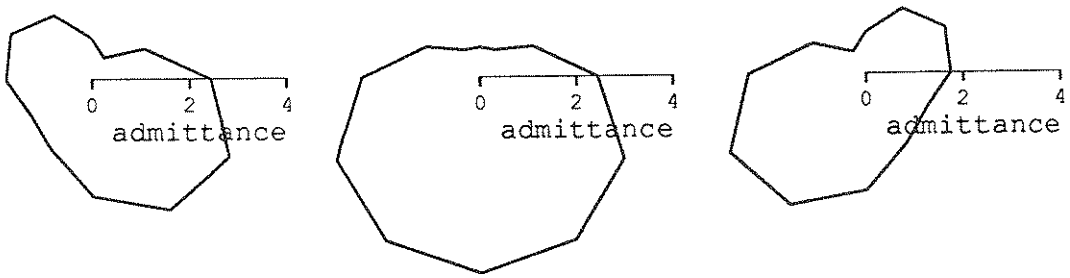

b-admittance of the cylinders

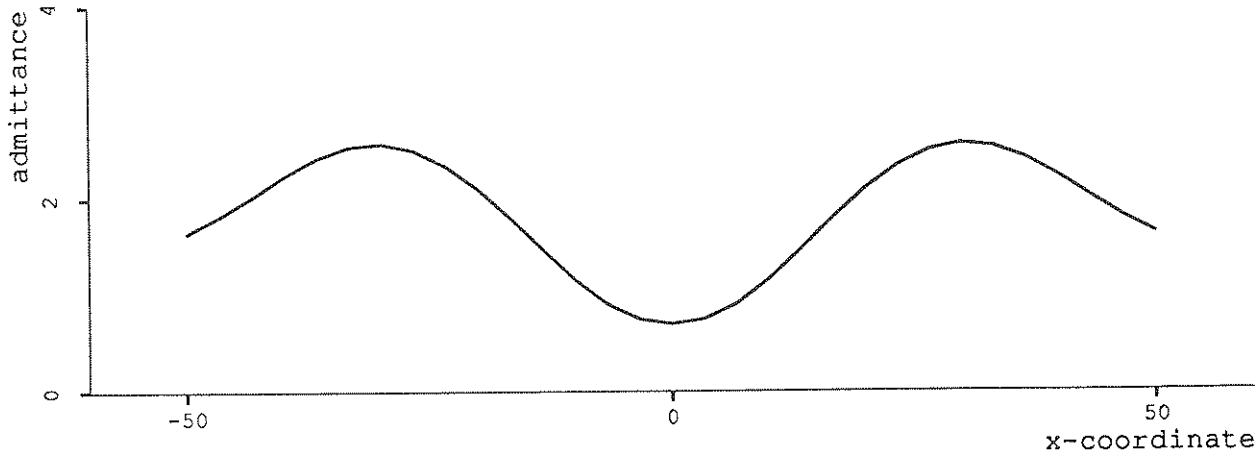

c-admittance of lower interface

FIGURE 3-11 Admittance for tunnels in a layered half space with a hill—vertical incidence

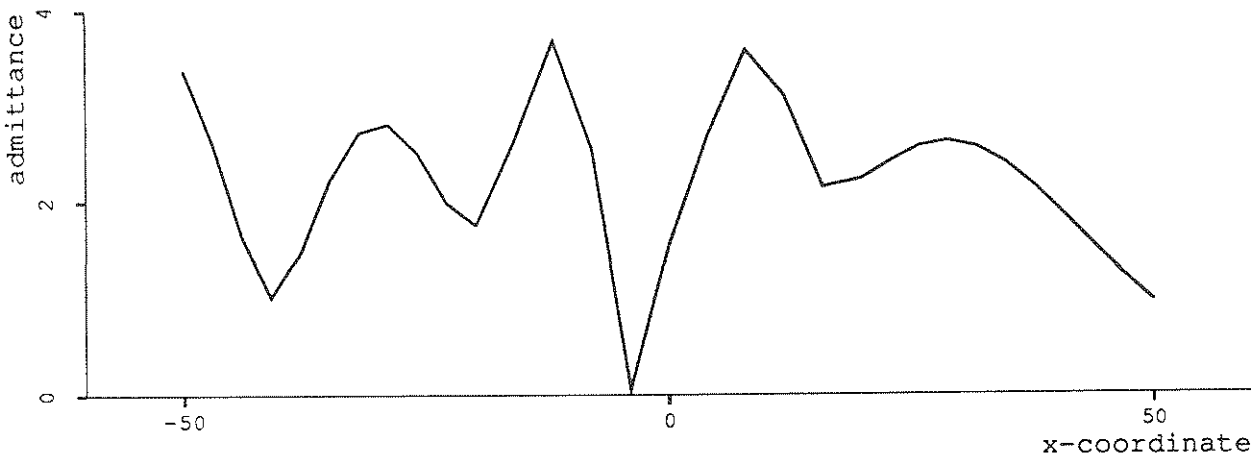

a-admittance of the free surface

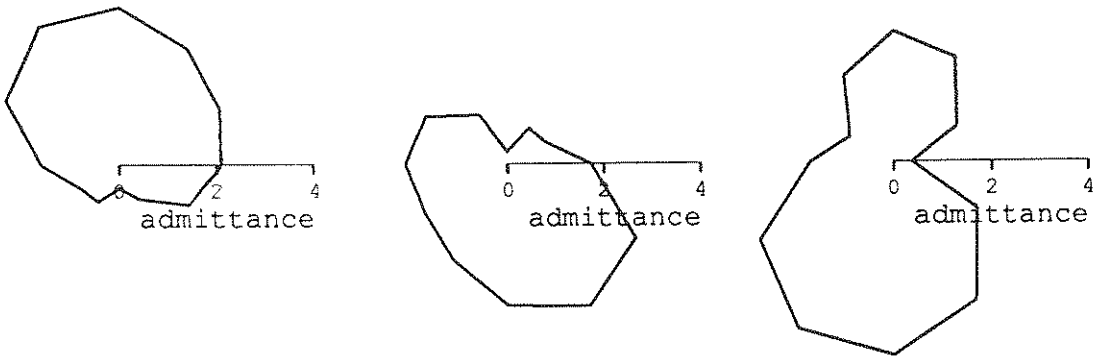

b-admittance of the cylinders

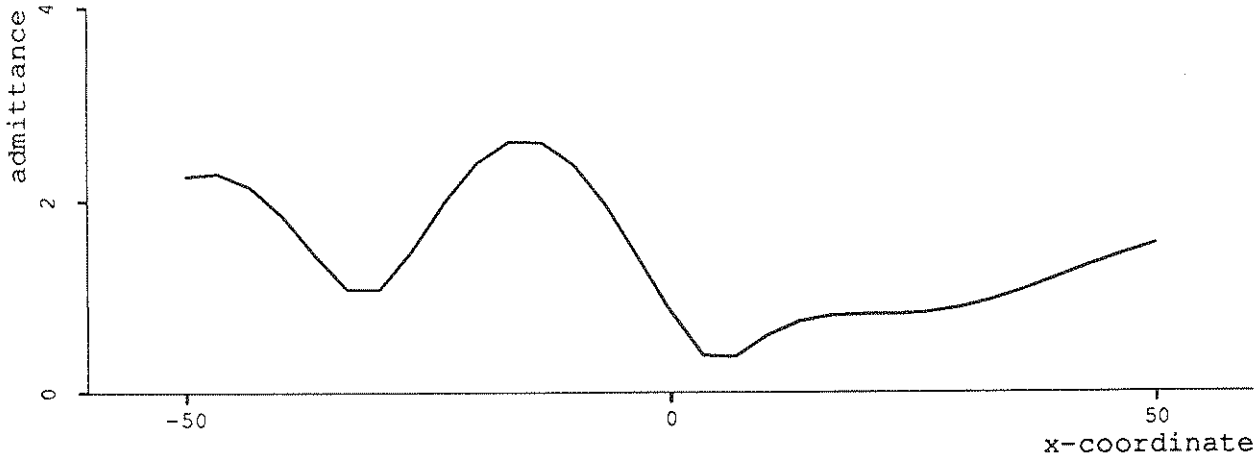

c-admittance of the lower interface

FIGURE 3-12 Admittance for tunnels in a layered half space with a hill—45° incidence

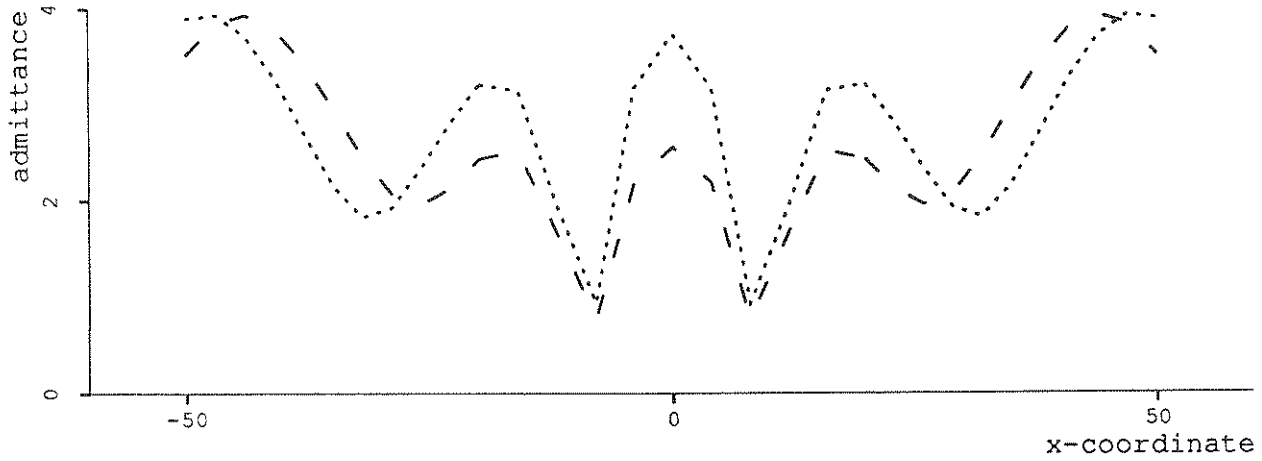

a-admittance of the free surface

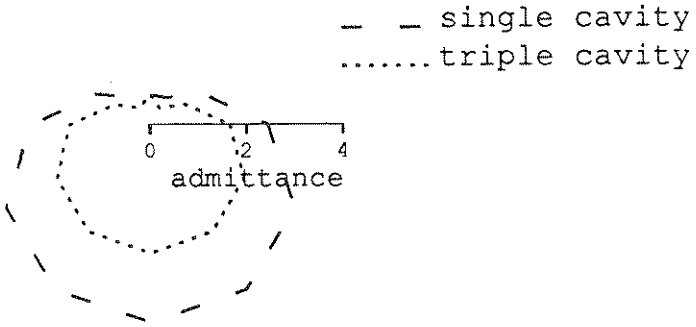

b-admittance of the cylinders

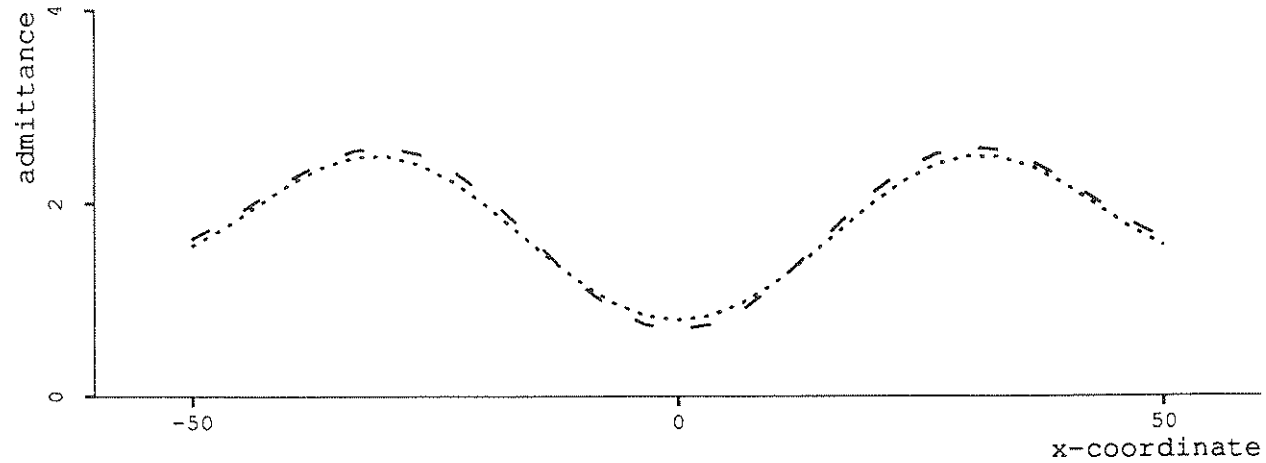

c-admittance of lower interface

FIGURE 3-13 Comparison of responses for one- and three-tunnel profiles—vertical incidence

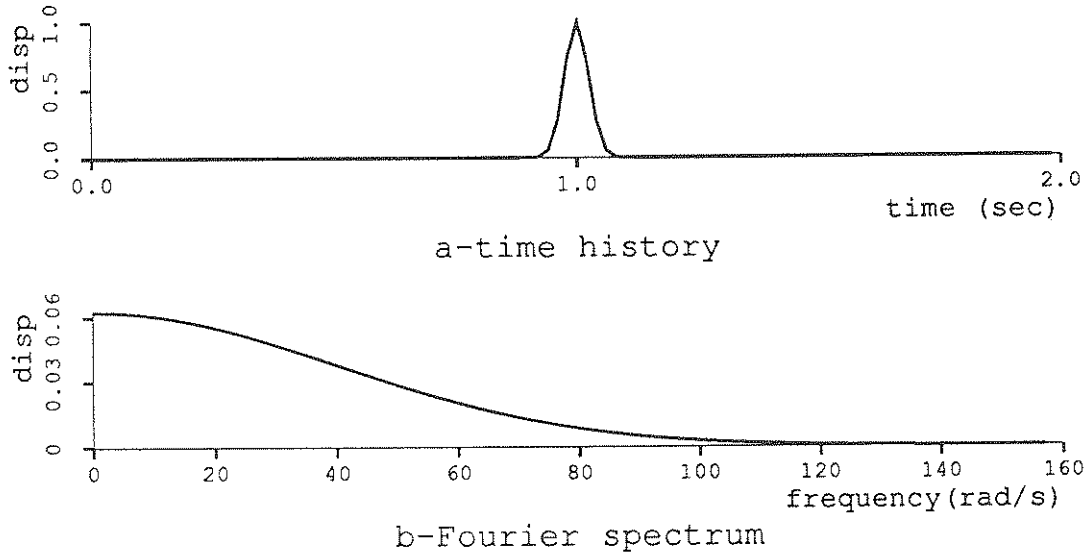

FIGURE 3-14 Time history and Fourier transform of Gaussian pulse

---

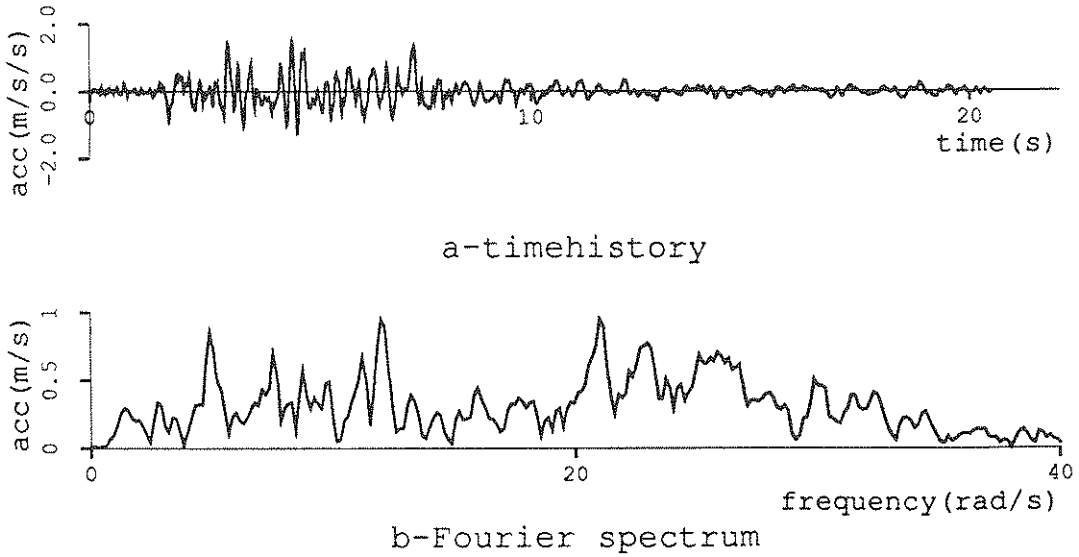

FIGURE 3-15 Acceleration history and displacement spectrum of San Fernando earthquake

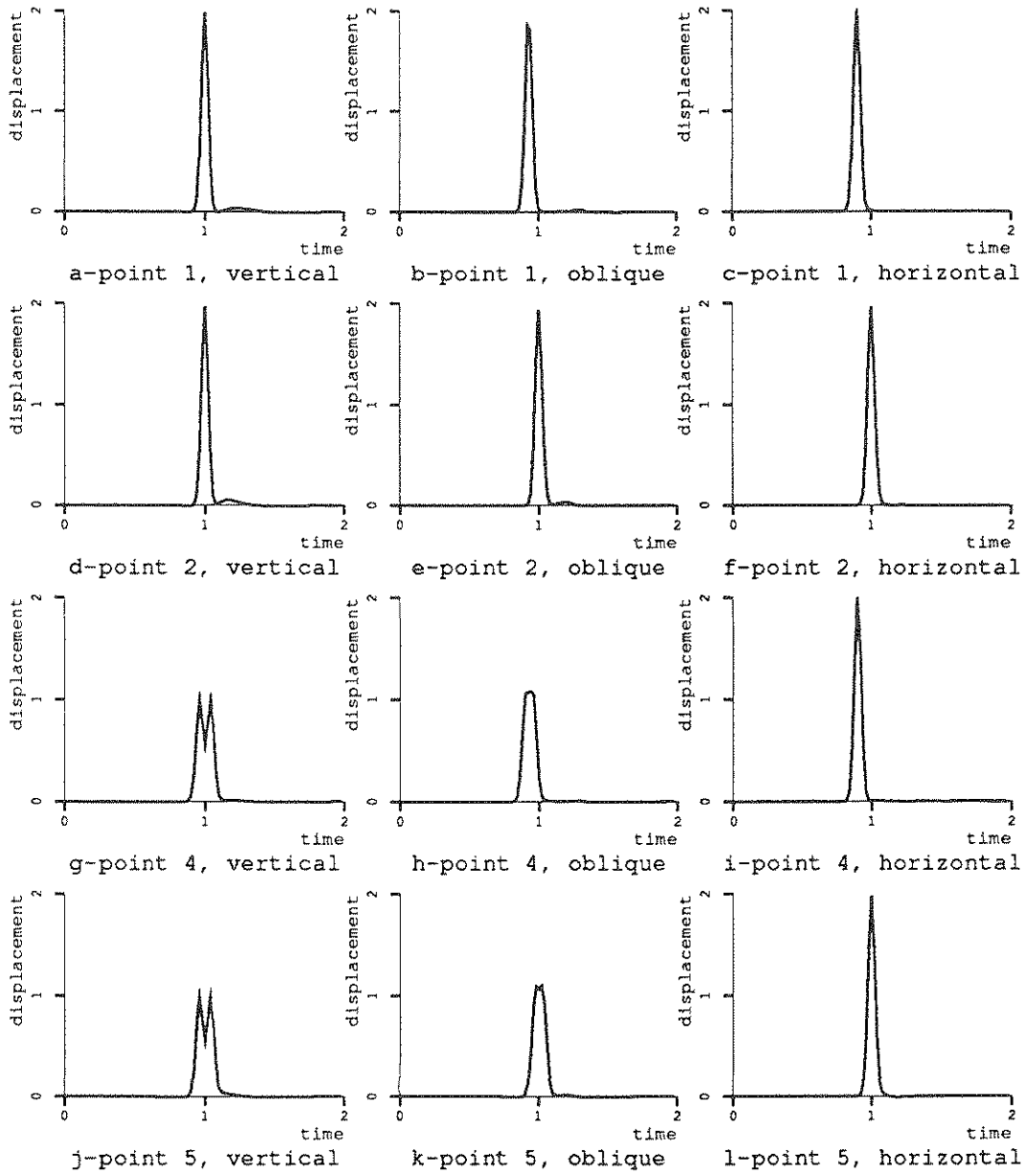

FIGURE 3-16 Time response of four points in homogeneous half space to the Gaussian pulse

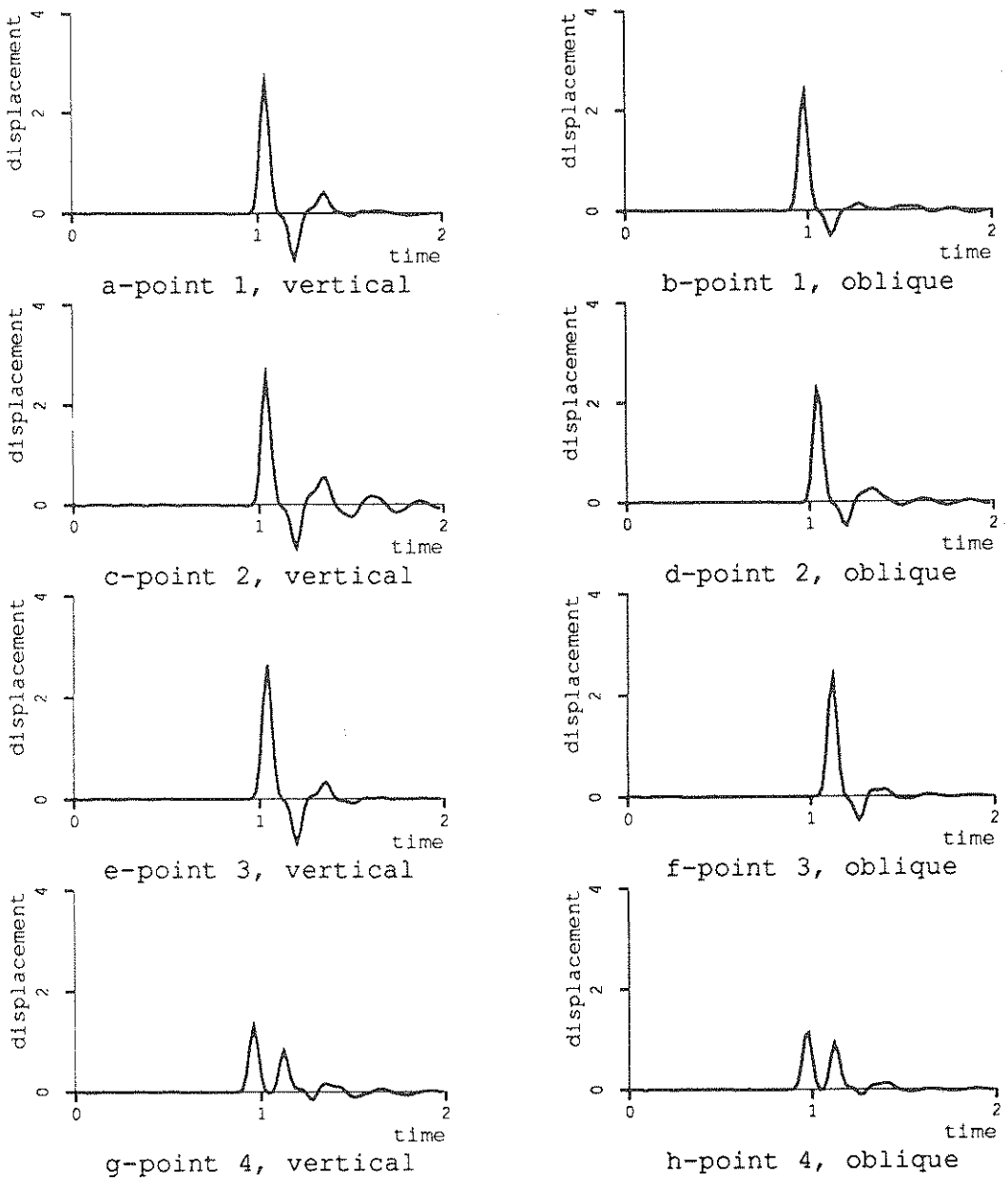

FIGURE 3-17 Time response of four points in heterogeneous half space to the Gaussian pulse

the profile. This is, of course, what one would expect and validates the process of the Fourier analysis.

Plots g-l are for points on the interface layer and show that for horizontal incidence (plots i and l) the incident and reflected wave arrive together while for the vertical and 45° incidences, the energy travels to the surface and is reflected, thereby causing the double spikes in those plots and a pattern of constructive interference in time.

Figures 3-18 and 3-19 show the response of the tunnel in a half space with a hill shown in figure 3-7 to the Gaussian pulse at vertical and 45° incidence respectively. In each figure plot a is the response of point 3 at the crest of the hill, plot b is the response of point 7 on the left side of the cylindrical cavity, and plot c is the response of point 11 which is directly beneath the tunnel,the midpoint of the interface line.

By comparing these two figures, one can see that the angle of incidence is a potentially important parameter and that analytical methods should have the capacity to take it into account.

Figures 3-21 and 3-22 show the responses of the same three points to a vertically incident wave but in the profile with three tunnels.

Figure 3-23 gives a comparison of the response of the same three points (points 3, 7, and 11) in figure 3-7 (the single cavity profile) and figure 3-10 (the triple cavity profile) to the Gaussian pulse at vertical incidence. Previously, the difference in response in the frequency domain was noted. This figure shows that there can be differences in the time domain as well.

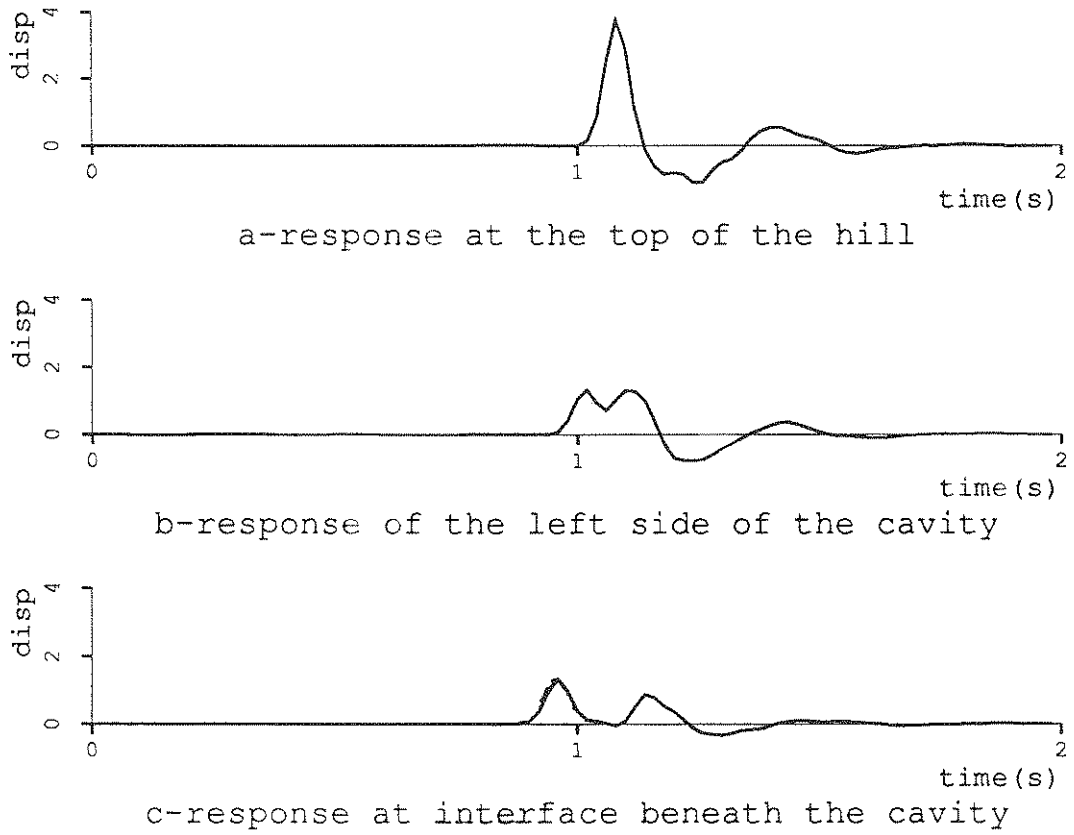

FIGURE 3-18 Response of the single tunnel profile to the Gaussian pulse vertically incident

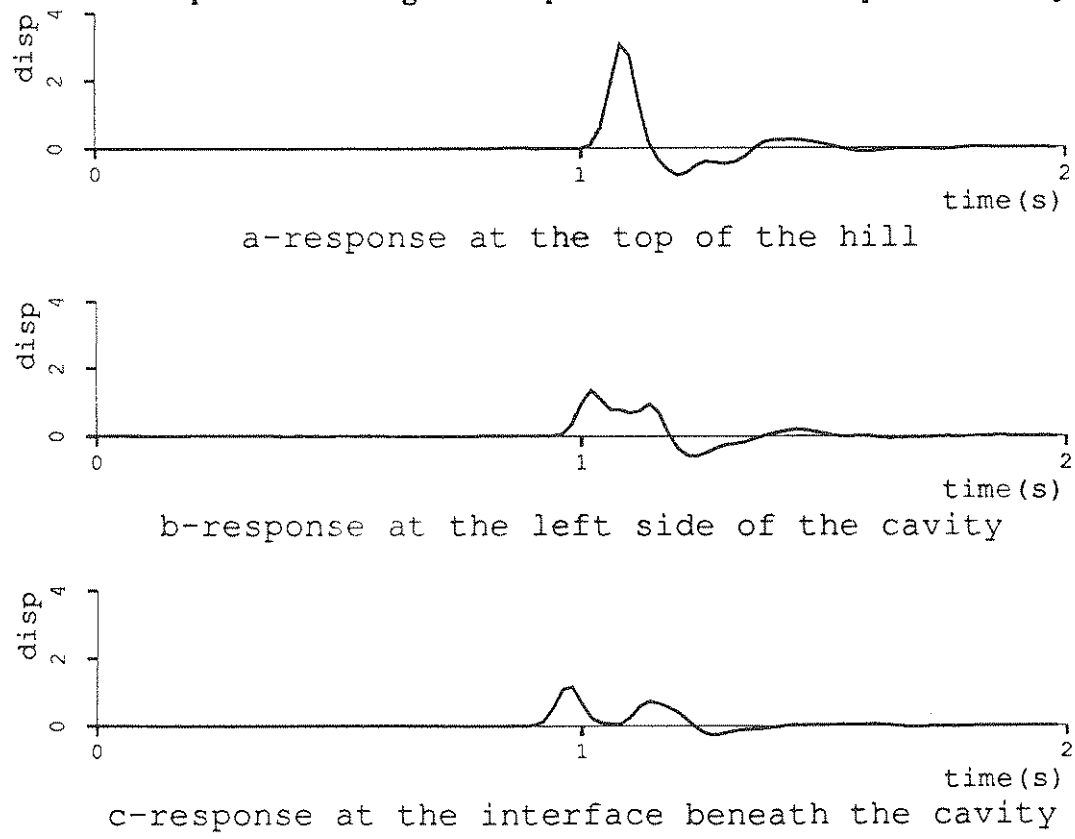

FIGURE 3-19 Response of the single tunnel profile to the Gaussian pulse at 45°

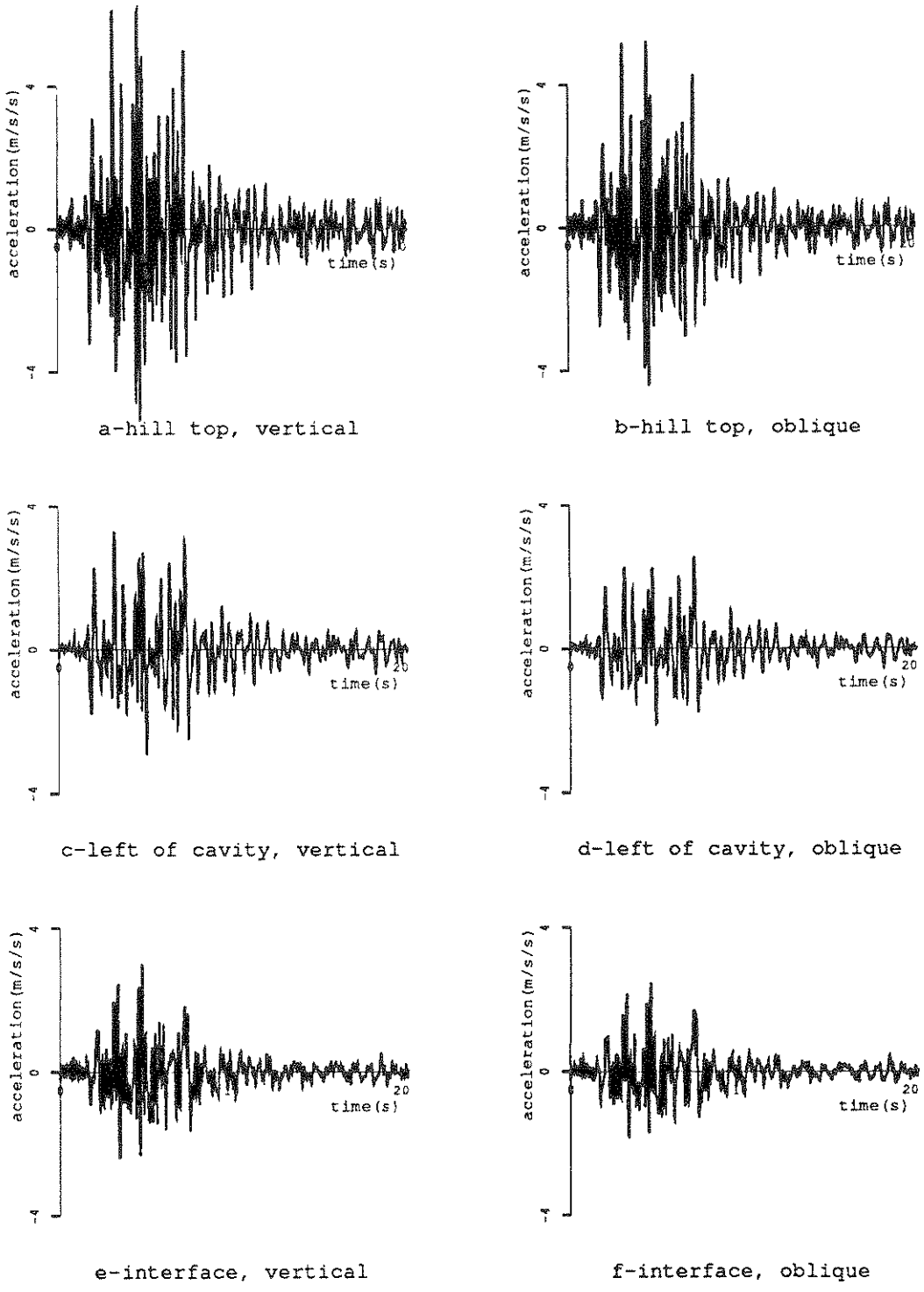

FIGURE 3-20 Response of the single tunnel profile to the San Fernando earthquake

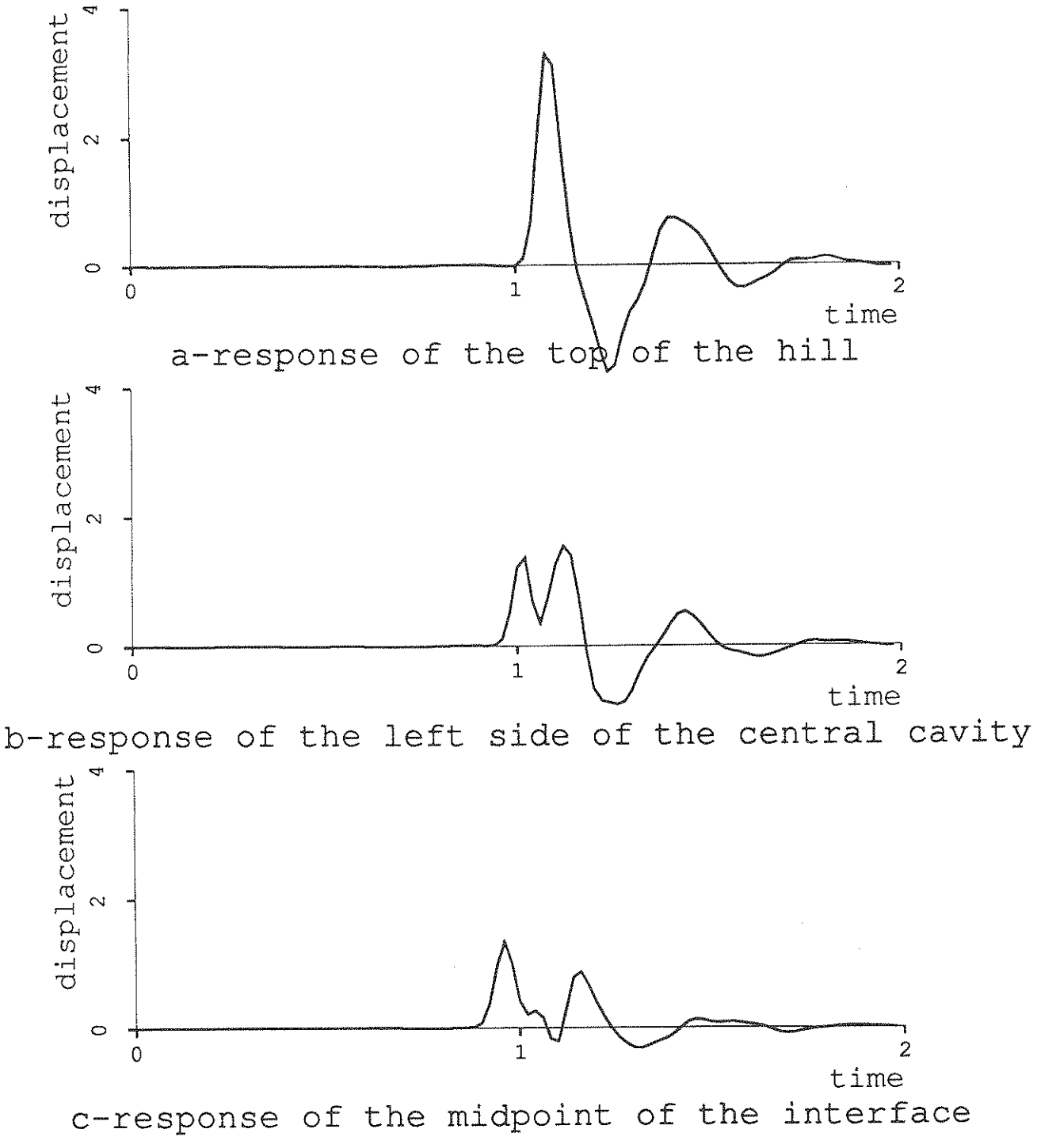

FIGURE 3-21 Response of the triple tunnel profile to the Gaussian pulse

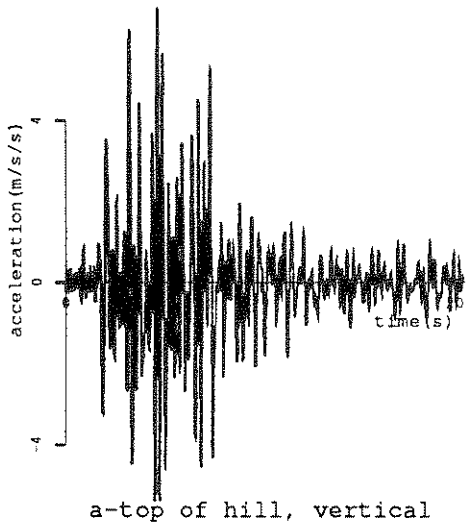

a-top of hill, vertical

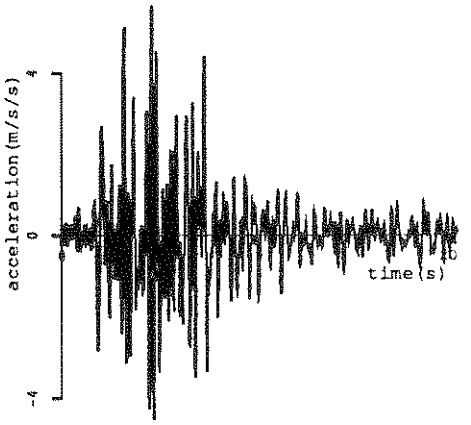

b-top of hill, oblique

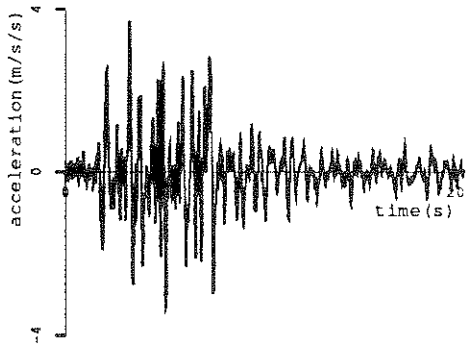

c-side of central tunnel, vertical

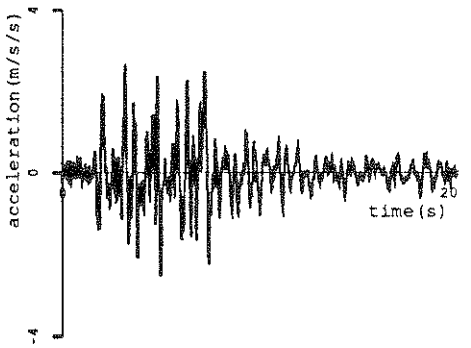

d-side of middle tunnel, oblique

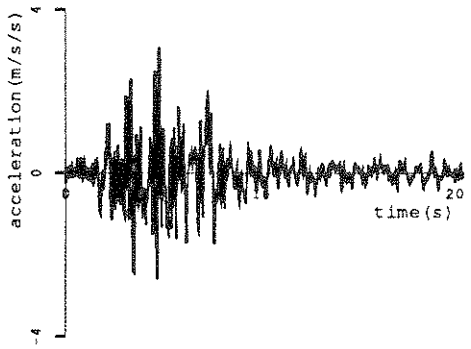

e-midpoint of interface, vertical

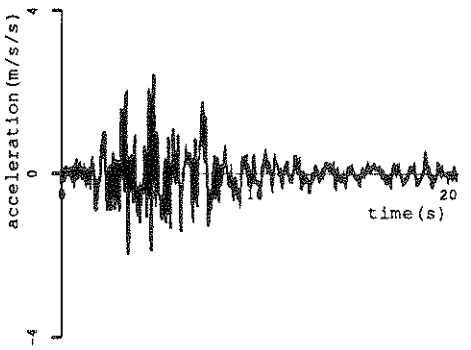

f-midpoint of interface, oblique

FIGURE 3-22 Response of the triple tunnel profile to the San Fernando earthquake

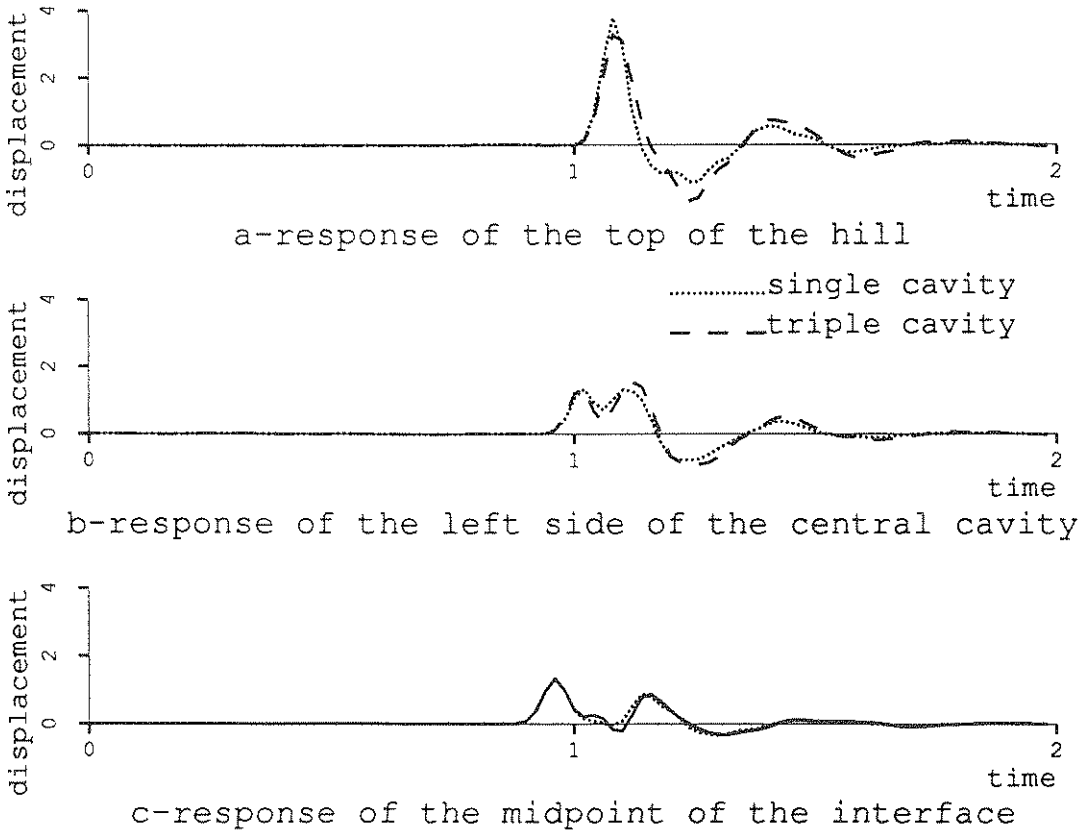

FIGURE 3-23 Comparison of time responses for vertical incidence

3.5 Conclusions

The boundary integral method is an effective way to perform a frequency-domain analysis of the behaviour of a nonhomogeneous profile subjected to SH waves. Where compared to known solutions, it is found to have small errors. The examples given in this section show the wide variety of problems to which the method can be applied:

problems with different soil properties
problems with multiple inclusions
problems with infinite width as long as the edges behave as parallel layers
problems with surficial topographies which are not flat.

The results computed for individual frequencies can be convoluted back into the time domain to find the time history of the response of points in the profile. Results show that the interaction of buried structures does modify behaviour and therefore indicates the limitation of a one-dimensional analysis and the desirability of a multidimensional analysis.

SECTION 4
INTERSECTION POINTS

Section 2 presents the basic theory for the wave scattering problem in homogeneous media. Section 3 extends this theory for nonhomogeneous profiles but does not address the case when two interface lines intersect as shown in figure 4-1.

The purpose of this section is to extend the theory and implementation to include problems where three media are in contact at one point. First, the analytical theory is extended, then the implications of that extension for the numerical scheme are examined. Finally, examples of the use of this extension are given.

4.1 Analytical theory

As was shown in section 2, the integral equation for steady-state harmonic wave scattering in a bounded homogeneous elastic medium is

$$(1-\alpha)\,\bar{w} + P\int_{S'} (\bar{w}\frac{\partial g}{\partial n'} - g\frac{\partial \bar{w}}{\partial n'})dS' = \bar{w}^i \tag{4.1}$$

In this equation, α, which comes from the singularity in the Hankel function, is equal to $\frac{\theta}{2\pi}$ or that portion of a circle which integration proceeds around. Thus, for the typical case of a line or smoothly changing curve, α is always 0.5 and $1-\alpha$ is 0.5. For the case of a sharp corner, this no longer obtains. In figure 4-1 the value of α at point B is 0.5 in the lower medium, 0.8334 in medium a, and 0.6667 in medium b. Because the integrations are done with respect to an outward-pointing normal, α becomes the portion of the circle on the outside of the medium and $1-\alpha$ becomes the portion inside. Thus the values of $1-\alpha$ for the three media are 0.5, 0.1667, and 0.3333.

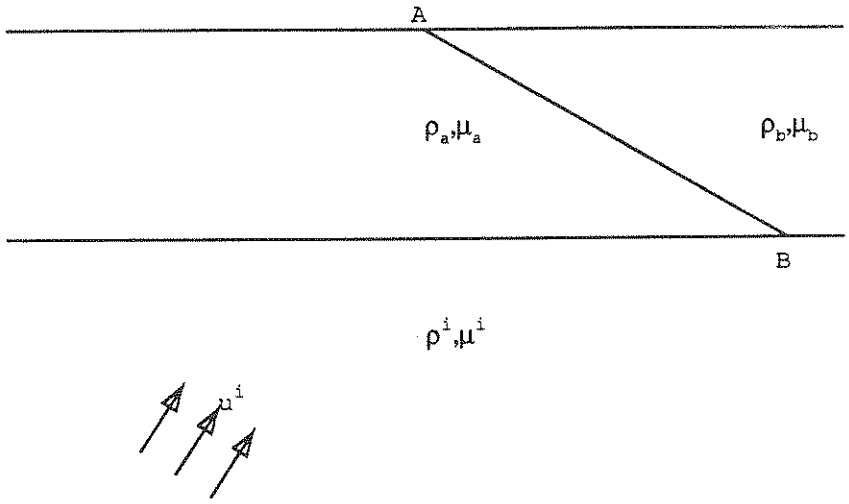

FIGURE 4-1 Statement of problem for joined layers

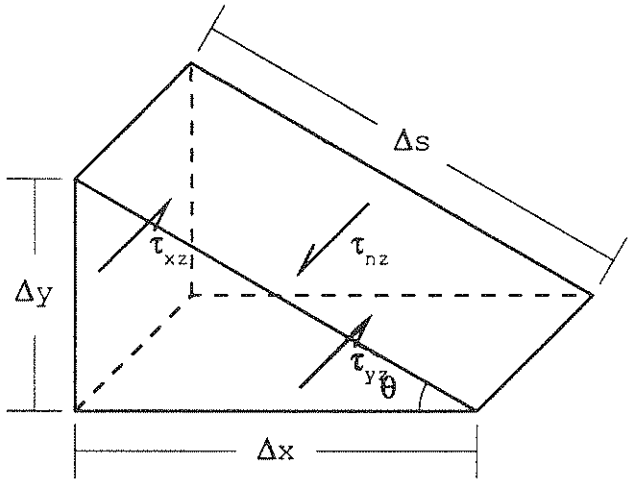

FIGURE 4-2 Material element showing antiplane stresses

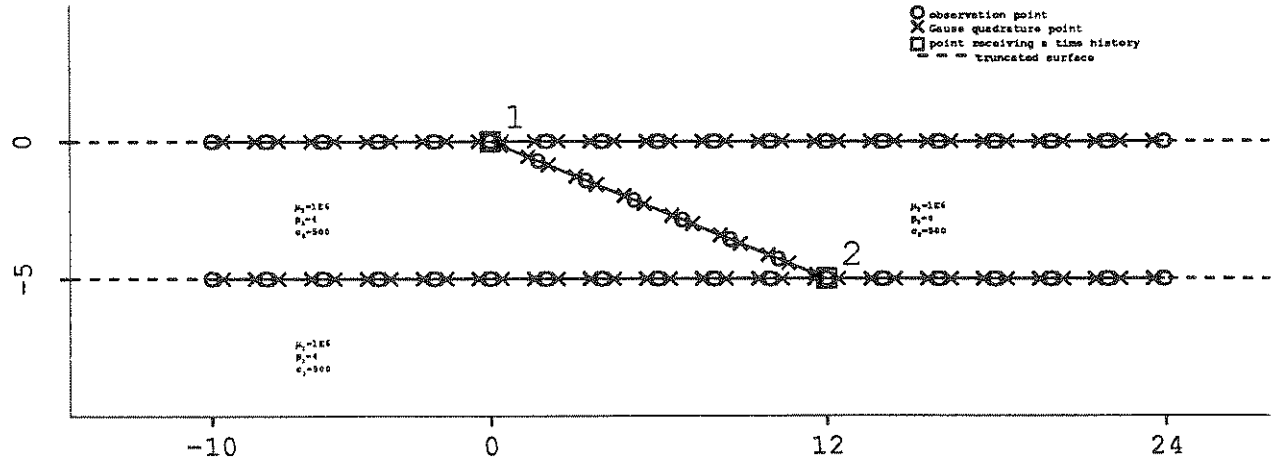

FIGURE 4-3 A homogeneous half space solved as a wedged profile

There is also a difficulty in choosing the unknown for the stress term in equation (1). The stress term, τ is supposed to be the shear stress on the outward surface. If there is only one line at a given point, the stress on the surface is the obvious choice for use in the equations. However, the points where two or more lines meet can have several different outward normals. The choice of stresses with which to express the equation must be consistent with theory and amenable to use.

Fortunately, this is a very minor problem. Figure 4-2 shows a stress block with two surfaces parallel to the coordinate axes and one parallel to a surface in the profile of figure 4-1. Basic considerations as reproduced in appendix C show that

$$\tau_{nz} = \tau_{xz}\cos\theta + \tau_{yz}\sin\theta \qquad (4.2)$$

For this reason all the normal stresses on all the surfaces meeting at a point can be expressed in terms of two independent stresses. One need know only the orientations of the surfaces.

At the point of intersection of surfaces there are three independent unknown variables, displacement, $\bar{w}$ and the two stresses, τ_{xz} and τ_{yz}. If there are three media meeting at the same point, then the balance between number of unknowns and number of equations is preserved.

The present discussion can also be applied to points at a free surface such as point A in figure 4-1. Again, for this angle α=0.8333 *or* 0.6667 and 1–α = 0.1667 *or* 0.3333. Because two of the surfaces are free surfaces, the shear stresses are zero. On the third surface (AB) there is no need to apportion the stress trigonometrically.

In like manner, sharp corners in a free surface can be handled by adjusting the singularity.

4.2 Numerical representation of the joints

From the discussion in the previous section, it should be clear that the implementation of these joints of several surfaces is a small extension to the numerical problem. Primarily, the task is that of establishing the proper bookkeeping procedures to keep straight the coefficients of the two stresses and to check the endpoints of each surface to determine whether the term for the singularity $(1-\alpha)$ should be modified. Apart from this all the integrations remain the same because along any surface there is no ambiguity as to which stress to use or about the value of the singularity.

4.3 Examples

This section contains a small set of examples showing the reasonableness of this extension and some of the new geometries which are now susceptible to solution.

4.3.1 Examples of problems possessing analytical solutions

Figure 4-3 shows a homogeneous elastic half space divided as if it were composed of several layers. Because it is homogeneous, it possesses an analytical solution. Figures 4-4 to 4-6 show the admittance for the three surfaces of figure 4-3 subjected to vertical, 45°, and horizontal incident wave fields. As can be seen, there is close agreement between the analytical solution and the numerical solution.

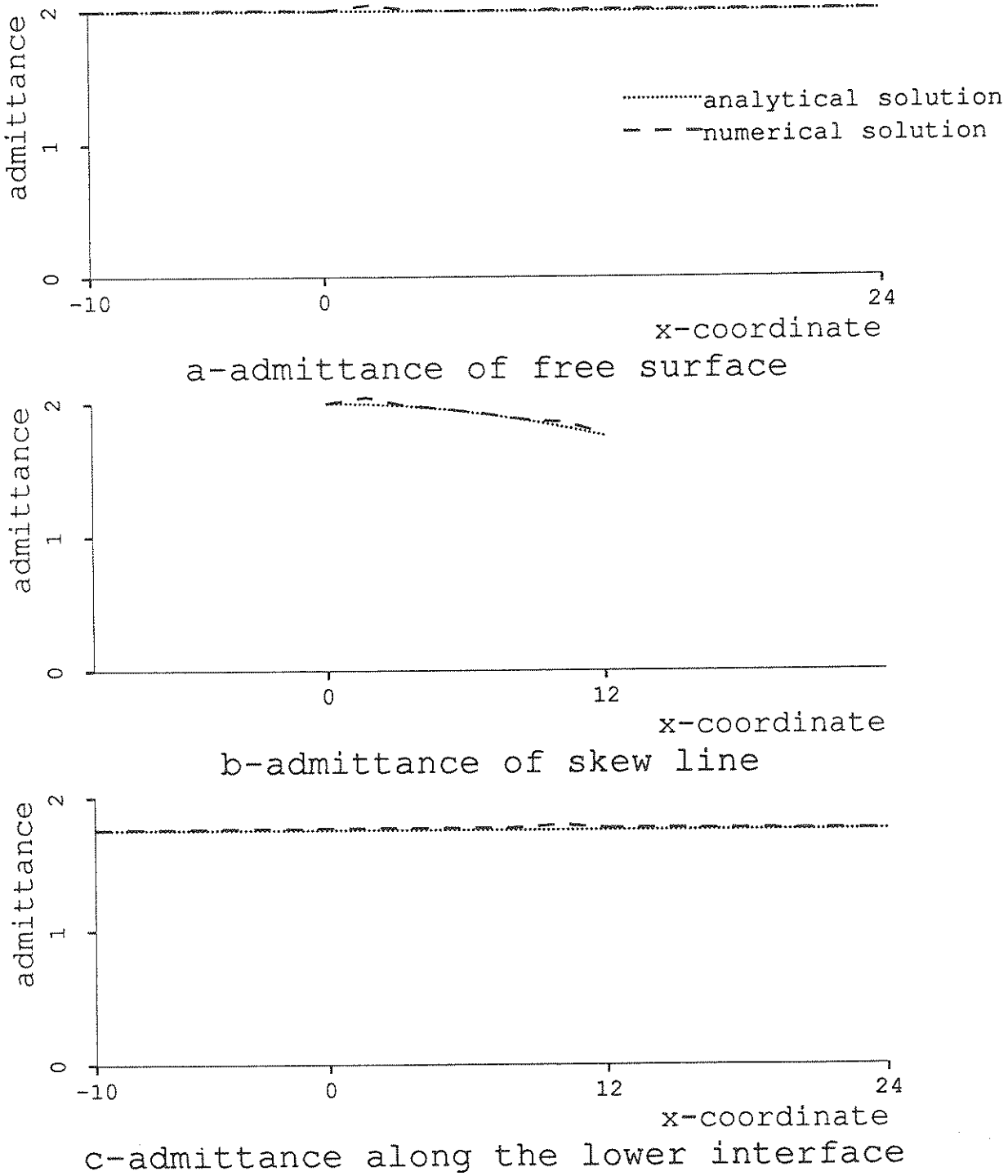

FIGURE 4-4 Admittance of homogeneous halfspace for ω=50 rad/s—vertical incidence

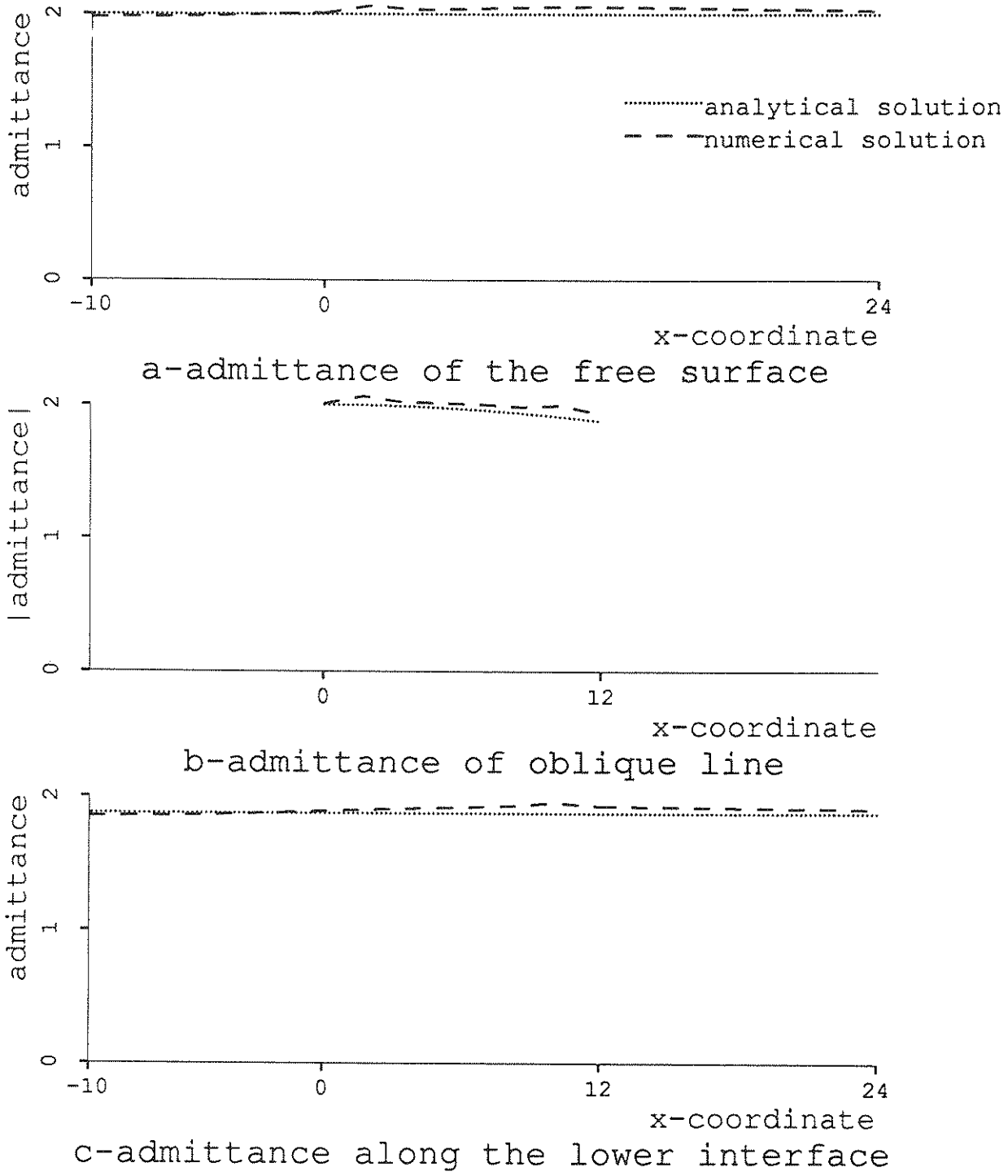

FIGURE 4-5 Admittance of homogeneous halfspace for ω=50 rad/s—45° incidence

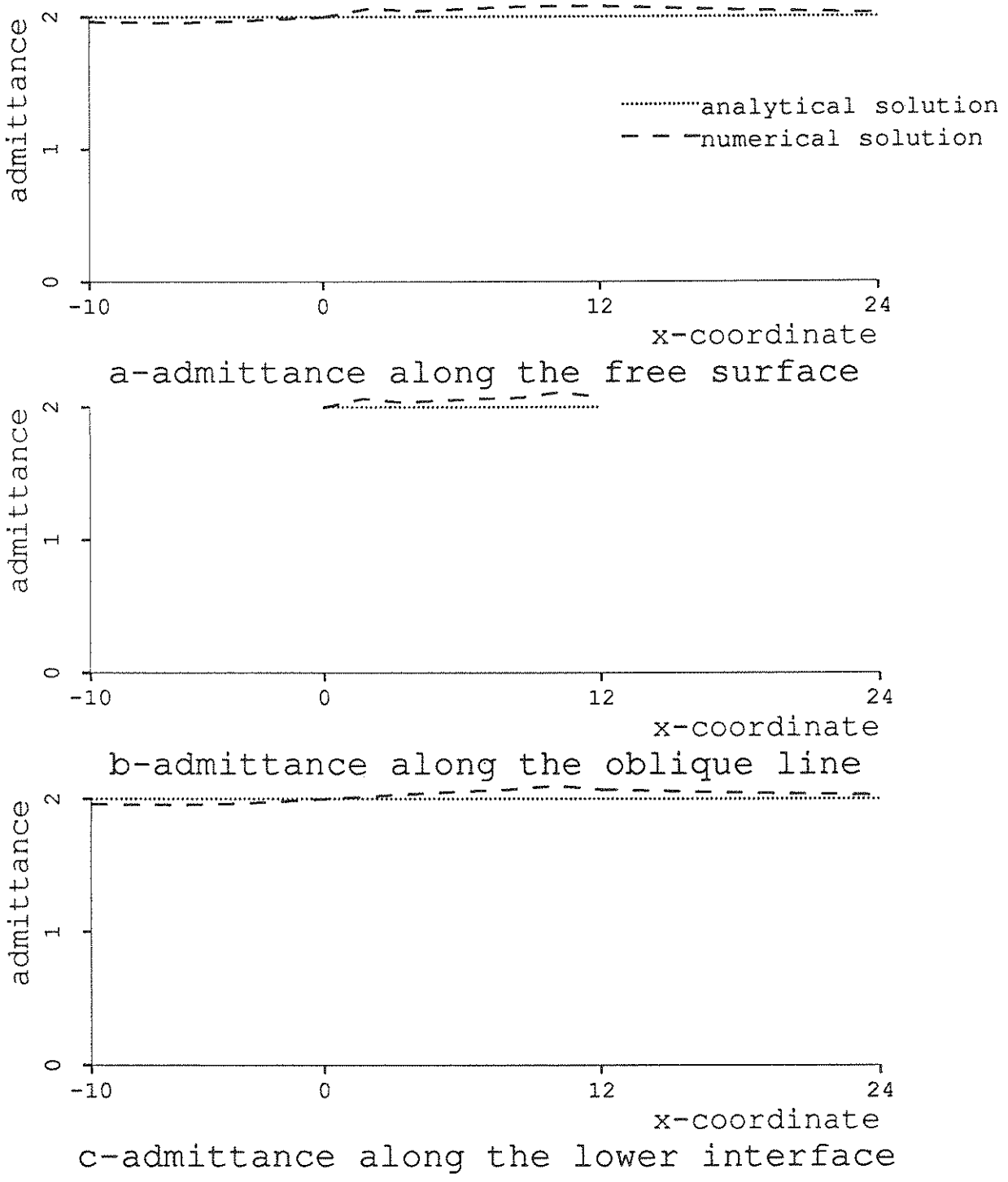

FIGURE 4-6 Admittance of homogeneous halfspace for ω=50 rad/s—horizontal incidence

4.3.2 Examples of problems not possessing analytical solutions

Figure 4-7 shows the same geometry as figure 4-3 but with the upper right layer composed of a softer material than the rest of the profile. Figures 4-8 to 4-10 show the admittances of this profile at ω=50 rad/sec for various angles of incidence.

4.3.3 Time histories

Figure 4-11 shows a profile of a semicylinder of soft material in a stiffer half space. Figure 4-12 gives the response in time of the five points marked to the Gaussian pulse. The columns are for horizontal, 45°, and vertical angles of incidence. The soft inclusion modifies the behaviour over what one would expect from a homogeneous half space. For the horizontal incidence shown in the left column, points to the left of the kettle (plots d,g,m) experience a response similar to that which they would undergo in a homogeneous half space though they do see some waves reflected or otherwise modified by the kettle. For the point on the surface in the middle of the soft soil (plots j,k,l), there is a significant amplification effect as one would expect. The fact that there is little variation with respect to angle of incidence is probably due to the fact that the kettle is cylindrical in shape.

The point on the far side from the point of incidence (plots a,b) shows how the original clean signal loses some of its coherence on passing through the softer medium. Of course, this effect is even more pronounced where the reflection arrives later than the incident wave (plots g,h,i and m,n,o). The existence of inhomogeneities can affect the behavior of other points in the profile. Figure 4-13 is the profile of a soft wedge of soil overlying a stiffer half space. The responses of the four numbered points to the Gaussian pulse of figure 2-10 are shown in figure 4-14 for horizontal, 45°, and vertical incident waves. Again, there is

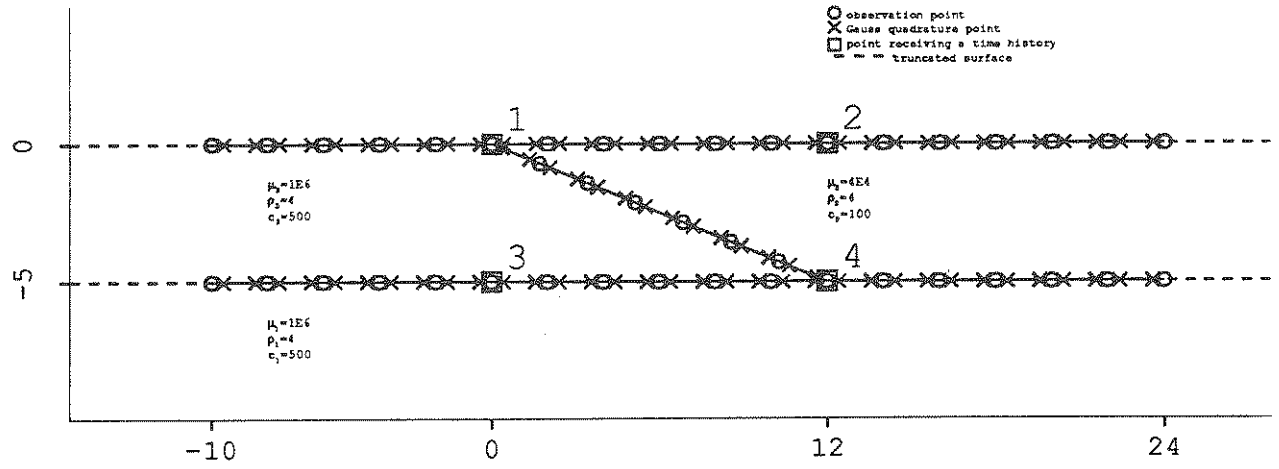

FIGURE 4-7 Halfspace overlain by a wedge of softer material

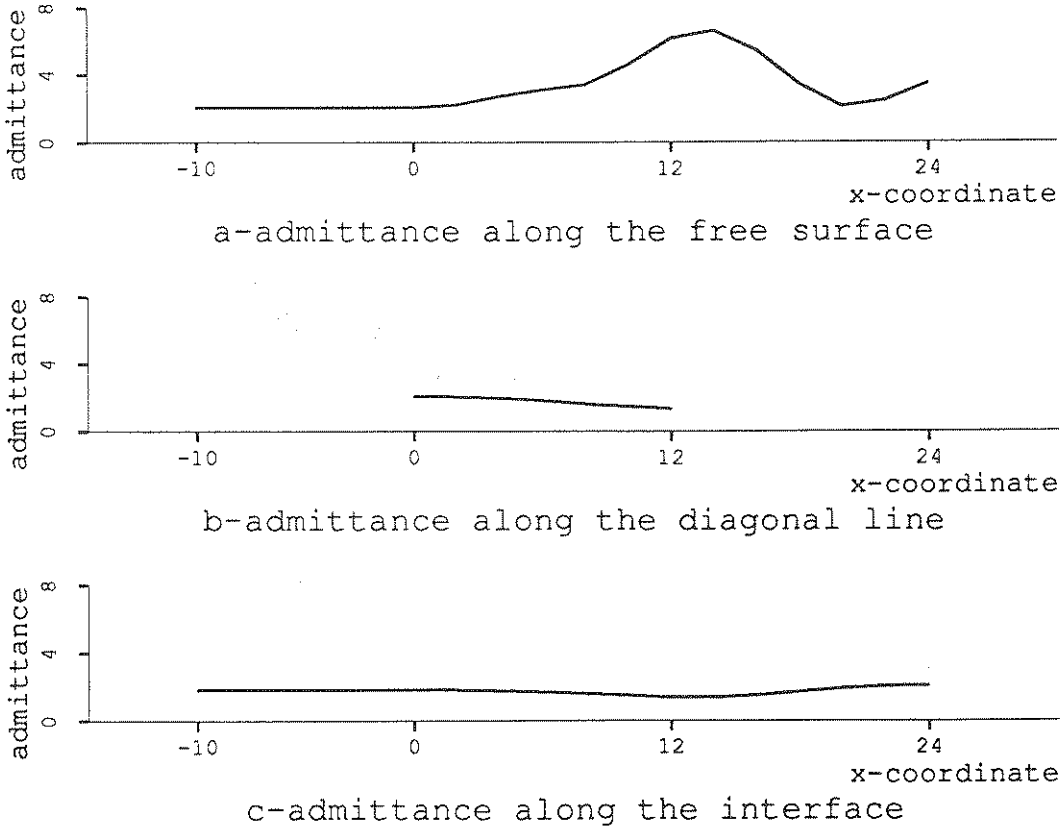

FIGURE 4-8 Nonhomogeneous half space with vertical incident wave at ω=50 rad/s

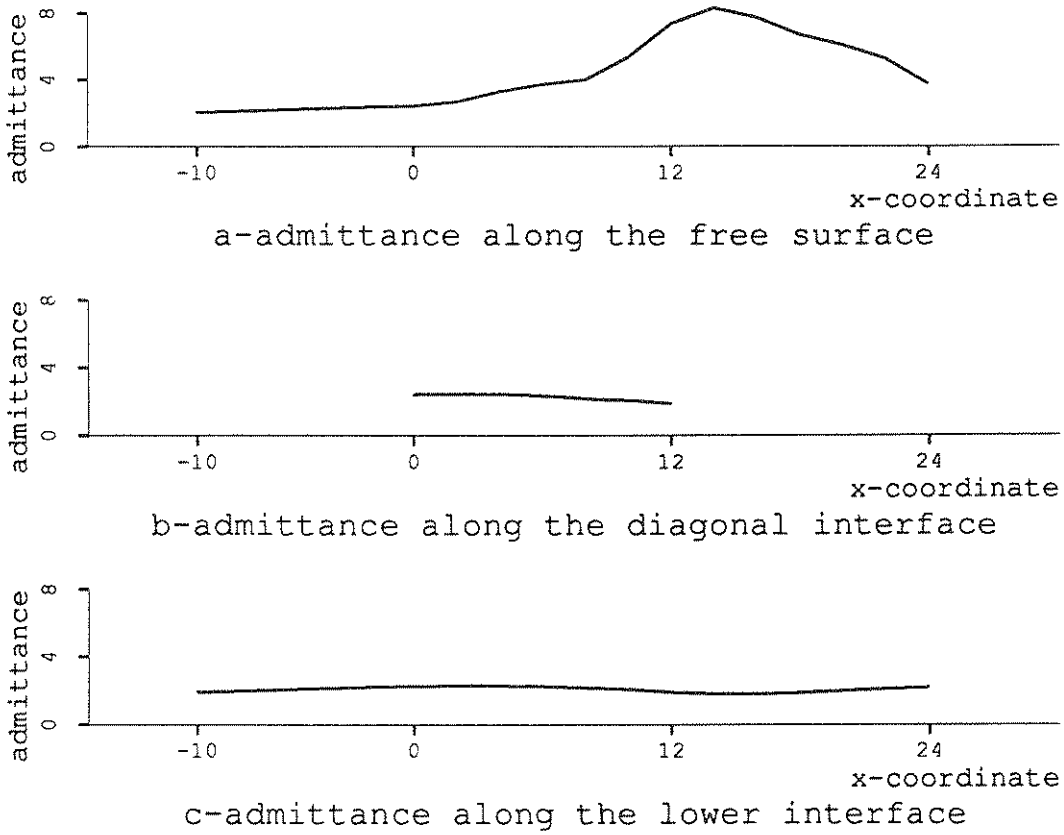

FIGURE 4-9 Nonhomogeneous half space with 45° incident wave at 50 rad/s

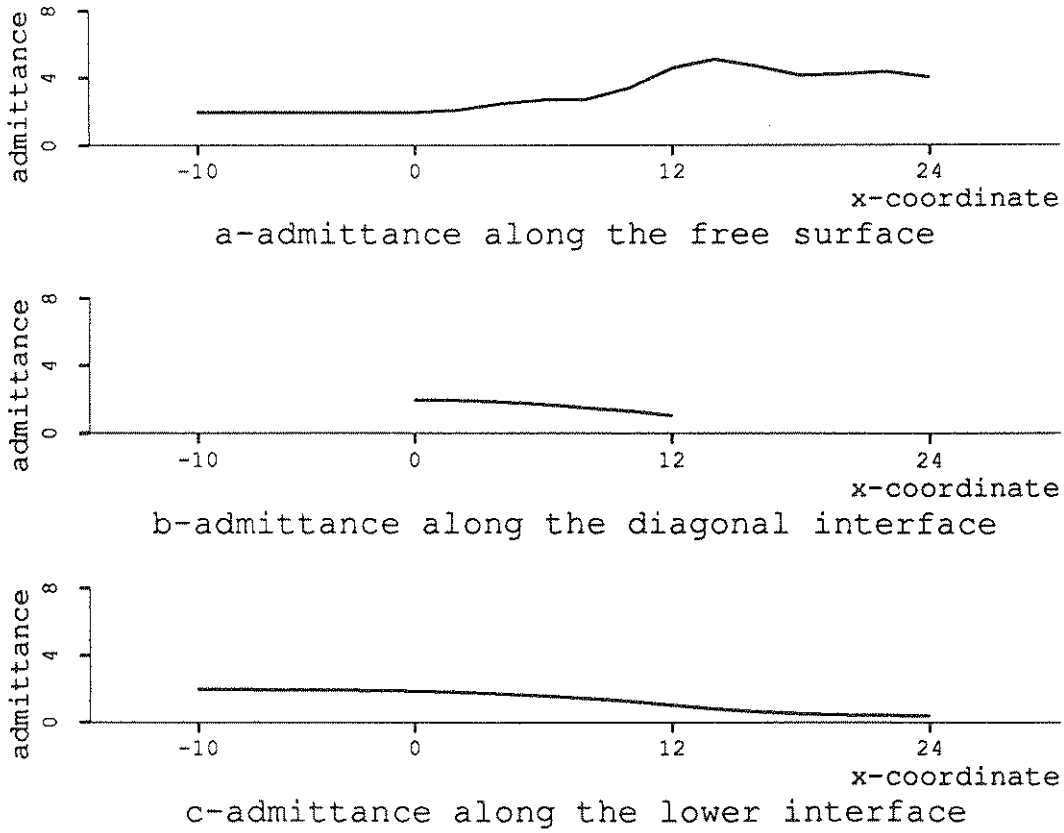

FIGURE 4-10 Nonhomogeneous half space with horizontal incident wave at ω=50 rad/s

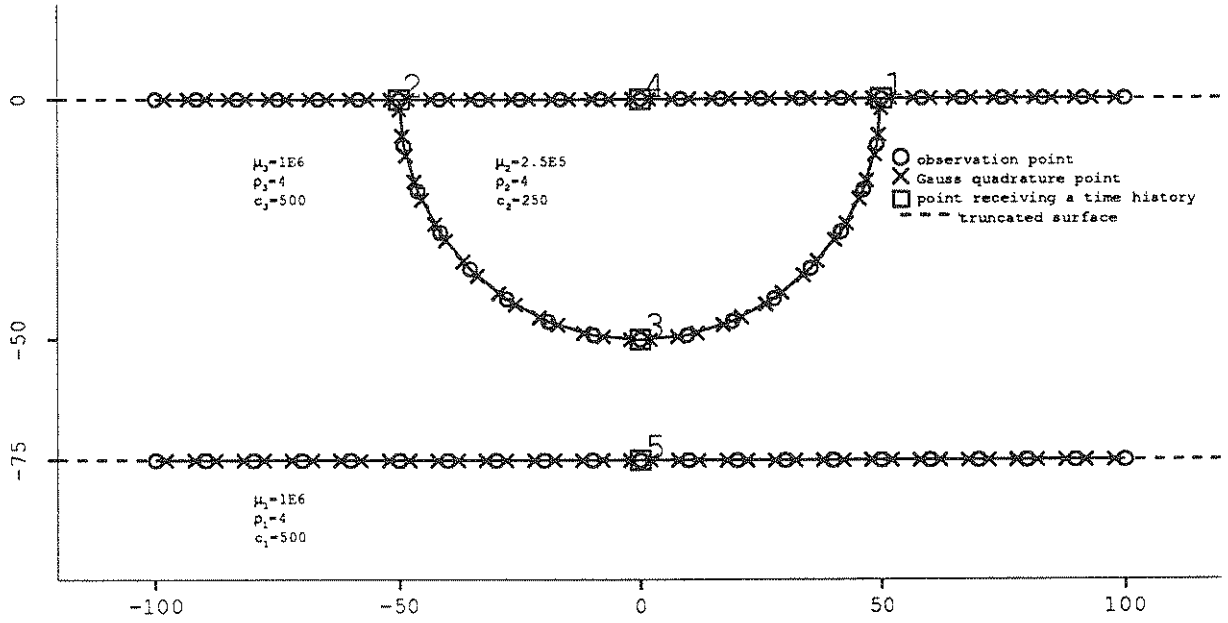

FIGURE 4-11 Geometry profile of a soft cylindrical valley in a firm half space

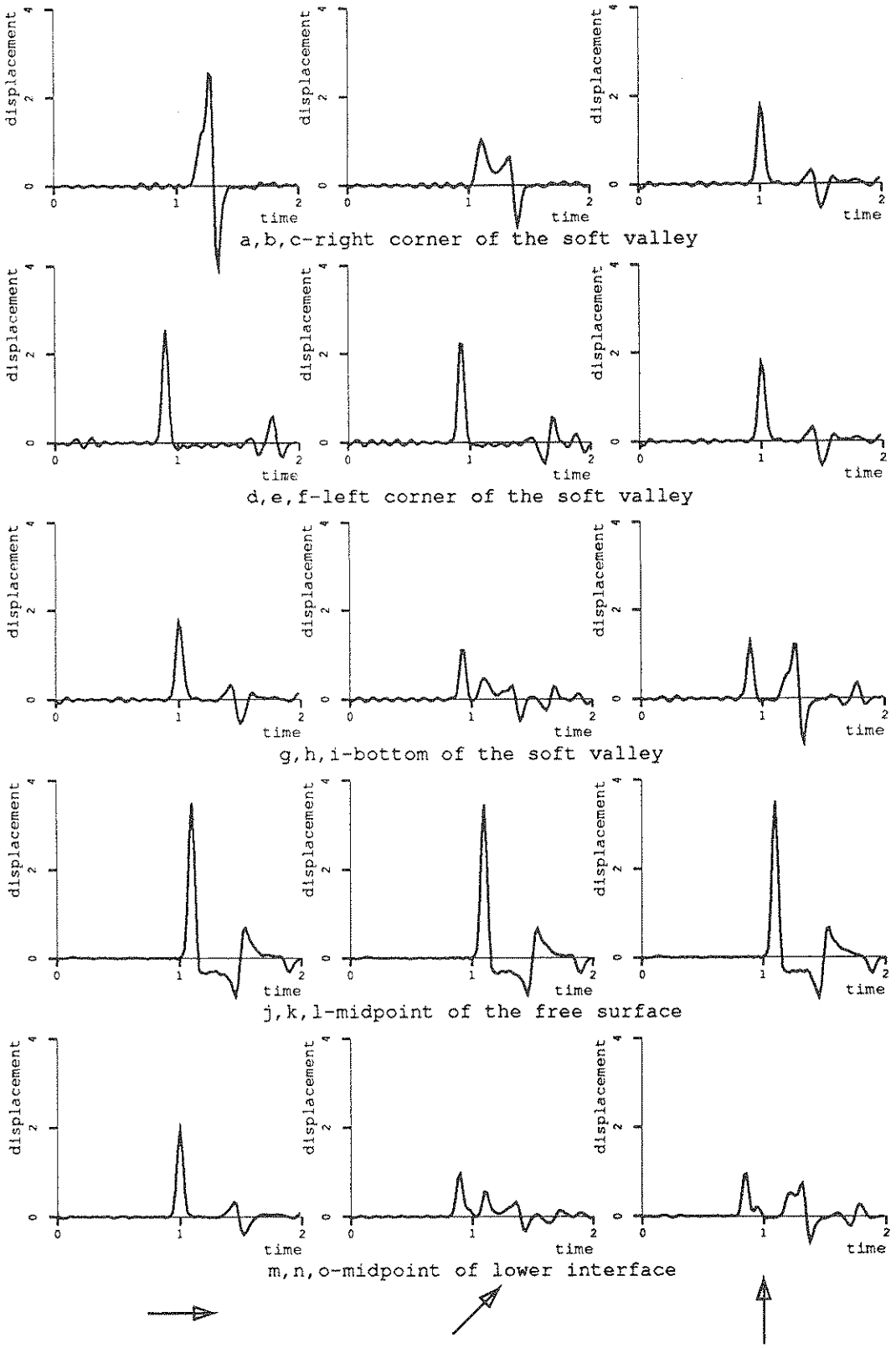

FIGURE 4-12 Time response of the soft valley profile

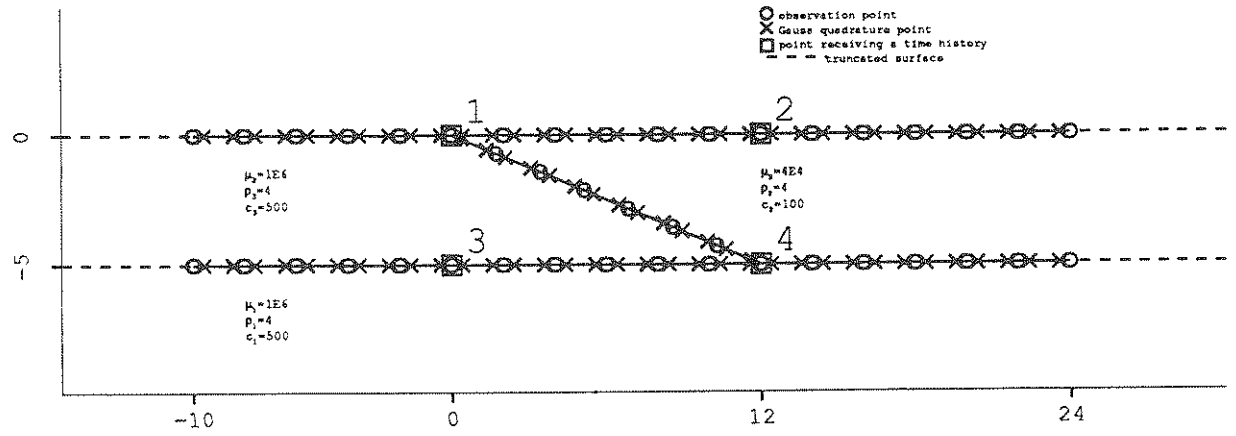

FIGURE 4-13 Soft wedge overlying a half space

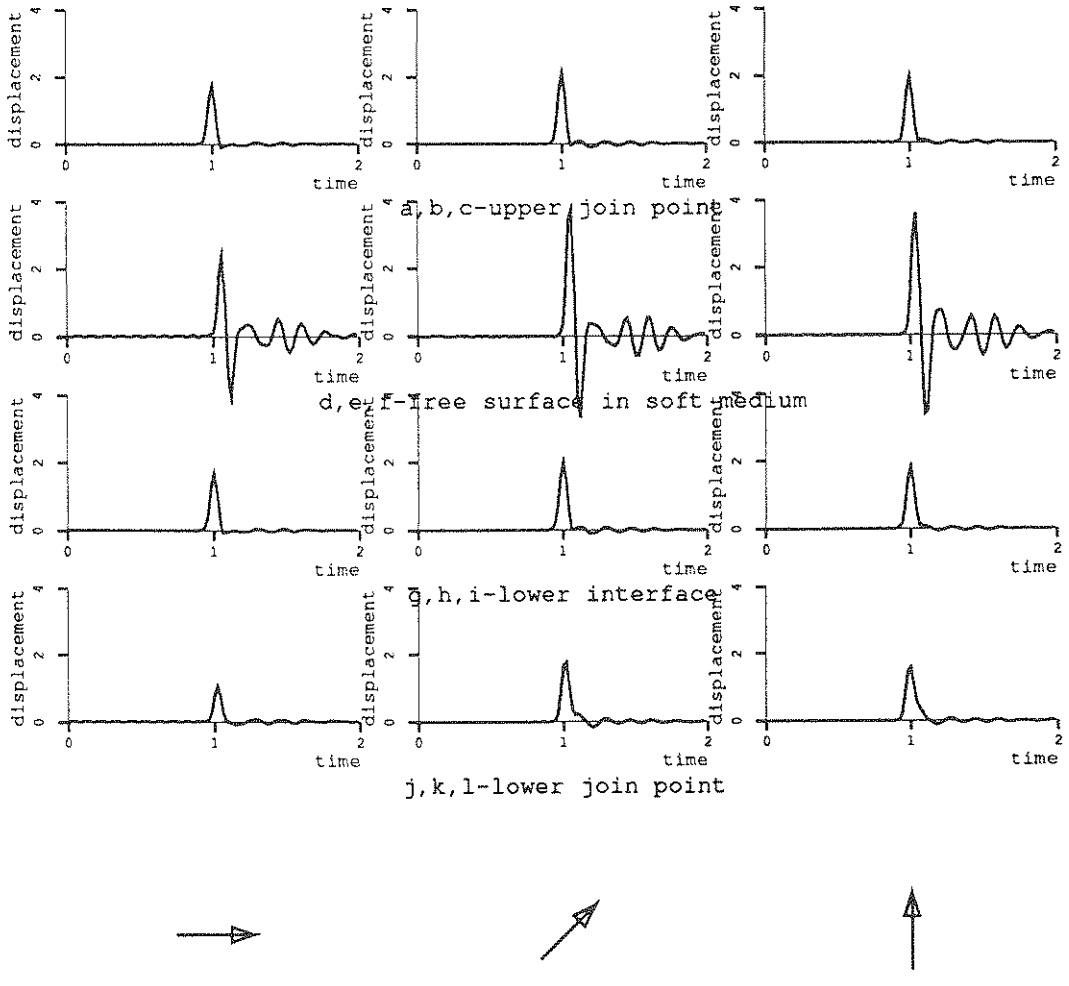

FIGURE 4-14 Response of soft wedge on a half space to Gaussian pulse

amplification in the soft material but very little deviation in the other points from what would be expected in a half space. This result is understandable since the points used are all on the incident (upwind) side of the soft layer.

4.4 Conclusions

In this section the techniques of the earlier sections were extended to handle cases where three media meet at one spot. The success of this extension means that the boundary element method is a promising tool for analyzing profiles with lenses, soft pockets, and valleys. As in the previous cases, the convolution back to the time domain is also shown to be possible. The combination of these approaches gives the method a wide range of applicability.

SECTION 5
SANTA FELICIA EARTH DAM

In this chapter the techniques previously described are applied to a real problem—the Santa Felicia earth dam in California subjected to the San Fernando earthquake of 1971. A recorded accelerogram is used as input and the output is compared to an accelerogram recorded at an observation point in the profile. Figure 5-1 shows a plan view and an idealized section of the Santa Felicia earth dam. This dam has been studied by Abdel-Ghaffar and Scott [7] and a nonlinear dynamic finite element analysis for in-plane displacements has been done by Lacy [8]. The material properties used in this project were taken from Lacy's work. The accelerogram and Fourier spectrum shown in figure 5-2 is the record taken at the outlet works during the San Fernando earthquake of 1971. The input record used was derived from this output record by these steps:

(1) the spectrum was divided by the admittance function at the downstream point labeled 5 in figure 5-1 to produce the supposed corresponding input at the reference point of the incident wave,

(2) this new spectrum was clipped of high spikes which are more an artifact of the profile than of the input earthquake,

(3) the corresponding time history was produced and truncated to eliminate the wrapping due to the offset from the reference point to the point.

This input (shown in figure 5-3) was then convoluted in the usual manner with the admittance functions of the top of the dam (point 1) and the downstream point (point 5). These results are presented in figures 5-4 and 5-5. Figure 5-6 shows the measured response of the crest of the earth dam during the San Fernando earthquake of 1971. This measured response

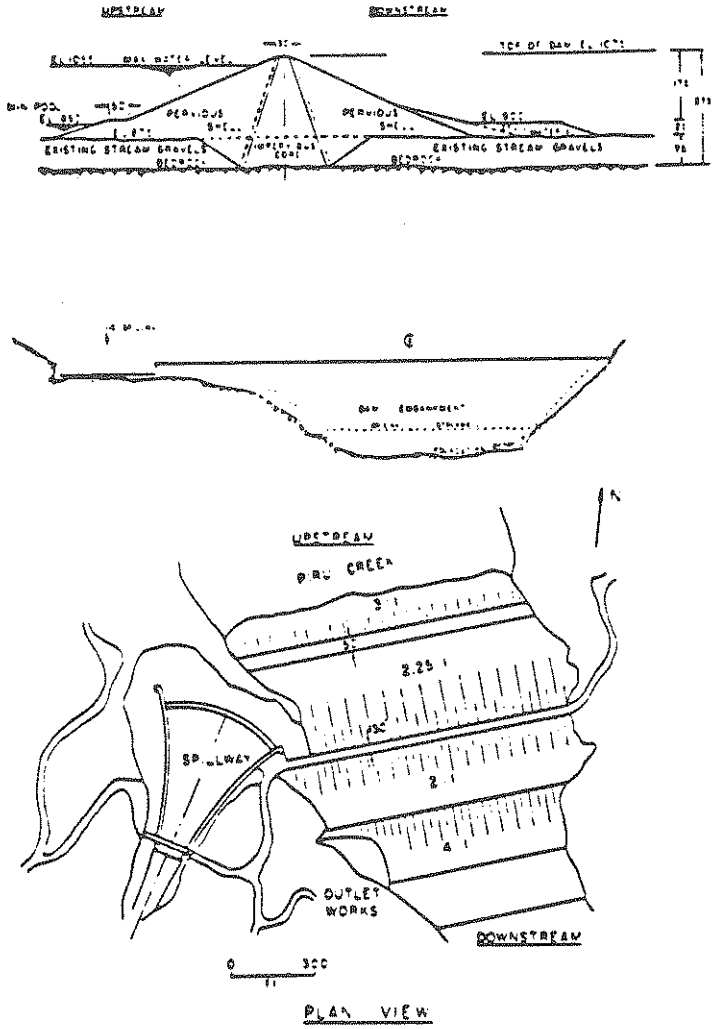

FIGURE 5-1 Geometry of the Santa Felicia earth dam

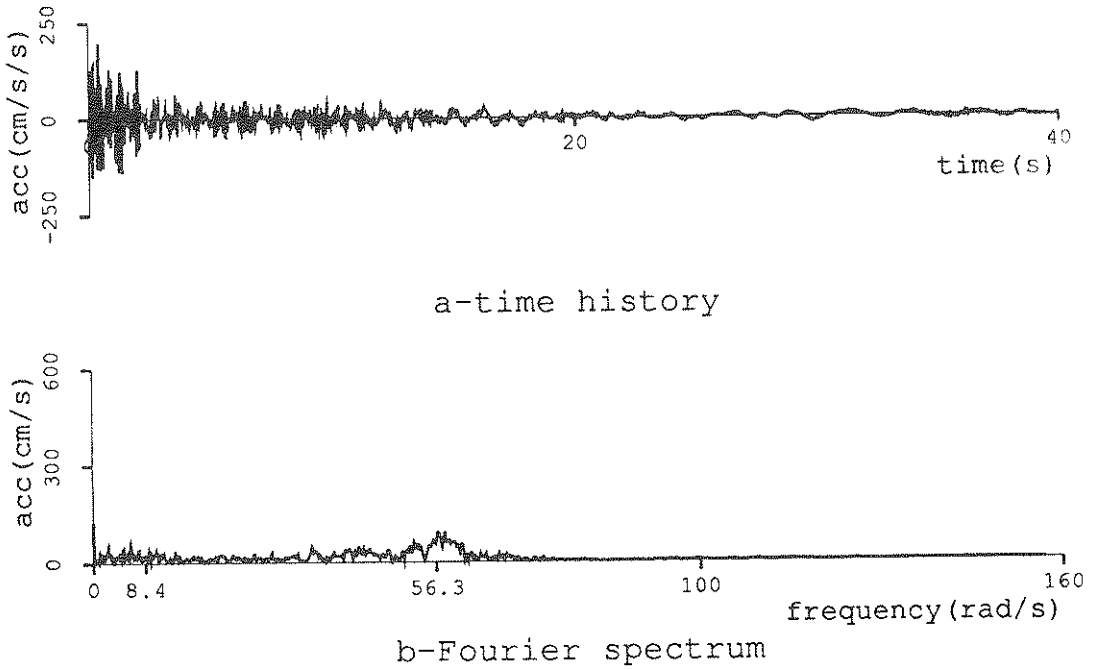

FIGURE 5-2 Accelerogram recorded at outlet of dam

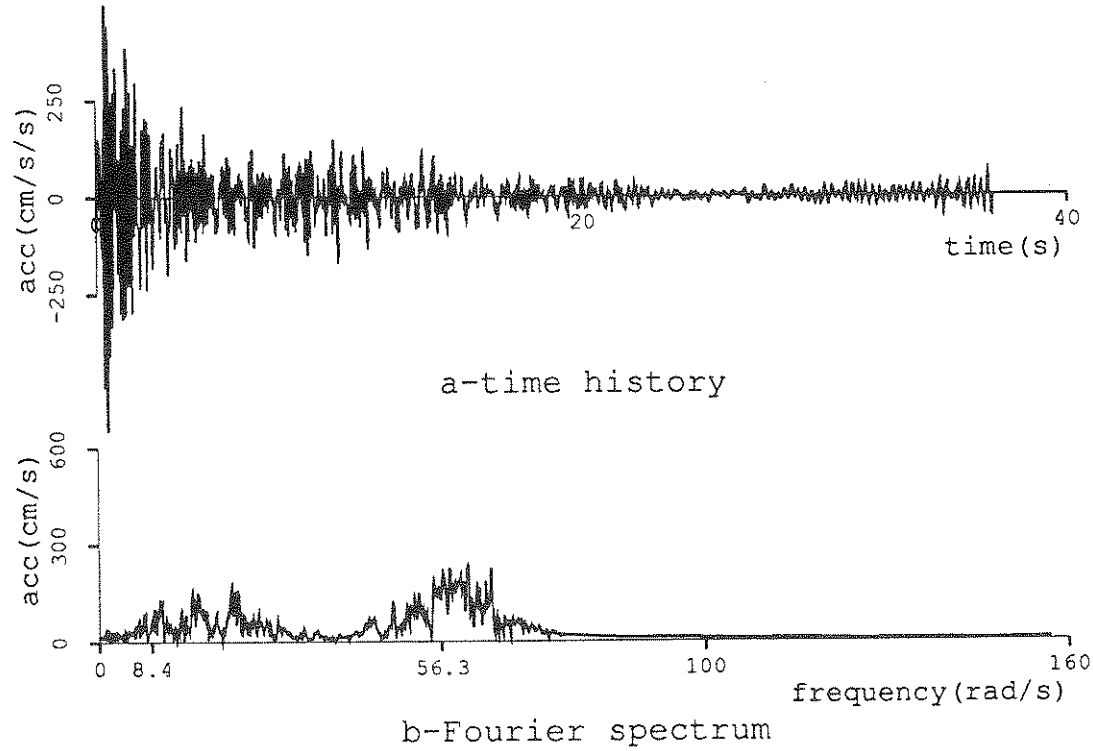

FIGURE 5-3 Input earthquake for the Santa Felicia dam

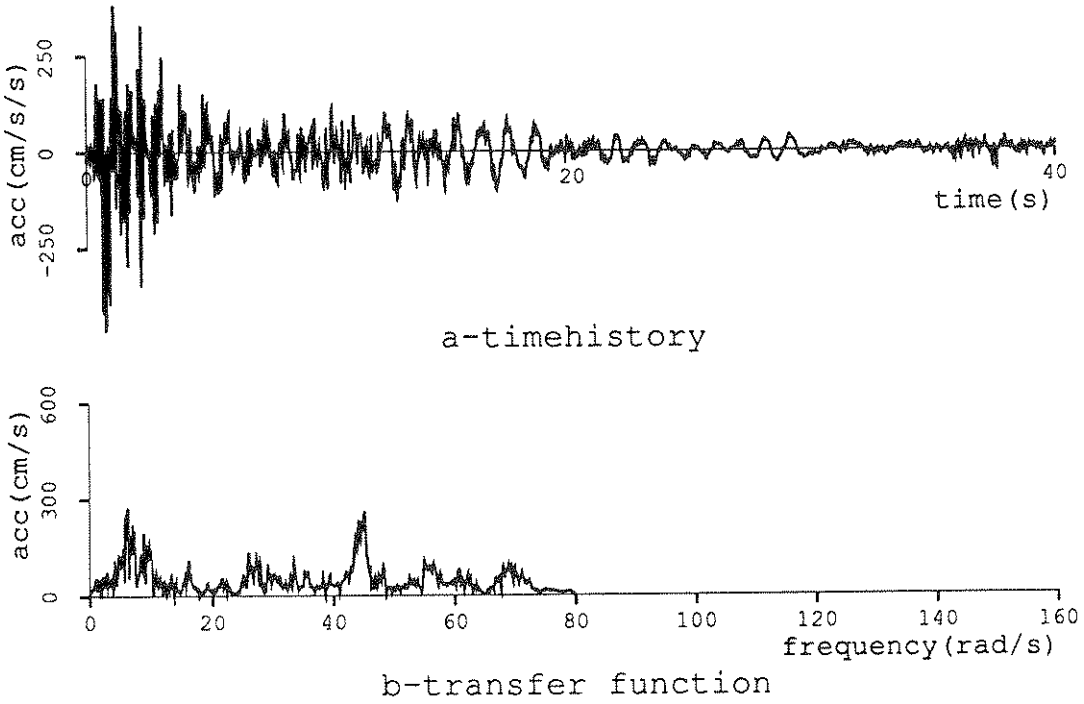

FIGURE 5-4 Computed response at the crest of the dam

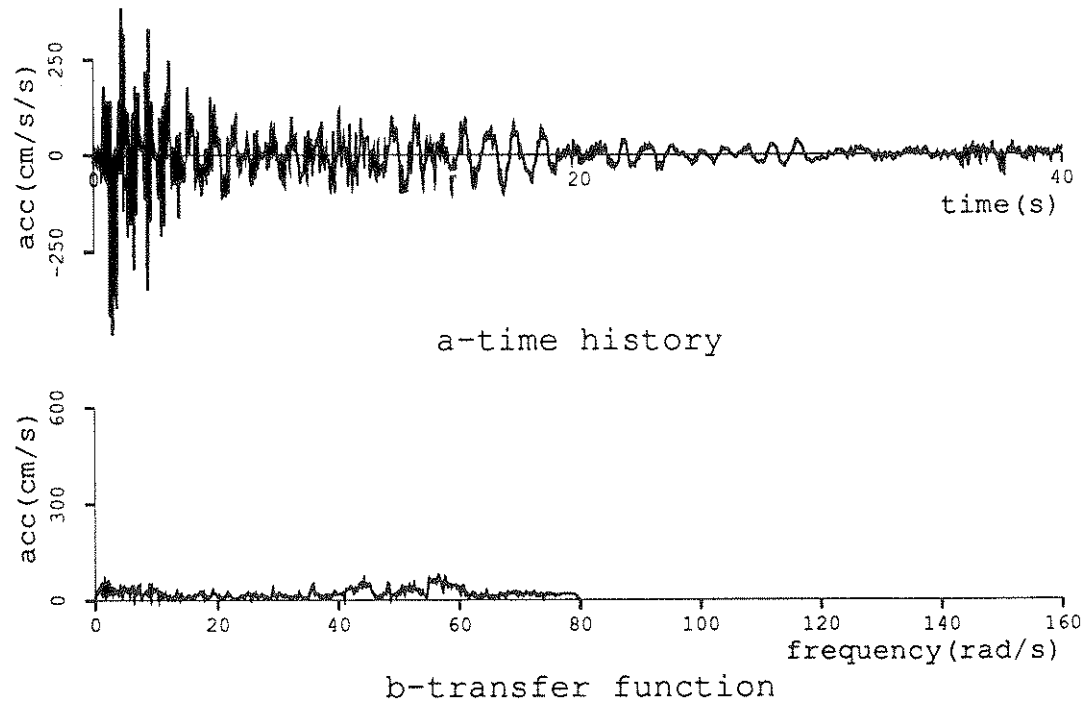

FIGURE 5-5 Computed response downstream

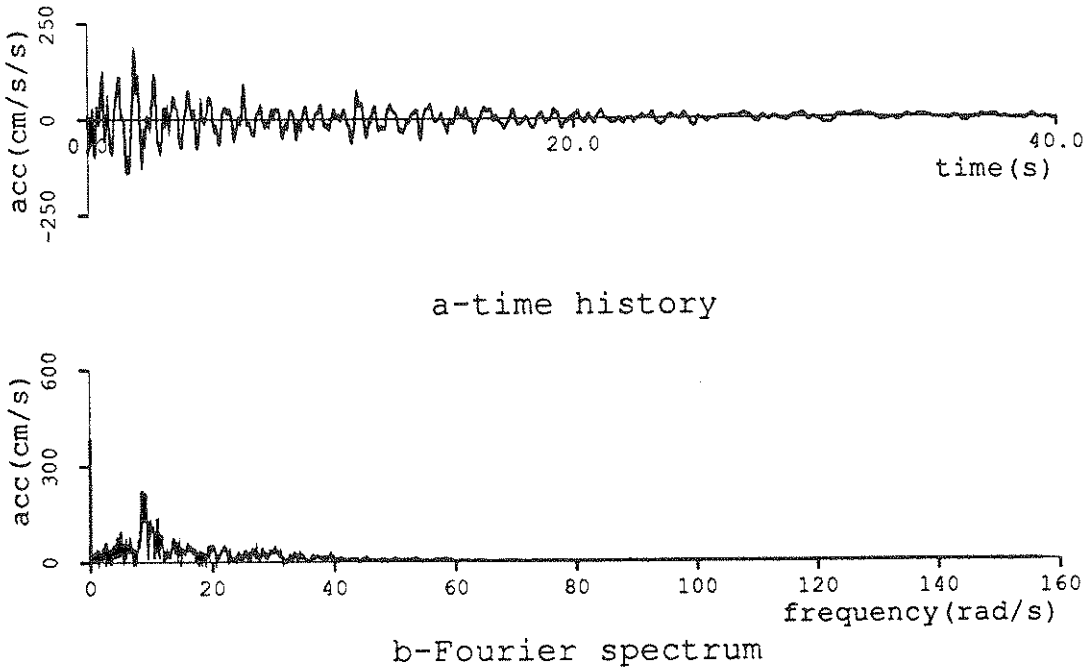

FIGURE 5-6 Accelerogram recorded at crest of dam

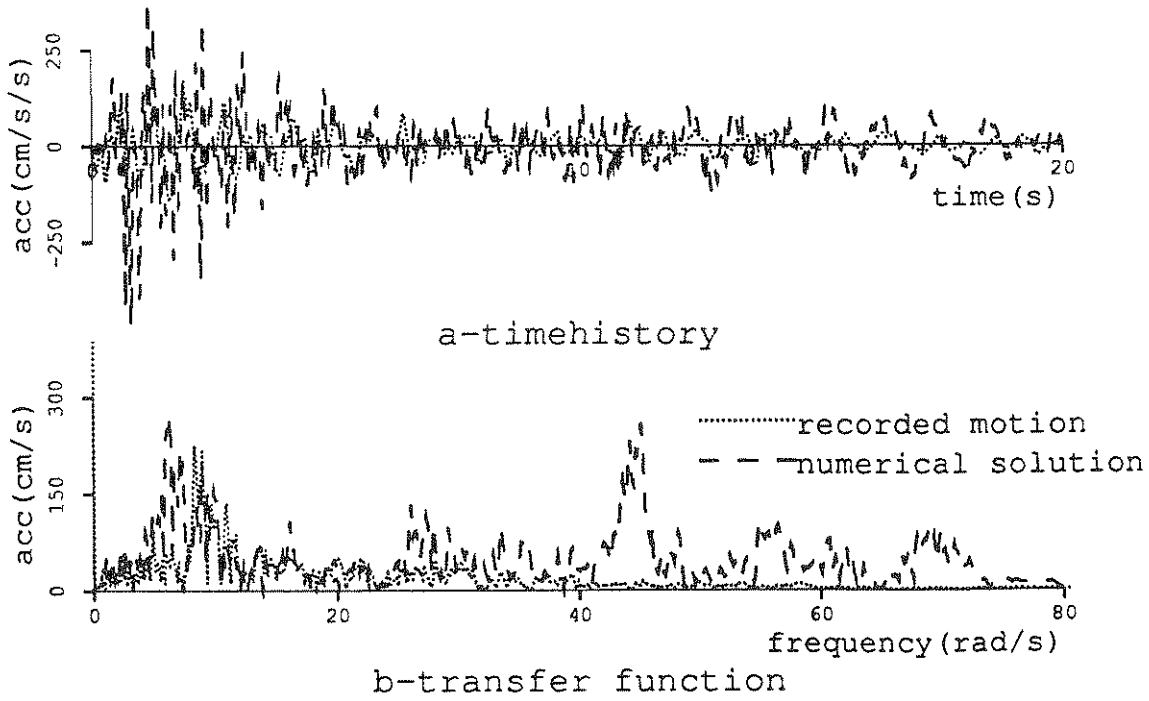

FIGURE 5-7 Comparison of measured and computed crest response

is compared to the computed response of figure 5-4 in figure 5-7. Examination of this figure shows that once again the numbers are of the right order but differ in the frequencies where resonance occurs and have large spikes at the higher frequencies. This is probably also explainable by the simplification in the geometry and the lack of damping.

In like manner, figure 5-8 compares the measured and computed responses at the down-stream point. The similarity of these responses is not surprising when one considers the derivation of the incident earthquake as described above. It does show that the record was not destroyed completely.

5.1 Conclusions

These results show that the boundary element method produces results which can compare well with the results observed for real earthquakes in real soil profiles. However, the model as currently constituted is elastic and the introduction of damping into it might improve the predictive power of this approach.

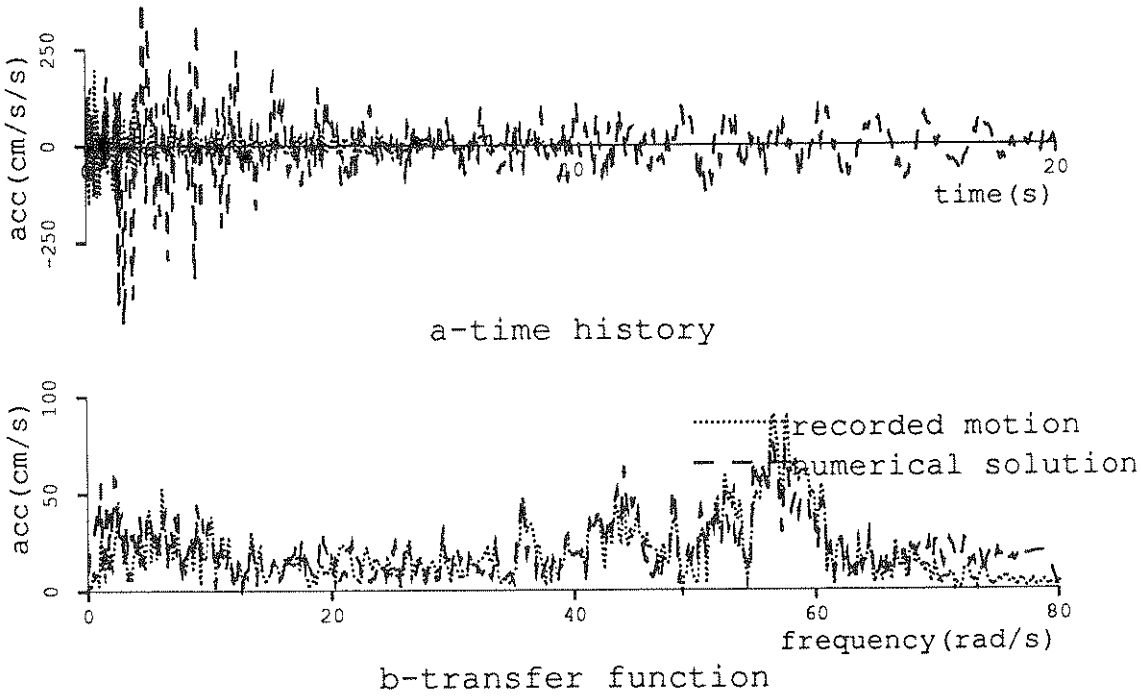

FIGURE 5-8 Comparison of computed and measured responses downstream

SECTION 6
CONCLUSIONS

The boundary element method is shown to be an appropriate tool for solving the elastic wave scattering problem for antiplane waves in a two-dimensional profile. Where there are analytical solutions, the results of the numerical method match them closely. For simple geometries which do not possess analytical solutions, the results seem reasonable. This implies the accuracy of the technique for the more complicated geometries.

Because the boundary element method can be used to construct an admittance function over a large range of frequencies, it can be used to solve for the response of most profiles to a transient input. This Fourier analysis makes it a promising approach for research and analysis.

6.1 Suggestions for future work

There are several directions which this research can take from this point:

(1) Extension to SV and P waves can be done with similar techniques as Altay [5] has shown for the homogeneous case.

(2) Similar methods could also be applied to the three-dimensional problem. Practical applications for transient loading might be limited by the extravagant use of computer time which the solving of the several matrices would entail. Accordingly,

(3) A more efficient method of solving the matrices would make the entire process economically more feasible. There have been some promising results with a modified Gauss-Seidel method of estimating the solution at the current frequency using the solu-

tion of the previous frequency as a starting point. Unfortunately, this approach seems to be unstable for more complicated geometries.

(4) Quasi-hysteretic damping (viscous within a single frequency) should be attainable as a simple extension to the current methods.

(5) By making a surface rigid and movable, the dynamics of machine foundations should be findable with these techniques.

SECTION 7
REFERENCES

(1) Sanchez-Sesma, F.J., I. Herrera, and J. Aviles, "A boundary method for elastic wave diffraction: Application to scattering of SH waves by surface irregularities," **72** Bull. Seism. Soc., 1982, p.473 (1982)

(2) Altay, S., A. Askar, P. Hadley, and A.S. Cakmak, "Explicit integration of boundary integral equations in the frequency domain for wave scattering problems," *Recent Applications in Computational Mechanics*, New Orleans (1986)

(3) Banaugh, R.P. and W. Goldsmith, "Diffraction of steady elastic waves by surfaces of arbitrary shape," *J Appl Mech*, **30**, p589-597 (1963)

(4) Beskos, D.E. and D.C. Karabalis, "Dynamic response of three-dimensional foundations, Final Report part A," National Science Foundation Earthquake Hazards Mitigation Program, University of Minnesota

(5) Altay, S., *Explicit Integration of Boundary Integral Equations in the Frequency Domain for Wave Scattering Problems*, a doctoral dissertation in the Department of Civil Engineering at Princeton University, Princeton (1986)

(6) Eringen, A.C. and E.S. Suhubi, *Elastodynamics II: Linear Theory*, Academic Press, New York, New York (1975)

(7) Abdel-Ghaffar, A.M. and R.F. Scott, "Vibration tests of a full-scale earth dam," *Journal of the Geotechnical Division*, ASCE,**107**, p241 March, 1981

(8) Lacy, S.J., *Numerical Procedures for Nonlinear Transient Analysis of Two-phase Soil Systems*, a doctoral dissertation in the Department of Civil Engineering at Princeton University, Princeton (1986)

(9) Newton, I., *Principia Mathematica*

(10) Pao, Y.H. and C.C. Mow, *Diffraction of Elastic Waves and Dynamic Stress Concentrations*, Crane-Russak, New York (1971)

(11) Hildebrand, F.B., *Advanced Calculus for Applications*, Prentice-Hall, Inc., Englewood Cliffs, New Jersey (1976)

(12) Graff, K.F., *Wave Motions in Elastic Solids*, Ohio State University Press, Columbus, Ohio (1975)

(13) IMSL, *User's Manual, IMSL library*, Houston (1985)

APPENDIX A
DERIVATION OF FUNDAMENTAL RELATIONSHIPS

The purpose of this appendix is to give the derivation of the basic mathematics used in the current work. Starting from Newton's second law, the equation of motion is transformed into the integral equation of the steady-state wave propagation problem. The solution to this equation gives the admittance function for an incident harmonic wave. These solutions can, therefore, be convoluted with the forward Fourier transform of an incident wave back into the time domain to render the time response of any point within the profile to the given incident field.

The derivation in this appendix is limited to the case of a two-dimensional homogeneous profile with arbitrary surface. The extension to a heterogeneous profile is made in appendix C.

A.1 Statement of the problem

Figure A-1 shows a generalized two-dimensional profile subjected to incident SH waves, u^i. As these waves strike the surfaces shown (the tunnels, the hill, or the flat ground surface), they are reflected. The combined effect of these reflections from all of the surfaces is the scattered field, u^s. The total response,u^t, of any point x to the incident field is the sum of the incident and scattered fields.

$$u^t=u^i+u^s \tag{A.1}$$

The derivation in this appendix assumes that the profile is homogeneous, linear, elastic, and isotropic. A further limitation is antiplane strain—that there is no variation in the z– or x_3–direction ($\frac{\partial}{\partial z}=\frac{\partial}{\partial x_3}=0$) and that the wave motion is entirely in that direction ($u_1=u_2=0$).

The incident wave may be transient or harmonic.

The problem solved in this dissertation is the computation of the total wave field, u^t, as a result of an incident SH wave, $u^i(x,t)$, for a two-dimensional profile.

A.2 Equation of motion

In his *Principia* [9], Professor Newton states that an object in motion tends to maintain its velocity unless it is acted upon by unbalanced forces. This can be rendered into simpler form as

$$F = ma \tag{A.2}$$

Applying this to the element of material in figure A-2, yields the stress equation of motion

$$\tau_{ij,j}+\rho f_j=\ddot{u}_j \tag{A.3}$$

where: τ = stress,

ρ = mass density,

f = the body force,

u = displacement, and

subscripts are to be interpreted according indicial notation.

For a linear, elastic, isotropic, homogeneous material the constitutive equation can be represented as

$$\tau_{ij}=c_{ijkl}\varepsilon_{kl}=\lambda\varepsilon_{kk}\delta_{ij}+2\mu\varepsilon_{ij} \tag{A.4}$$

where: c = the elasticity tensor,

ε = strain, and

λ,μ = the Lame constants.

Substituting this relation into equation (A.3) yields the displacement equation of motion

$$(\lambda+\mu)u_{i,ij}+\mu u_{j,ii}+\rho f_j=\rho\ddot{u}_j \tag{A.5}$$

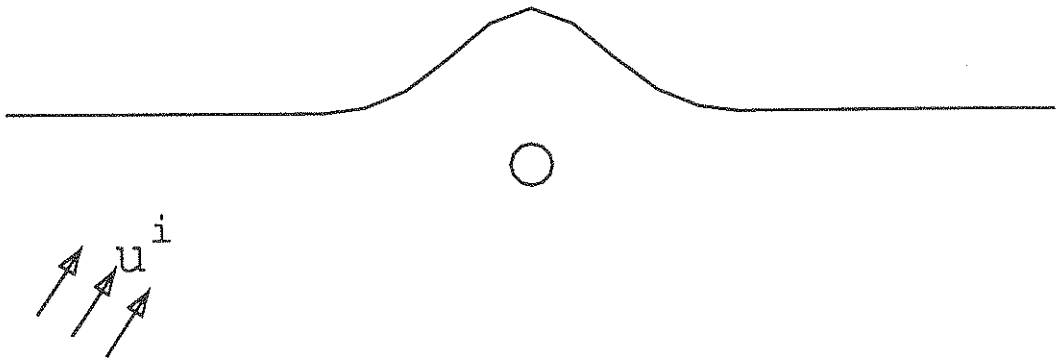

FIGURE A-1 Depiction of the problem

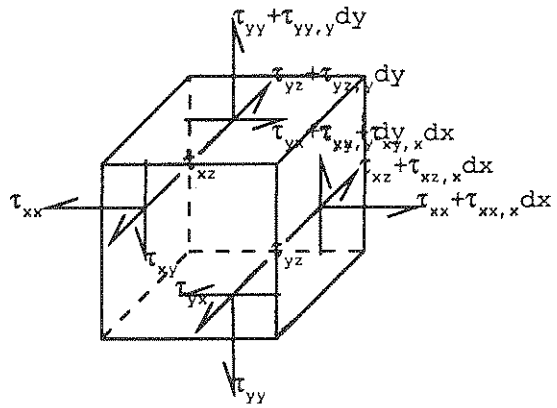

FIGURE A-2 Stress element in a material

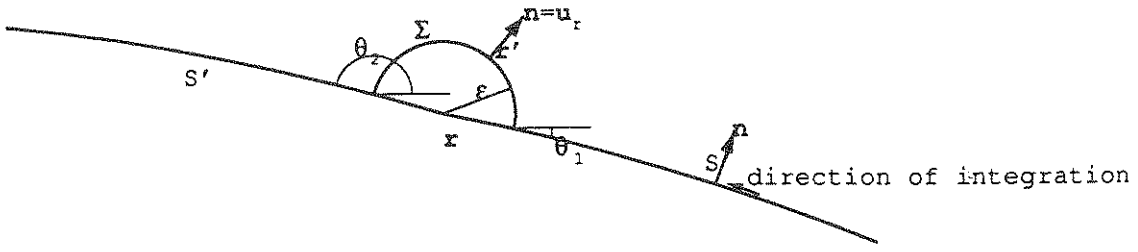

FIGURE A-3 Evaluation of the singularities

For large-scale problems of soil dynamics, the body force is negligible ($f_j = 0$). This simplification leaves us with the equation for wave propagation in a three-dimensional, homogeneous, linear, elastic, isotropic medium:

$$(\lambda+\mu)u_{i,ij}+\mu u_{j,ii}=\rho\ddot{u}_j \tag{A.6}$$

Furthermore, the current study is limited to the case of antiplane (SH) waves. Therefore, $u_1=u_2=0$ and $\frac{\partial}{\partial x_3}=0$. Thus,

$$\mu(u_{3,11}+u_{3,22})=\rho\ddot{u}_3 \tag{A.7}$$

or

$$\mu(w_{,11}+w_{,22})=\mu\nabla^2 w=\rho\ddot{w} \tag{A.8}$$

where: $w = u_3$=displacement in the $z-$ or x_3- direction

This is the differential equation governing the propagation of SH waves through a two-dimensional elastic medium. The excitation can be transient or harmonic.

A.3 Forward Fourier transform

In order to simplify equation (A.8) further, a forward Fourier transform is applied. This operation removes the time dependence of the equation and gives an equation which can be solved at single frequencies of harmonic excitation. The Fourier transform is defined as

$$\bar{w}(\mathbf{x},\omega)=\int_0^\infty w(\mathbf{x},t)e^{i\omega t}dt \tag{A.9}$$

where: $\bar{w}(\mathbf{x},\omega)$ = the forward Fourier transform of w at $\mathbf{x}$ at frequency ω

$\mathbf{x}$ = position vector of the point of observation

Applying this definition to equation (A.8) yields the reduced wave equation

$$\mu\bar{w}_{,ii}=\nabla^2\bar{w}=-\rho\omega^2\bar{w} \tag{A.10}$$

or

$$\nabla^2\bar{w}+\xi^2\bar{w}=0 \tag{A.11}$$

where: $\xi^2=\frac{\omega^2}{c_2^2}=\frac{\rho\omega^2}{\mu}$

$\xi=\frac{\omega}{c_2}=\frac{2\pi}{\lambda}$ (where λ is the wavelength) is the wave number for a shear wave in the medium at the given frequency, ω.

Accordingly, we now have a differential equation dependent only on position, **x**, and the parameter, ω. This equation, when solved for $\bar{w}$, gives the forward transform of the time history of the displacement. Thus, to solve for the time history, it is now necessary to solve the reduced equation only in space.

A.4 Integral equation and Green's functions

In order to solve the reduced wave equation (A.11), it is recast into its integral form using the Green's function approach. The Green's function is developed in three dimensions and is reduced to the two-dimensional problem by integrating z or x_3 from $-\infty$ to ∞.

By definition the three-dimensional Green's function for equation (A.11) must satisfy the equation

$$(\nabla^2+\xi^2)G(\mathbf{x},\mathbf{x}')=-\delta(\mathbf{x}-\mathbf{x}') \tag{A.12}$$

where: $G(\mathbf{x},\mathbf{x}')$ = the Green's function,

δ = the Dirac delta function,

$\mathbf{x}$ = the position vector of the observation point, and

$\mathbf{x}'$ = the position vector of the source point.

(Throughout the following discussion, primed quantities represent the source points or the path of integration while their unprimed counterparts represent the observation point or the

point around which the equation is written.)

Premultiplying equation (A.12) by $\bar{w}$, premultiplying equation (A.11) by G, and subtracting yields

$$G(\nabla^2+\xi^2)\bar{w}-\bar{w}(\nabla^2+\xi^2)G=\bar{w}\delta$$

which simplifies to

$$G\nabla^2\bar{w}-\bar{w}\nabla^2G=\bar{w}\delta \tag{A.13}$$

Integrating over the volume of the medium, V,

$$\iiint_{V'}(G\nabla'^2\bar{w}-\bar{w}\nabla'^2G)dV'=\begin{cases}\bar{w} \text{ for } \mathbf{x}\in V'\\ 0 \text{ for } \mathbf{x}\notin V'\end{cases} \tag{A.14}$$

To transform the equation from the three-dimensional volume integral to a surface integral, Green's theorem is applied to obtain

$$\iint_{A'}(G\frac{\partial\bar{w}}{\partial n'}-\bar{w}\frac{\partial G}{\partial n'})\,dA'=\begin{cases}\bar{w} \text{ for } \mathbf{x}\in V'\\ 0 \text{ for } \mathbf{x}\notin V'\end{cases} \tag{A.15}$$

Because there is no variation in the $z-$ or x_3–direction, this equation can be transformed into a two-dimensional equation by integrating out that coordinate to yield

$$\int_{S'}(\bar{w}(\mathbf{r}')\frac{\partial g}{\partial n'}-g(\mathbf{r},\mathbf{r}')\frac{\partial\bar{w}}{\partial n'}|_{\mathbf{r}'})\,dS'=\begin{cases}\bar{w} \text{ for } \mathbf{r}\in V'\\ 0 \text{ for } \mathbf{r}\notin V'\end{cases} \tag{A.16}$$

where: $g=\int_{x_3=-\infty}^{\infty}G\,dx_3'$,

S' = the line bounding the cross–section of the volume.

$\mathbf{r}$ = two–dimensional position vector of the observation point, and

$\mathbf{r}'$ = two–dimensional position vector of the integration point.

Mow and Pao [10] show that the Green's function for equation (A.10) is

$$G(\mathbf{x},\mathbf{x}')=\frac{e^{i\xi\rho}}{4\pi\rho}=G(\mathbf{x}',\mathbf{x}) \tag{A.17}$$

where: $\rho=|\mathbf{x}-\mathbf{x}'|=\sqrt{(x-x')^2+(y-y')^2+(z-z')^2}$

For the two-dimensional case of equation (A.11), this Green's function becomes

$$g = \int_{z=-\infty}^{\infty} G dz = \int_{z=-\infty}^{\infty} \frac{e^{i\xi\rho}}{4\pi\rho} dz = \int_{z=-\infty}^{\infty} \frac{e^{i\xi\sqrt{\bar{r}^2+z^2}}}{4\pi\sqrt{\bar{r}^2+z^2}} = \frac{iH_0^{(1)}(\xi\bar{r})}{4} \tag{A.18}$$

where: $\bar{r} = \sqrt{(x-x')^2+(y-y')^2}$=distance from observation point to integration point

$H_0^{(1)} = J_0(\bar{r})+iY_0(\bar{r})$=the Hankel function of the first kind of zeroeth order

A.5 Application to the incident and scattered fields

Mow and Pao [10] point out that in equation (A.16), the incident field which originates at infinity is not singular within the volume of integration. Therefore,

$$\int_{S'}(g\frac{\partial \bar{w}^i}{\partial n'} - \bar{w}^i \frac{\partial g}{\partial n'})dS' = 0 \tag{A.19}$$

The scattered field originates at the surfaces shown in the profile and is singular. Therefore,

$$\int_{S'}(g\frac{\partial \bar{w}^s}{\partial n'} - \bar{w}^s \frac{\partial g}{\partial n'})dS' = \bar{w}^s \tag{A.20}$$

Adding these two equations yields

$$\int_{S'}(g\frac{\partial(\bar{w}^i+\bar{w}^s)}{\partial n'} - (\bar{w}^i+\bar{w}^s)\frac{\partial g}{\partial n'})dS' = \bar{w}^s$$

or

$$\int_{S'}(g\frac{\partial \bar{w}^t}{\partial n'} - \bar{w}^t \frac{\partial g}{\partial n'})dS' = \bar{w}^s \tag{A.21}$$

Further references to this equation drop the superscript ^{t} so that $\bar{w}$ is understood to be the total field, $\bar{w}^t$.

A.6 Singularities in the Green's functions

Equation (A.21) gives an expression for the steady-state harmonic coefficient of displacement for any point $r \in V$ for the given frequency, ω, as an integral around the boundary of the profile. The goal of this work is to be able to compute the coefficients of the displacement

and the normal derivative at points on the boundary. To do this by a boundary method, it is necessary to move the observation point to the boundary. Unfortunately, this causes the Green's functions to be singular where the integration point approaches the observation point ($\mathbf{r}=\mathbf{r}'$) because $\bar{r}=|\mathbf{r}-\mathbf{r}'|=0$. In this section we extract those singularities and interpret the integral in the Cauchy principal value sense. Accordingly, when the observation point is on the boundary, equation (A.21) becomes

$$\alpha\bar{w}-\beta\frac{\partial\bar{w}}{\partial n'}+P\int_{S'}(g\frac{\partial\bar{w}}{\partial n'}-\bar{w}\frac{\partial g}{\partial n'})dS'=\bar{w}^s \qquad \text{(A.22)}$$

where: α = the singularity in $\frac{\partial g}{\partial n'}$, and

β = the singularity in g

For future convenience, we add and subtract $\bar{w}^i$ on the right side to get

$$\alpha\bar{w}-\beta\frac{\partial\bar{w}}{\partial n'}+P\int_{S'}(g\frac{\partial\bar{w}}{\partial n'}-\bar{w}\frac{\partial g}{\partial n'})dS'=\bar{w}^s+\bar{w}^i-\bar{w}^i=\bar{w}-\bar{w}^i$$

This equation is rearranged to get

$$(1-\alpha)\bar{w}+\beta\frac{\partial\bar{w}}{\partial n'}+P\int_{S'}(\bar{w}\frac{\partial g}{\partial n'}-g\frac{\partial\bar{w}}{\partial n'})dS'=\bar{w}^i \qquad \text{(A.23)}$$

Assuming that the singularity is tractable, the equation can be dealt with on the basis of these singularities. The next two subsections explain the evaluation of these singularities.

A.6.1 Evaluation of the singularity in the Green's function

β is the singularity in the Green's function for the case when $\mathbf{r}'\to\mathbf{r}$. Therefore, its evaluation requires examining its behaviour in the vicinity of $\mathbf{r}$. Figure A-3 shows this vicinity. To extract the singularity, the integral, $\int_{\Sigma} g\frac{\partial\bar{w}}{\partial n'}dS'$ is evaluated in terms of ε and then ε is allowed to approach 0.

The green's function is

$$g=\frac{iH_0^{(1)}(\xi\bar{r})}{4}=\frac{i}{4}(J_0(\xi\bar{r})+iY_0(\xi\bar{r})) \tag{A.24}$$

For small arguments (that is, as $\varepsilon\to 0$), the Bessel functions approach

$$J_0(\xi\varepsilon)\sim 1-\frac{\xi^2\varepsilon^2}{4}\sim 1 \text{ and}$$

$$Y_0(\xi\varepsilon)\sim\frac{2}{\pi}\ln(\xi\varepsilon)$$

Thus, the asymptotic form for the Green's function for small arguments is seen to be

$$g(\xi\varepsilon)\sim\frac{i}{4}(1+i\frac{2}{\pi}\ln(\xi\varepsilon)) \tag{A.25}$$

which has a logarithmic singularity.

For $\mathbf{r}'\in\Sigma$, $\bar{r}=\varepsilon$, $dS'=\varepsilon\, d\theta$, and $\frac{\partial\bar{w}}{\partial n'}\sim\frac{\partial\bar{w}}{\partial n'}(\mathbf{r})$. Therefore, we can evaluate β by

$$\beta\frac{\partial\bar{w}}{\partial n'}=\lim_{\varepsilon\to 0}\int_\Sigma g\frac{\partial\bar{w}}{\partial n'}dS'\sim\lim_{\varepsilon\to 0}\int_{\theta_1}^{\theta_2}\frac{i}{4}(1+\frac{2i}{\pi}\ln(\xi\varepsilon))\frac{\partial\bar{w}}{\partial n'}\,\varepsilon d\theta=\frac{i(\theta_2-\theta_1)}{4}\lim_{\varepsilon\to 0}\varepsilon[1+i\frac{2}{\pi}\ln(\xi\varepsilon)]=0 \tag{A.26}$$

That $\varepsilon\cdot 1$ vanishes with ε should be obvious. $\varepsilon\ln(\xi\varepsilon)$ vanishes because a logarithmic singularity is weaker than first order.

From the above discussion, we see that $\beta=0$ and the singularity in the $\frac{\partial\bar{w}}{\partial n'}$ term vanishes.

A.6.2 Evaluation of the singularity in the derivative

α is the singularity in the normal derivative of the Green's function for the case when $\mathbf{r}\to\mathbf{r}'$. Figure A-3 shows the vicinity of $\mathbf{r}$. To extract the singularity, α, the integral $\int_\Sigma\bar{w}\frac{\partial g}{\partial n'}dS'$ is evaluated along Σ in terms of ε and then ε is allowed to approach zero. The derivative of the Green's function is

$$\frac{\partial g}{\partial n'} = \mathbf{n}' \cdot \nabla' g = n_r \frac{\partial g}{\partial \rho} + n_\theta \frac{\partial g}{\partial \theta} = \frac{\partial g}{\partial \bar{r}} = \frac{-i\xi}{4} H_1^{(1)}(\xi \bar{r})$$

For points on the arc Σ the outward normal is in the r-direction. Therefore, $n_r=1$ and $n_\theta=0$.

The derivative of $H_0^{(1)}$ is $-\xi H_1^{(1)}$ [11].

For small argument, ε, the first-order Bessel functions approach

$$J_1(\xi\varepsilon) \sim \frac{\xi\varepsilon}{2}$$

$$Y_1(\xi\varepsilon) \sim \frac{-2}{\pi\xi\varepsilon}$$

Thus, the asymptotic form for the first-order Hankel function is seen to be

$$H_1^{(1)} \sim \frac{\xi\varepsilon}{2} - i\frac{2}{\pi\xi\varepsilon} \tag{A.27}$$

For $\mathbf{r} \in \Sigma$, $\bar{r}=\varepsilon$, $dS'=\varepsilon d\theta$, $\bar{w}(\bar{r}') \sim \bar{w}(\mathbf{r})$, and $\frac{\partial g}{\partial n'} \sim \frac{-i\xi}{4}\left(\frac{\xi\varepsilon}{2} - i\frac{2}{\pi\xi\varepsilon}\right)$. Thus, to evaluate α,

$$\begin{aligned}
\alpha\bar{w} &= \lim_{\varepsilon\to 0}\int_{\Sigma} -\bar{w}\frac{\partial g}{\partial n'} dS' \\
&= \lim_{\varepsilon\to 0}\int_{\theta_1}^{\theta_2} -\bar{w}\left(\frac{-i\xi}{4}\right)\left(\frac{\xi\varepsilon}{2} - i\frac{2}{\pi\xi\varepsilon}\right)\varepsilon d\theta \\
&= -(\theta_2-\theta_1)\bar{w}\left(\frac{-i\xi}{4}\right)\lim_{\varepsilon\to 0}\varepsilon\left(\frac{\xi\varepsilon}{2} - i\frac{2}{\pi\xi\varepsilon}\right) \\
&= -\bar{w}\Delta\theta\left(\frac{-i\xi}{4}\right)\left(\frac{-i2}{\pi\xi}\right) \\
&= \bar{w}\frac{\Delta\theta}{2\pi}
\end{aligned} \tag{A.28}$$

From this it is seen that the singularity, $\alpha=\frac{\Delta\theta}{2\pi}$ where $\Delta\theta$ is the change in angle around the outside of the point, $\mathbf{r}$. Typically, this value is π but for the cases where there is a sharp corner at a point, it will be different. Accordingly, in most cases $\alpha=½$ and $(1-\alpha)=½$.

Recognizing that β vanishes and that α does not, equation (A.23) becomes

$$(1-\alpha)\bar{w} + P\int_{S'}\left(\bar{w}\frac{\partial g}{\partial n'} - g\frac{\partial \bar{w}}{\partial n'}\right)dS' = \bar{w}^i \tag{A.29}$$

which is the principal analytic equation for the current work. This equation is solved for the

steady-state coefficient of displacement at a given frequency, ω.

A.7 Response in the time domain

Equation (A.29) gives the steady-state response of all points on the boundary (and, therefore, in the interior) to an incident harmonic wave $\bar{w}^i$ at the given frequency. In order to find the response in the time domain to a transient incident wave, w^i, it is necessary to reverse the Fourier transform of equation (A.9).

The forward transform gives the frequency content of the incident wave. Equation (A.29) gives the response at a given frequency for points in the medium. To get the response of a particular point for the frequency content of the incident field, the two can be multiplied. Thus, by superposition, the convolution of the forward transform from equation (A.9) and the admittance function from equation (A.29) yields the time response of the given point to the given incident field. The inverse transform would be

$$w(\mathbf{r},t)=\int_0^\infty \bar{w}(\mathbf{r},\omega)e^{-i\omega t}\,d\omega \qquad \text{(A.30)}$$

A.8 Summary

Starting from $F=ma$, the displacement equation of motion was developed for SH waves. The time dependence of this equation was handled by the use of a Fourier transform and the reduced spatially dependent equation was converted to its integral form through the use of Green's function. After investigating the singularities in the Green's functions, a boundary equation for the admittance was derived. The solution of this equation is then convoluted with the forward transform of the incident wave field to obtain the response of a point in the

profile to the given incident wave. An example of this process is given in appendix E.

APPENDIX B
NUMERICAL IMPLEMENTATION FOR HOMOGENEOUS PROFILES

The purpose of this appendix is to present the implementation of a numerical solution method for the equations derived in appendix A. The procedure is to discretize the surfaces of the medium, represent the displacement and stress as interpolants of their values at the endpoints of the discrete segments, and integrate the representations of these functions along each of the segments.

The final section of the appendix presents the discrete Fourier transform.

B.1 Numerical solution of the steady-state wave equation

The boundary integral form of the steady-state wave equation (A.11) is

$$(1-\alpha)\,\bar{w} + P\int_{S'}\left(\bar{w}\frac{\partial g}{\partial n'} - g\frac{\partial \bar{w}}{\partial n'}\right)dS' = \bar{w}^i \qquad \text{(B.1)}$$

and is applicable to a homogeneous medium as shown in figure B-1. Because this equation is soluble for only a very small number of problems, numerical techniques are used. The numerical method used for this work entails a discretization of the problem boundaries, a Gaussian quadrature over the segments generated, and the solution of the matrix equation generated.

B.1.1 Discretization of the domain

The first step of the numerical process is to discretize the problem domain. Accordingly, figure B-1 is divided into segments as exemplified in figure B-2. In that figure the endpoints of each segment are denoted by o's. The unknown quantities in the matrix equation are the displacement, $\bar{w}$, and the normal derivative, $\frac{\partial \bar{w}}{\partial n'}$ at each of these points. These quantities are assumed to

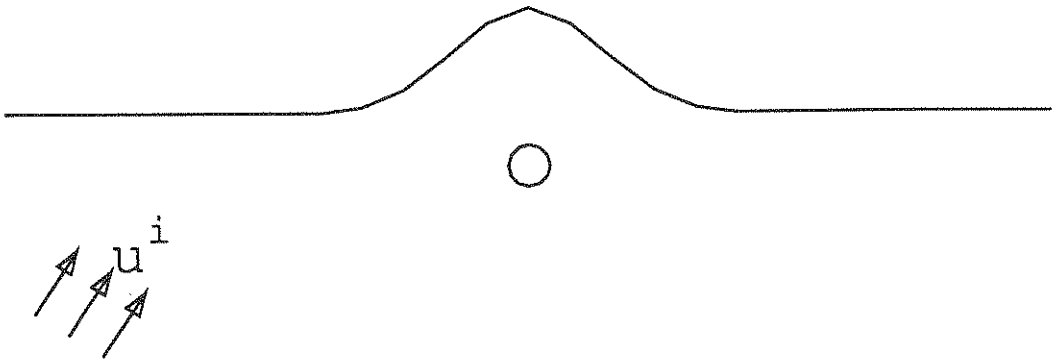

FIGURE B-1 Homogeneous medium

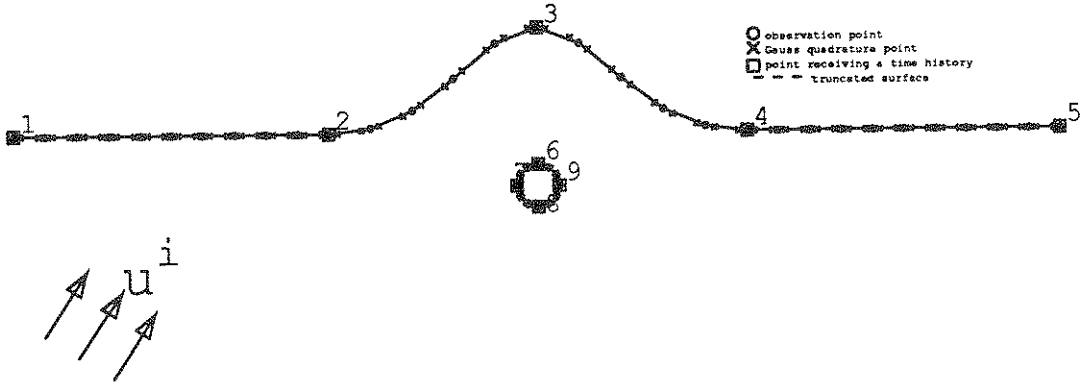

FIGURE B-2 Discretization of the domain

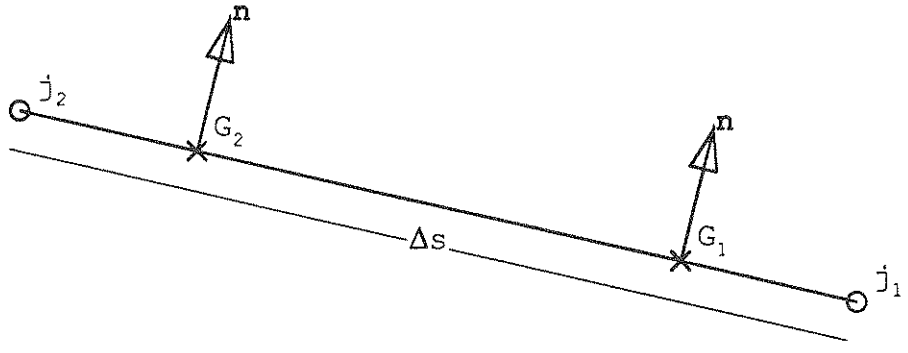

FIGURE B-3 Segment of the boundary

vary linearly between the endpoints.

Instead of integrating over the whole boundary, the integration can now be conducted over each segment and equation (B.1) becomes

$$(1-\alpha)\bar{w}+\sum_{j=1}^{N_{el}} P\int_{el_j}(\bar{w}\frac{\partial g}{\partial n'}-g\frac{\partial \bar{w}}{\partial n'})dS'=\bar{w}^i \qquad \text{(B.2)}$$

where: N_{el} = number of segments on surface and $\int_{el_j}$=integration over the j[th] segment

Accordingly, if an expression is developed for integration over a single segment, this integration can be repeated for each segment. In this work Gaussian quadrature is used.

Figure B-3 shows a single segment of the boundary. The task here is to obtain an expression for $\int_{el_j}(\bar{w}\frac{\partial g}{\partial n'}-g\frac{\partial \bar{w}}{\partial n'})dS'$ in terms of $\bar{w}$ and $\frac{\partial \bar{w}}{\partial n'}$ at the endpoints of the segments. The following notation is used:

E1 is the first endpoint
E2 is the second endpoint
G1 is the first Gauss point
G2 is the second Gausspoint
W_1 is the first weighting factor for the quadrature (0.789)
W_2 is the second weighting factor (0.211)
s is distance from the first endpoint
Δs is the length of the segment

Assuming that $\bar{w}$ and $\frac{\partial \bar{w}}{\partial n'}$ may be well approximated in the segment by linear interpolation between the endpoints,

$$\bar{w}(s)\simeq \bar{w}\,|_{E1}(\frac{\Delta s-s}{\Delta s})+\bar{w}\,|_{E2}(\frac{s}{\Delta s}) \text{ and}$$

$$\frac{\partial \bar{w}}{\partial n'}(s)\simeq \frac{\partial \bar{w}}{\partial n'}|_{E1}(\frac{\Delta s-s}{\Delta s})+\frac{\partial \bar{w}}{\partial n'}|_{E2}(\frac{s}{\Delta s})$$

Therefore, at the Gauss points

$$\bar{w}\,|_{G1}\simeq W_1\bar{w}\,|_{E1}+W_2\bar{w}\,|_{E2}$$

$$\bar{w}\,|_{G2} \approx W_2 \bar{w}\,|_{E1} + W_1 \bar{w}\,|_{E2}$$

$$\frac{\partial \bar{w}}{\partial n'}\,|_{G1} \approx W_1 \frac{\partial \bar{w}}{\partial n'}\,|_{E1} + W_2 \frac{\partial \bar{w}}{\partial n'}\,|_{E2}$$

$$\frac{\partial \bar{w}}{\partial n'}\,|_{G2} \approx W_2 \frac{\partial \bar{w}}{\partial n'}\,|_{E1} + W_1 \frac{\partial \bar{w}}{\partial n'}\,|_{E2}$$

Two-point Gauss quadrature tells us that the integral over the segment can be approximated as

$$\int_{el_j} \left(\bar{w} \frac{\partial g}{\partial n'} - g \frac{\partial \bar{w}}{\partial n'} \right) dS' \approx \left[\left(\bar{w} \frac{\partial g}{\partial n'} - g \frac{\partial \bar{w}}{\partial n'} \right) |_{G1} + \left(\bar{w} \frac{\partial g}{\partial n'} - g \frac{\partial \bar{w}}{\partial n'} \right) |_{G2} \right] \frac{\Delta s}{2}$$

Substituting the above approximations for $\bar{w}$ and $\frac{\partial g}{\partial n'}$ at the Gauss points yields

$$\int_{el_j} \left(\bar{w} \frac{\partial g}{\partial n'} - g \frac{\partial \bar{w}}{\partial n'} \right) dS' \approx \left[(W_1 \bar{w}\,|_{E1} + W_2 \bar{w}\,|_{E2}) \frac{\partial g}{\partial n'}\,|_{G1} - (W_1 \frac{\partial \bar{w}}{\partial n'}\,|_{E1} + W_2 \frac{\partial \bar{w}}{\partial n'}\,|_{E2}) g\,|_{G1} \right.$$

$$\left. + (W_2 \bar{w}\,|_{E1} + W_1 \bar{w}\,|_{E2}) \frac{\partial g}{\partial n'}\,|_{G2} - (W_2 \frac{\partial \bar{w}}{\partial n'}\,|_{E1} + W_1 \frac{\partial \bar{w}}{\partial n'}\,|_{E2}) g\,|_{G2} \right] \frac{\Delta s}{2}$$

Collecting the like terms produces

$$\int_{el_j} \left(\bar{w} \frac{\partial g}{\partial n'} - g \frac{\partial \bar{w}}{\partial n'} \right) dS' \approx \left[(W_1 \frac{\partial g}{\partial n'}\,|_{G1} + W_2 \frac{\partial g}{\partial n'}\,|_{G2}) \bar{w}\,|_{E1} + (W_2 \frac{\partial g}{\partial n'}\,|_{G1} + W_1 \frac{\partial g}{\partial n'}\,|_{G2}) \bar{w}\,|_{E2} \right. \tag{B.3}$$

$$\left. - (W_1 g\,|_{G1} + W_2 g\,|_{G2}) \frac{\partial \bar{w}}{\partial n'}\,|_{E1} - (W_2 g\,|_{G1} + W_1 g\,|_{G2}) \frac{\partial \bar{w}}{\partial n'}\,|_{E2} \right] \frac{\Delta s}{2}$$

Using this equation to integrate the terms of equation (B.2) yields an approximate expression relating $\bar{w}$ and $\frac{\partial \bar{w}}{\partial n'}$ at all the segment endpoints on the surface to $\bar{w}$ and $\bar{w}^i$ at the observation point. In order to make a well-posed problem out of this, the observation point is moved to one of the segment endpoints.

$$(1-\alpha)\bar{w}_i + \sum P \int_{el_j} \left(\bar{w} \frac{\partial g}{\partial n'} - g \frac{\partial \bar{w}}{\partial n'} \right) dS' = \bar{w}^i{}_i \tag{B.4}$$

This equation can be written for each of the segment endpoints (for $i=1\ N_{points}$) to formulate a simultaneous system of equations.

At each of the segment endpoints an equation can be written (N_{points} points). Also at each of the points, there is a boundary condition (typically $\tau=0$). Thus, there are $2N_{points}$ equations.

At each of the points there are two unknown quantities, $\bar{w}$ and $\frac{\partial \bar{w}}{\partial n'}$, which means that there are $2N_{points}$ unknowns. Accordingly, the system of equations is well posed. Of course, in practice the boundary conditions are used to eliminate an unknown and not to generate a new equation. The matrix equation which results from this numerical method will then have N_{points} equations in N_{points} unknowns. This set of equations can be conveniently represented as

$$H_{ij}\,\bar{w}_j = \bar{w}^i{}_i \tag{B.5}$$

where: H_{ij} = the influence of the j^{th} unknown on the i^{th} equation

$\bar{w}_j$ = the j^{th} unknown (typically, the displacement at the j^{th} point), and

$\bar{w}^i{}_i$ = the incident field coefficient at the observation point

It should be observed that H_{ij} is the integral of Green's functions relating the displacement at the observation point (i) to the unknown (j) at the integration point. Therefore, the matrix is not necessarily symmetric. Furthermore, it need not be positive-definite nor even well conditioned. Because the matrix relates all of the unknowns on the boundary to the displacement at the observation points, it is dense and, quite possibly, completely full. These make some of the more sophisticated methods of storage and solution inappropriate.

B.2 The discrete Fourier transform

Equations (A.9) and (A.30) give the forward and inverse Fourier transforms for a continuous variable. Digital computers are discrete by nature and acceleration information for earthquakes is generally discretized at intervals of 0.02 seconds. These two considerations make it reasonable to use a discrete Fourier transform. The discrete Fourier transform pair is

$$\bar{w}(\omega_l)=\sum_{k=1}^{N_{terms}} w(t_k)e^{i\omega_l t_k}\Delta t \qquad \text{and} \qquad w(t_k)=\sum_{k=1}^{N_{terms}} w(\omega_l)e^{-i\omega_l t_k}\Delta\omega \tag{B.6}$$

where: $\bar{w}(\omega_l)$ = the transform for the l^{th} frequency,

$w(t_k)$ = the k^{th} term in the time history data, and

N_{terms} = the number of terms in the time series.

The algorithm used is the Cooley-Tukey algorithm (fast Fourier transform) as implemented by IMSL [13]

B.3-Summary

The equation derived in appendix A has been solved approximately through the use of Gaussian quadrature of the unknown quantities and a fast Fourier transform of the incident wave.

APPENDIX C
EXTENSION TO NONHOMOGENEOUS PROFILES

The purpose of this appendix is to present the extension of the derivation of appendix A to the case where a profile contains more than one material as shown in figure C-1. The derivation is again limited to antiplane (SH) waves and, though the profile may have several different media within it, each medium is homogeneous.

C.1 Statement of the problem

Figure C-1 shows a profile containing several different media. The problem addressed in this appendix is the mathematical relationship between the several media and the extension of the numerical methods for homogeneous media discussed in appendix B to the nonhomogeneous case. This extension is in two parts—the simple extension for layered profiles with non-intersecting interfaces and the more complicated extension to intersecting interfaces such as points A and B in figure C-1.

C.2-Governing equation

In appendix A the governing equation for shear wave propagation in a homogeneous medium was presented as equation (A.29). Within each of the media of figure C-1, the medium is homogeneous. Therefore, within each of these media, the development of appendix A applies. In particular, equation (A.29) still applies. Therefore, within each medium

$$(1-\alpha)\,\bar{w} + P\int_{S'}(\bar{w}\frac{\partial g}{\partial n'} - g\frac{\partial \bar{w}}{\partial n'})dS' = \bar{w}^i \qquad \text{(C.1)}$$

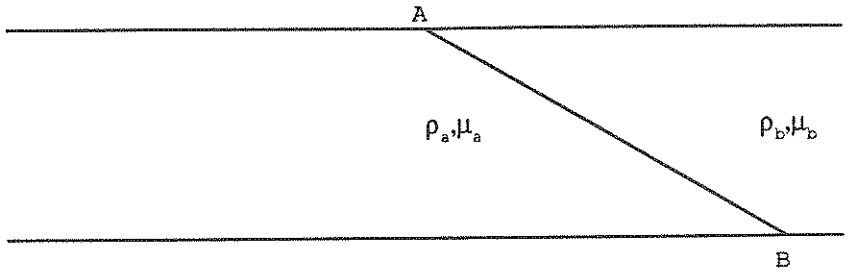

FIGURE C-1 General problem of a heterogeneous profile

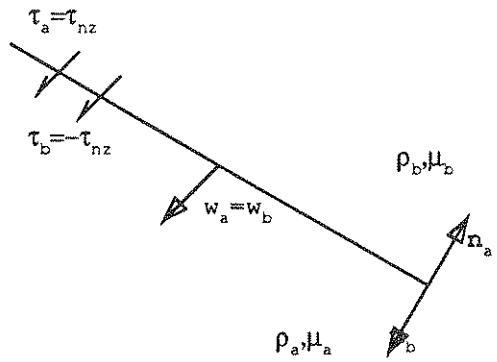

FIGURE C-2 Continuity conditions across an interface

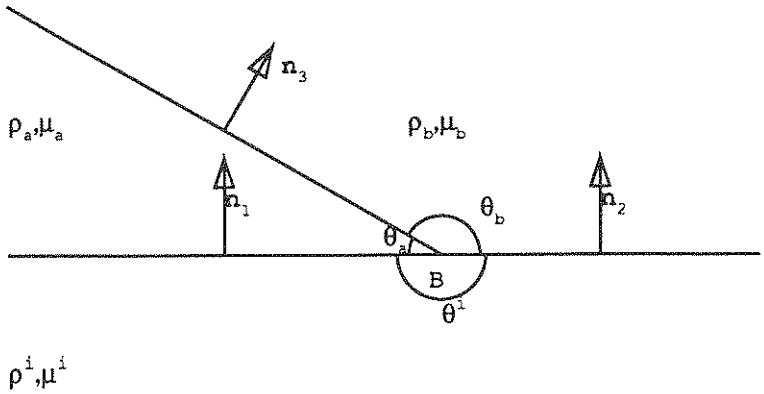

FIGURE C-3 Expanded view of interface intersection

where: S' = the surface bounding the particular medium.

In the case where a profile consists of a single medium, the surfaces of that medium have boundary conditions which typically eliminate one of the unknowns, $\bar{w}$ or $\frac{\partial \bar{w}}{\partial n'}$, or at least establish a relationship between them. In particular a free surface has no stress so that $\tau=\frac{\partial \bar{w}}{\partial n'}=0$ and equation (C.1) becomes

$$(1-\alpha)\bar{w}+P\int_{S'}\bar{w}\frac{\partial g}{\partial n'}dS'=\bar{w}^i$$

However, for the case where a surface is not free but is rather an interface with the adjacent medium, both unknowns will be present. Thus, all along the boundary in both media both unknowns exist. It is reasonable to expect that there is a relationship between the displacements and the derivatives on either side of the interface. The assumptions used here are that the displacements and stresses are continuous across the interface. In the terms illustrated in figure C-2,

$$\bar{w}_a=\bar{w}_b \quad \text{and} \quad \tau_a=\tau_b \tag{C.2}$$

The first relation is immediately usable. The second must first be understood in terms of displacements using the relation

$$\tau_{nz}=\mu\frac{\partial \bar{w}}{\partial n'}=\mu\mathbf{n}\cdot\nabla\bar{w} \tag{C.3}$$

There is a complication here because of the direction of integration. For adjacent media the directions of integration must be opposite and the outward normals, $\mathbf{n}_a$ and $\mathbf{n}_b$, must have opposite signs. Therefore, there is a sign change between the two quantities as used in the integrand of equation (C.1). Consequently, in the numerical formulation the coefficients of the stresses must have their signs changed for one medium.

In doing this we have at each observation point two unknowns and because the interface borders two media, we have two equations. Accordingly, the problem is still well-posed.

C.3 Numerical implementation

Because all of the mechanisms for dealing with coefficients for both displacement and stress are in place as described in appendix B, the only further extensions to the numerical problem are in bookkeeping. The program constructs the equations *seriatim* and therefore must know which point and which medium each equation is written for. It must keep track of which surfaces bound each medium. It must know the direction of the outward normal for each medium so that it may compute the proper value for $\frac{\partial g}{\partial n'}$ and assign the proper sign to the matrix coefficients of the $\frac{\partial \bar{w}}{\partial n'}$'s. Apart from these matters, the construction of the matrices proceeds as described in appendix B.

C.4 Intersections of interfaces

Figure C-1 which shows the general multi-media problem contains points where interface lines intersect (points A and B). Such points present two further complications—the fact that the singularity, α, of equation (C.1) is not ½ and that there the normals are not necessarily collinear.

An amplified view of point B of figure C-1 is presented in figure C-3. As can be seen from the figure, there are three interior angles, θ_a, θ_b, and θ^i and two (or possibly three) different orientations of the interface lines, $\mathbf{n}_1$, $\mathbf{n}_2$, and $\mathbf{n}_3$. Each of these will be important in constructing equation (C.1) for point B. Furthermore, since there are three media meeting at

point B, there are three different equations which can be written with B as the observation point. Therefore, it is desirable that there should be three independent unknown quantities at point B. This is indeed the case.

C.4.1 Evaluation of α

Section A.6.2 gives the extraction of the singularity, α, from the $\bar{w}\frac{\partial g}{\partial n'}$ term of the integrand of the principal equation. In that section it is shown that

$$\alpha=\frac{\Delta\theta}{2\pi} \tag{C.4}$$

where: θ = the angle measured around the outside of the boundary at the observation point.

For the typical point on an interface, α=½. At point B this is no longer true. However, under all circumstances, α may be understood as the portion of the circle which lies outside the medium. Since this is true, $(1-\alpha)$ may be understood as the portion of the circle which lies inside the medium. Thus, the leading coefficient of equation (C.1) may be understood as the interior angle of the medium at the observation point of the equation. For the equation written at point B and integrated around medium a,

$$(1-\alpha)=\frac{\theta_a}{2\pi}$$

and the singularities in media b and c may be handled similarly.

Having made this observation, the application of the numeric scheme is straightforward as it plugs directly into equation (B.5). The displacement, $\bar{w}$, is assumed to be the same in all three media.

C.4.2 Evaluation of normal derivatives

While τ_{nz} in medium a is equal and opposite to τ_{nz} in medium b along the length of line 3, there is not such a clear relationship at the point of intersection, B. Basic principles of stress are resorted to in order to determine the behaviour of the stresses at this point. Figure C-4 shows a wedge of the material where the inclined surface is parallel to line 1 of figure C-3. Simple equilibrium considerations dictate that

$$\tau_{nz}\, dn dz - \tau_{xz}\, dy dz - \tau_{yz}\, dx dz = 0$$

where: $dy = dn \sin\theta$ and $dx = dn \cos\theta$

Therefore,

$$\tau_{nz} = \tau_{xz} \sin\theta + \tau_{yz} \cos\theta \qquad \text{(C.5)}$$

Through this relation, the stress on a plane of any orientation may be referred to x– and y–coordinates. Therefore, there are at most two independent stresses at a given point. Because there are one displacement and two stresses, there are three independent unknown quantities at the point. As previously observed, there are also three media at this point and, therefore, three equations. The matrix is still well-posed.

An appropriate method for handling more than three media intersecting at a point has not been developed for the current work.

For the numerical formulation for such a point, equation (B.5) must be modified to include the additional unknown stress. The modified equation will be

$$H_{ij}\, w_j = f_i \qquad \text{(C.6)}$$

where w_j includes both displacements and stresses and where necessary includes both of the independent stresses at a point.

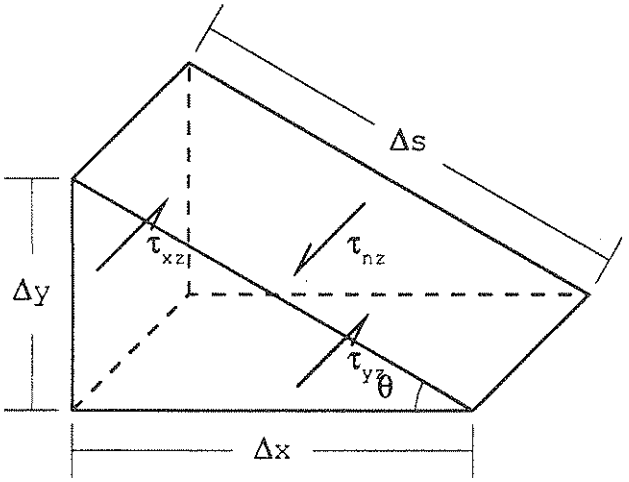

FIGURE C-4 Wedge of material showing the antiplane stresses

C.5 Summary

The methodology developed in appendices A and B has been extended to heterogeneous profiles. The continuity of displacement and stress were assumed and the implications of that assumption worked out for the numerical scheme. The case of intersecting interfaces was also developed both analytically and numerically. The scheme set forth in this appendix is applicable to a wide range of problems in earthquake wave propagation. In fact, any profile consisting of distinct media each of which is homogeneous should be amenable to solution by these methods.

APPENDIX D
TRUNCATED PORTIONS

Figure D-1 shows a typical profile which has been truncated to make the numerical process possible. Leaving these truncated regions out of the integrals introduces an error into the equations. Perhaps, this is best seen by examining the main equation (2.11)

$$(1-\alpha)\,\bar{w} + P\int_{S'}\left(\bar{w}\frac{\partial g}{\partial n'} - g\frac{\partial \bar{w}}{\partial n'}\right)dS' = \bar{w}^i \tag{D.1}$$

As this equation is applied to each medium, the integral is to be taken around the entire contour of that medium. This analytical integral consists of two parts—the part included in the numerical scheme and the part excluded from it. These two parts are identified in the figure as S_{num}, that part of the surface which is included in the numerical scheme, and S_{trunc}, that part which is truncated from the problem before the discretization and numerical integrations are performed. Using this division the following equation is written:

$$\int\left(\bar{w}\frac{\partial g}{\partial n'} - g\frac{\partial \bar{w}}{\partial n'}\right)dS' = \int_{S_{num}}\left(\bar{w}\frac{\partial g}{\partial n'} - g\frac{\partial \bar{w}}{\partial n'}\right)dS' + \int_{S_{trunc}}\left(\bar{w}\frac{\partial g}{\partial n'} - g\frac{\partial \bar{w}}{\partial n'}\right)dS' \tag{D.2}$$

Substituting this into equation (D.1) and rearranging yields

$$(1-\alpha)\bar{w} + P\int_{S_{num}}\left(\bar{w}\frac{\partial g}{\partial n'} - g\frac{\partial \bar{w}}{\partial n'}\right)dS' = \bar{w}^i - \int_{S_{trunc}}\left(\bar{w}\frac{\partial g}{\partial n'} - g\frac{\partial \bar{w}}{\partial n'}\right)dS' \tag{D.3}$$

In the numerical process described *supra*, the final integral is omitted. Thus, there is an error in each equation equal to the integral of the wave field around the truncated portion. Clearly, leaving this integral out of the formulation entirely is tantamount to assuming that both the displacement and the stress on these surfaces vanish. This reduces the magnitude of the computed response in the numerical portion. Figure D-2 shows the results of computations on a simple layered half-space ignoring the truncation. The solution is dragged down toward zero at the ends and is far from the correct solution (shown by the dotted line) over most of the domain.

D.1 Accounting for the truncation

Each medium of figure D-1 can be thought of as one of three separate media, one medium within the numerical region and the others in the truncated regions. These media are separated by an interface which has the same conditions of continuity in stress and displacement as discussed in appendix C. Figure D-3 shows the several parts of a medium cut up in this way. Equation (D.1) is applicable to each of these media. For any equation that we integrate in the numerical part, the observation point will be in the numerical region. For an observation point in the numerical region, the integral around the truncated portion of the medium will be zero. In other words, because the truncated portion is now a mathematically separate medium, it has no direct influence on the displacement of the observation point. Therefore, integration around one of the truncated portions on the side yields

$$\int_{S_{side}}\left(\bar{w}\frac{\partial g}{\partial n'} - g\frac{\partial \bar{w}}{\partial n'}\right)dS' + \int_{S_{trunc}}\left(\bar{w}\frac{\partial g}{\partial n'} - g\frac{\partial \bar{w}}{\partial n'}\right)dS' = 0 \tag{D.4}$$

This becomes

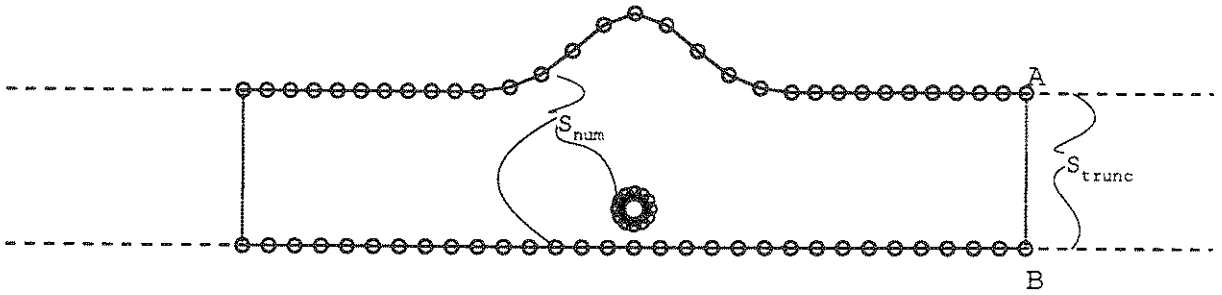

FIGURE D-1 A typical profile showing the truncated surfaces and regions

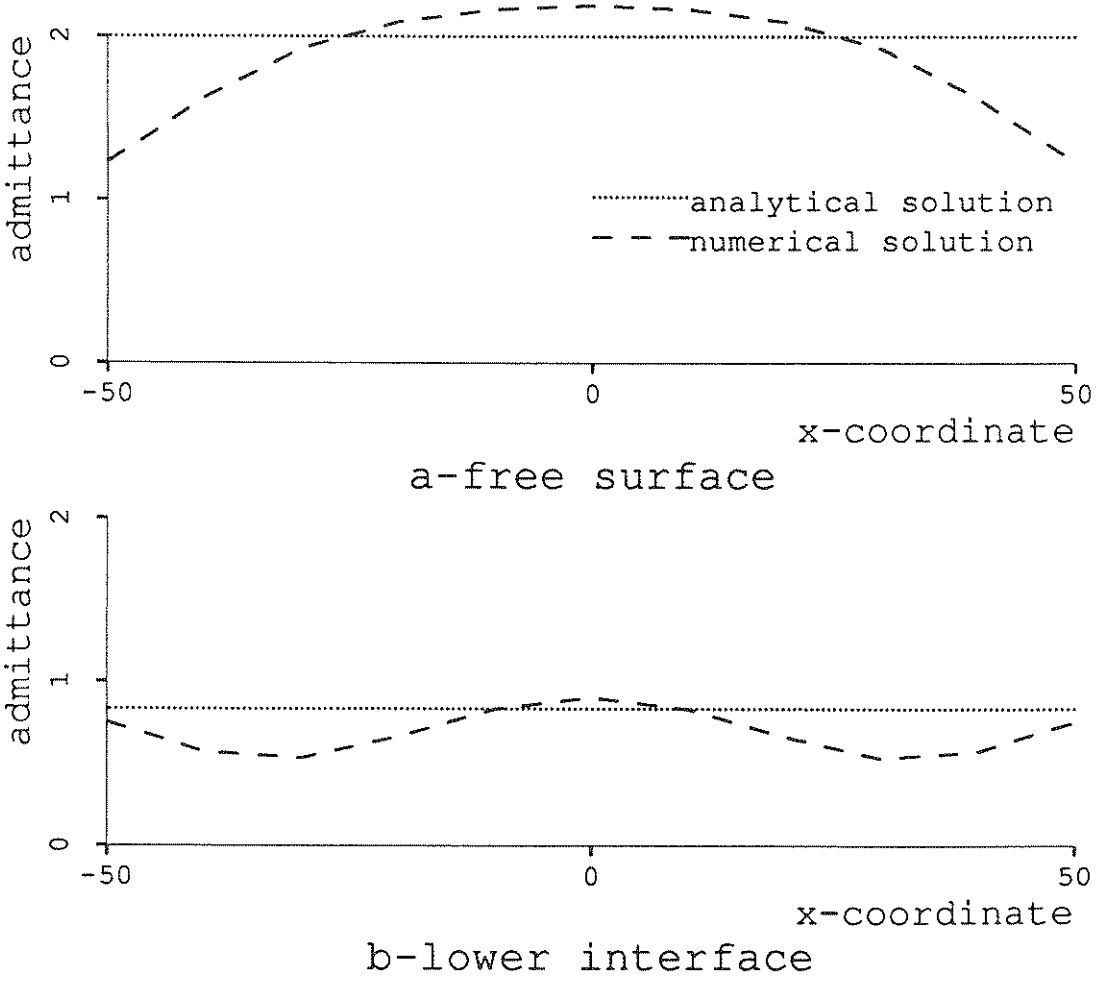

FIGURE D-2 Admittance functions obtained by ignoring the truncated regions

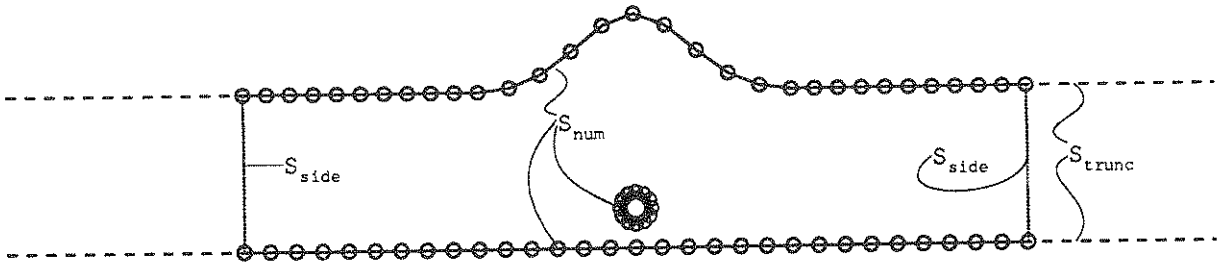

FIGURE D-3 The division of a truncated medium

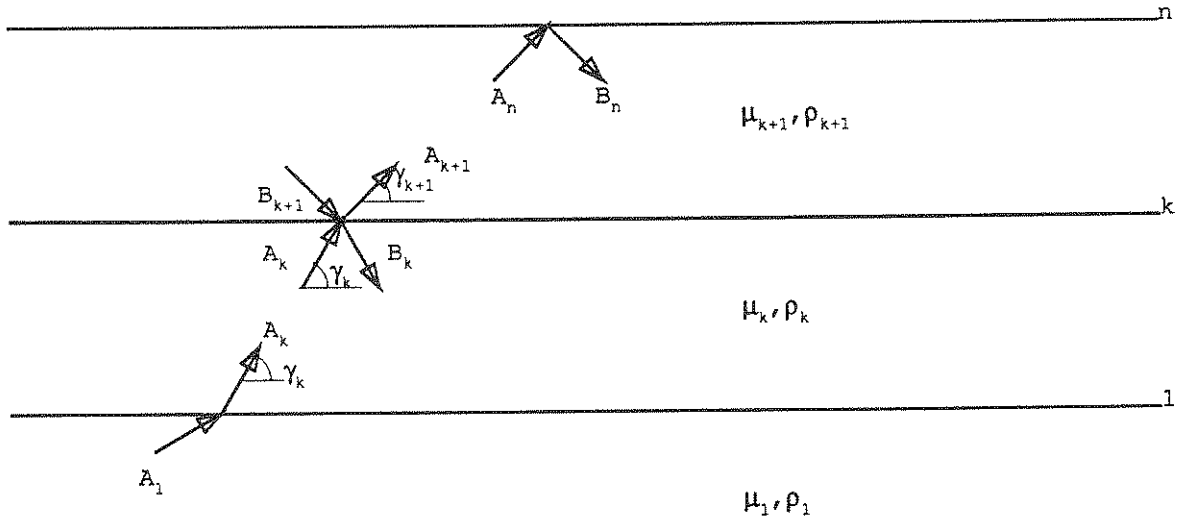

FIGURE D-4 Parallel infinite elastic layers showing the free-field solution

$$\int_{s_{num}} (\bar{w}\frac{\partial g}{\partial n'} - g\frac{\partial \bar{w}}{\partial n'})dS' = -\int_{s_{side}} (\bar{w}\frac{\partial g}{\partial n'} - g\frac{\partial \bar{w}}{\partial n'})dS' \quad \text{(D.5)}$$

From this equation it is seen that the problem of accounting for the truncated portion is reduced to finding the integral along the side of the numerical portion of the problem geometry. Equation (D.3) now becomes

$$(1-\alpha)\,\bar{w} + P\int_{S'} (\bar{w}\frac{\partial g}{\partial n'} - g\frac{\partial \bar{w}}{\partial n'})dS' = \bar{w}^i + \int_{s_{side}} (\bar{w}\frac{\partial g}{\partial n'} - g\frac{\partial \bar{w}}{\partial n'})dS' \quad \text{(D.6)}$$

D.1.1 The field in the truncated portion

This integral is of the same form as the principal integral of equation (D.1) and is integrable by similar methods. However, the wave field, $\bar{w}$, is not known. For the purposes of this project, its form and value are assumed.

At all points the total wave field is comprised of the incident and scattered fields ($\bar{w}=\bar{w}^i+\bar{w}^s$). For the case of infinite parallel layers the scattered field is simply the reflected field. Thus, for this simple case, $\bar{w}^s=\bar{w}^r$ and $\bar{w}=\bar{w}^i+\bar{w}^r$. This field is also identified as the free field, $\bar{w}^{ff}=\bar{w}^i+\bar{w}^r$.

The total field in these outlying regions can be thought of as the sum of the free-field wave and the waves scattered by the irregularities in the numerical portion of the problem. For the case shown in figure D-1, the scatterers would be the hill and the tunnel and the total wave field can be thought of as

$$\bar{w}^t=\bar{w}^i+\bar{w}^s=\bar{w}^i+\bar{w}^r+\bar{w}^\sigma \quad \text{(D.7)}$$

where $\bar{w}^\sigma$ = the scattering due to the internal scatterers, σ

The effect of the scatterer follows the shape of the Green's function, $g=\frac{iH_0^{(1)}(\xi\bar{r})}{4}$. Because the Green's function dies out with distance, $\bar{w}^\sigma$ does, too. Accordingly,

$$\bar{w}^\sigma \to 0 \quad as \quad \bar{r}\to\infty$$

and

$$\bar{w} \to \bar{w}^i+\bar{w}^r=\bar{w}^{ff} \quad as \quad \bar{r}\to\infty$$

It is, therefore, reasonable to assume that at some point $\bar{w}^\sigma$ is negligible. Using this assumption, the integral along the side becomes

$$\int_{S_{side}} (\bar{w}\frac{\partial g}{\partial n'} - g\frac{\partial \bar{w}}{\partial n'})dS' \sim \int_{S_{side}} ((\bar{w}^{ff})\frac{\partial g}{\partial n'} - g(\frac{\partial \bar{w}^{ff}}{\partial n'}))dS' \quad \text{(D.8)}$$

D.1.2 Computation of the free-field wave function The computation of the free-field wave form is a well-known solved problem in wave propagation [12]. It is briefly reproduced here. Figure D-4 shows a profile with infinite elastic layers. The wave in each layer has an ascending and a descending part with coefficients A_k and B_k, respectively. This means that the transform coefficient at a point (x,y) is

$$\overline{w}(x,y)=A_k e^{i\xi_k(x\cos\gamma_k+y\sin\gamma_k)}+B_k e^{i\xi_k(x\cos\gamma_k-y\sin\gamma_k)}$$

and

$$\frac{\partial\overline{w}}{\partial n'}=i\xi\sin\gamma_k(A_k e^{i\xi_k(x\cos\gamma_k+y\sin\gamma_k)}-B_k e^{i\xi_k(x\cos\gamma_k-y\sin\gamma_k)})$$

At each interface the displacement and the stress are assumed to be continuous. This means, for instance, that at interface k,

$$A_k e^{i\xi_k(x\cos\gamma_k+y_k\sin\gamma_k)}+B_k e^{i\xi_k(x\cos\gamma_k-y_k\sin\gamma_k)i}=A_{k+1}e^{i\xi_{k+1}(x\cos\gamma_{k+1}+y_k\sin\gamma_{k+1})}+B_{k+1}e^{i\xi_{k+1}(x\cos\gamma_{k+1}-y_k\sin\gamma_{k+1})}$$

and

$$i\mu_k\xi_k\sin\gamma_k[A_k e^{i\xi_k(x\cos\gamma_k+y_k\sin\gamma_k)}-B_k e^{i\xi_k(x\cos\gamma_k-y_k\sin\gamma_k)}]=i\mu_{k+1}\xi_{k+1}\sin\gamma_{k+1}[A_{k+1}e^{i\xi_{k+1}(x\cos\gamma_{k+1}+y_k\sin\gamma_{k+1})}-B_{k+1}e^{i\xi_{k+1}(x\cos\gamma_{k+1}-y_k\sin\gamma_{k+1})}]$$

In the bottom layer $A_1=\overline{w}^i$. At the free surface, there is no stress. There are, therefore, as many equations as there are unknown coefficients.

In order to allow a consistent solution,

$$\xi_k\cos\gamma_k=\xi_{k+1}\cos\gamma_{k+1} \quad \text{or} \quad \frac{\cos\gamma_k}{c_k}=\frac{\cos\gamma_{k+1}}{c_{k+1}}=\frac{\cos\gamma_1}{c_1} \tag{D.9}$$

$$A_k=\frac{1+R_k}{2}A_{k+1}e^{iy_k(xi_{k+1}\sin\gamma_{k+1}-\xi_k\sin\gamma_k)}+\frac{1-R_k}{2}B_{k+1}e^{-iy_k(xi_{k+1}\sin\gamma_{k+1}+\xi_k\sin\gamma_k)} \tag{D.10}$$

and

$$B_k=\frac{1-R_k}{2}A_{k+1}e^{iy_k(xi_{k+1}\sin\gamma_{k+1}+\xi_k\sin\gamma_k)}+\frac{1+R_k}{2}B_{k+1}e^{-iy_k(xi_{k+1}\sin\gamma_{k+1}-\xi_k\sin\gamma_k)} \tag{D.11}$$

where $R_k=\dfrac{\mu_{k+1}\xi_{k+1}\sin\gamma_{k+1}}{\mu_k\xi_k\sin\gamma_k}$

Starting at the top, the two coefficients, A_n and B_n, must be such that there is no stress at the surface.

$$B_n = A_n e^{i 2 y_n \xi_n \sin\gamma_n} \tag{D.12}$$

Coefficients of each layer can be expressed in terms of the coefficients of the layer above according to the equations above. Therefore, each coefficient is expressed in terms of A_n at the top. The whole set is corrected by the ratio of the value obtained for A_1 to the actual value of $\bar{w}^i$. Using this technique the $2n$ equations in $2n$ unknowns are solved without ever having to invert a matrix.

D.2 Examples of the effect of accounting for the truncated regions

In this section comparison is made of the solutions obtained ignoring the truncated portions with the solutions obtained using the above approximate restoration of its influence. Figure D-2 shows the results achieved with the numerical method without correcting for the truncated regions for a homogeneous layered half space. Figure D-5 shows the results for the same profile at the same frequency using the correction described above. Visual inspection shows great improvement. Table D-I gives the computed and analytical solutions for this same problem. Inspection of this table shows the quality of the results achieved.

Figure D-6 shows the admittances computed for a profile consisting of a soft layer overlying a stiffer half space subjected to an incident unit harmonic wave at a frequency of 50 rad/s and incident at a 45° angle. Again, the complete numerical solution (dashed line) shows very good agreement with the theoretical solution (dotted line).

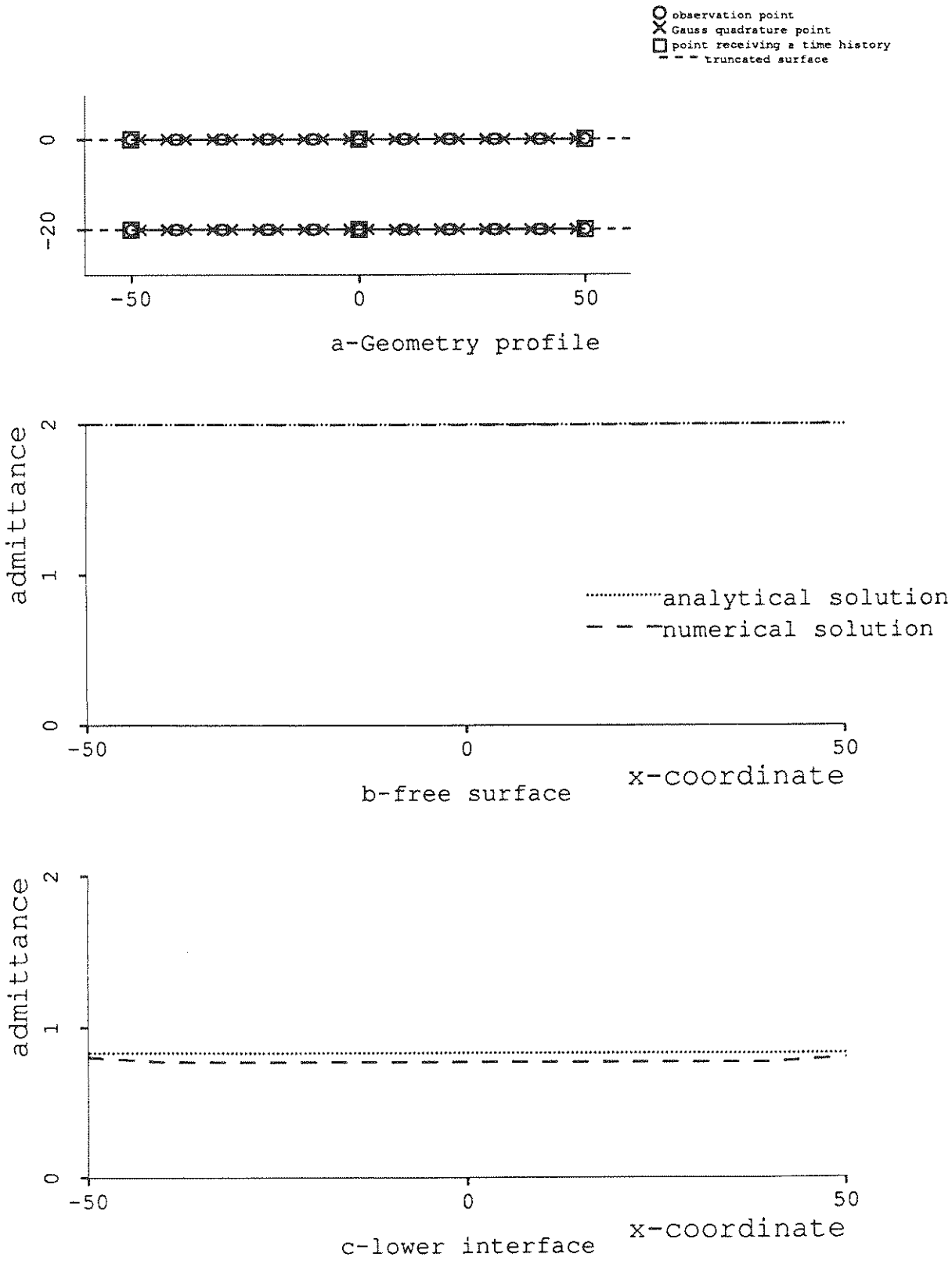

FIGURE D-5 Results correcting for the truncation, ω=50*rad/s*

TABLE D-I Comparison of numerical and analytical solutions correcting for truncation

		exact solution		numerical solution	
point	(location)	complex coefficient	magnitude	complex coefficient	magnitude
1	(50.00, 0.00)	(0.2001e+01,-0.3571e-02)	2.00117	(0.2000e+01, 0.00)	2.00000
2	(40.00, 0.00)	(0.1999e+01,-0.2178e-02)	1.99908	(0.2000e+01, 0.00)	2.00000
3	(30.00, 0.00)	(0.1998e+01,-0.1246e-02)	1.99779	(0.2000e+01, 0.00)	2.00000
4	(20.00, 0.00)	(0.1997e+01,-0.9451e-03)	1.99677	(0.2000e+01, 0.00)	2.00000
5	(10.00, 0.00)	(0.1996e+01,-0.1016e-02)	1.99595	(0.2000e+01, 0.00)	2.00000
6	(0.00, 0.00)	(0.1996e+01,-0.1094e-02)	1.99562	(0.2000e+01, 0.00)	2.00000
7	(-10.00, 0.00)	(0.1996e+01,-0.1016e-02)	1.99595	(0.2000e+01, 0.00)	2.00000
8	(-20.00, 0.00)	(0.1997e+01,-0.9449e-03)	1.99677	(0.2000e+01, 0.00)	2.00000
9	(-30.00, 0.00)	(0.1998e+01,-0.1246e-02)	1.99779	(0.2000e+01, 0.00)	2.00000
10	(-40.00, 0.00)	(0.1999e+01,-0.2177e-02)	1.99908	(0.2000e+01, 0.00)	2.00000
11	(-50.00, 0.00)	(0.2001e+01,-0.3570e-02)	2.00117	(0.2000e+01, 0.00)	2.00000
12	(50.00,-20.00)	(-0.8016e+00, 0.1100e-03)	0.80163	(-0.832295e+00,0.00)	0.83230
13	(40.00,-20.00)	(-0.7716e+00,-0.2542e-03)	0.77159	(-0.832295e+00,0.00)	0.83230
14	(30.00,-20.00)	(-0.7714e+00,-0.6943e-03)	0.77144	(-0.832295e+00,0.00)	0.83230
15	(20.00,-20.00)	(-0.7715e+00,-0.1189e-02)	0.77154	(-0.832295e+00,0.00)	0.83230
16	(10.00,-20.00)	(-0.7717e+00,-0.1615e-02)	0.77169	(-0.832295e+00,0.00)	0.83230
17	(0.00,-20.00)	(-0.7718e+00,-0.1786e-02)	0.77176	(-0.832295e+00,0.00)	0.83230
18	(-10.00,-20.00)	(-0.7717e+00,-0.1615e-02)	0.77169	(-0.832295e+00,0.00)	0.83230
19	(-20.00,-20.00)	(-0.7715e+00,-0.1189e-02)	0.77154	(-0.832295e+00,0.00)	0.83230
20	(-30.00,-20.00)	(-0.7714e+00,-0.6944e-03)	0.77144	(-0.832295e+00,0.00)	0.83230
21	(-40.00,-20.00)	(-0.7716e+00,-0.2545e-03)	0.77159	(-0.832295e+00,0.00)	0.83230
22	(-50.00,-20.00)	(-0.8016e+00, 0.1097e-03)	0.80163	(-0.832295e+00,0.00)	0.83230

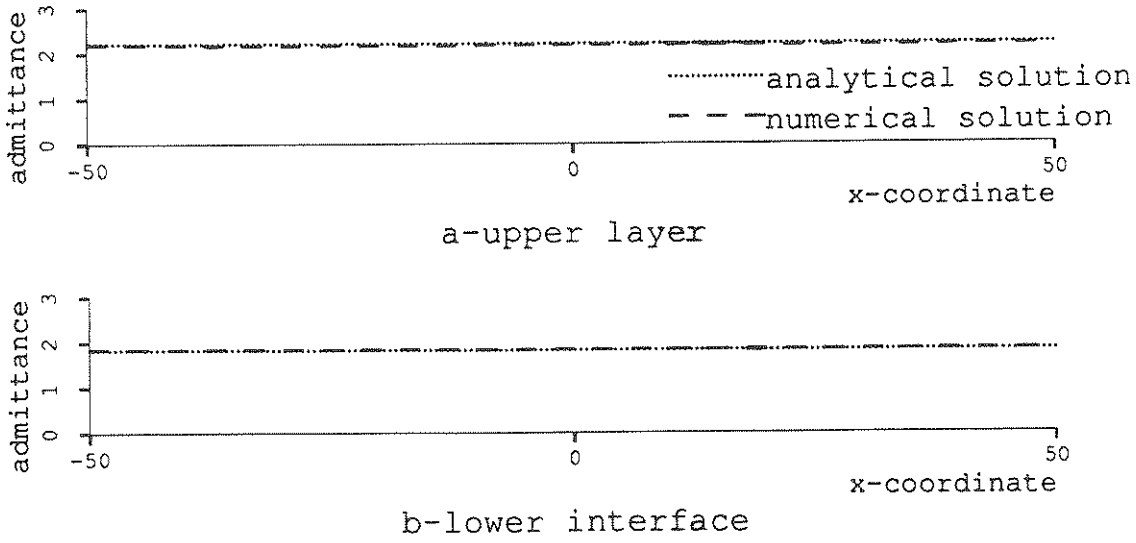

FIGURE D-6 Heterogeneous half space subjected to a wave at oblique incidence

APPENDIX E
EXAMPLE OF THE PROCEDURE

Figure E-1 shows the principal steps in computing the time history of point 1 of plot (a) subjected to a vertically incident earthquake as recorded in (b). The surface(s) of the profile are first divided into discreet portions by defining observation points which are marked by o's in plot (a). The resulting segments are then represented by their lengths and their two Gauss quadrature points which are marked by x's. The points (1, 2, and 3) at which time histories are to be generated are then chosen.

After establishing the geometry of the profile, the next step is to create a transfer function for each of the points (1, 2, and 3) for which a time history is to be computed. This is done frequency by frequency where it is necessary to compute the response of all the observation points to a unit incident harmonic wave at each frequency. This is accomplished through the discretization of the domain and the numerical analysis as described previously. These results are shown for two frequencies in plots (c) and (d).

When these values are computed, the responses at the points of interest are kept and the rest are discarded. After the results have been reserved for each of the evenly spaced frequencies from 0 to 157 rad/s (=50π/rad/s=25 Hz), each point has an admittance function as shown in plot (e) where the steady-state response of the point is given for each of the harmonic incident frequencies.

These admittance functions (or their interpolates) are then multiplied by the Fourier transform of the incident earthquake, shown in (f), to obtain the transfer function (g) of the point in response to the incident wave. This transfer function is the forward Fourier transform of the response of the point.

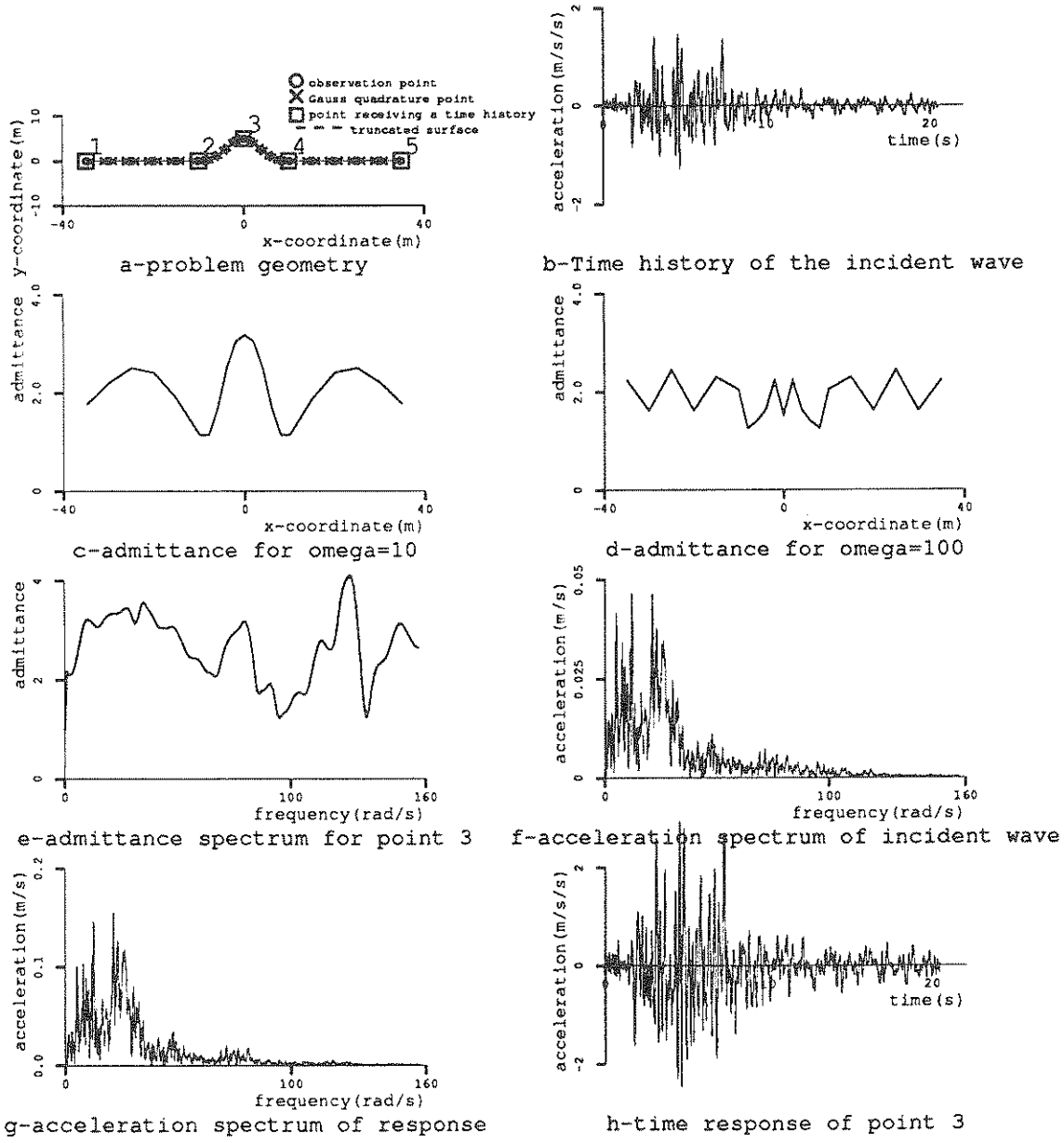

FIGURE E-1 Example of the process

Accordingly, the application of the inverse (or backward) transform to the transfer function results in the time history of the response of the point to the given incident earthquake. This response in the time domain is given in plot (h). Thus, within the limits of the numerical processes, plot (h) contains the response of point 1 in plot (a) to the incident field of plot (b).

NATIONAL CENTER FOR EARTHQUAKE ENGINEERING RESEARCH
LIST OF PUBLISHED TECHNICAL REPORTS

The National Center for Earthquake Engineering Research (NCEER) publishes technical reports on a variety of subjects related to earthquake engineering written by authors funded through NCEER. These reports are available from both NCEER's Publications Department and the National Technical Information Service (NTIS). Requests for reports should be directed to the Publications Department, National Center for Earthquake Engineering Research, State University of New York at Buffalo, Red Jacket Quadrangle, Buffalo, New York 14261. Reports can also be requested through NTIS, 5285 Port Royal Road, Springfield, Virginia 22161. NTIS accession numbers are shown in parenthesis, if available.

NCEER-87-0001 "First-Year Program in Research, Education and Technology Transfer," 3/5/87, (PB88-134275/AS).

NCEER-87-0002 "Experimental Evaluation of Instantaneous Optimal Algorithms for Structural Control," by R.C. Lin, T.T. Soong and A.M. Reinhorn, 4/20/87, (PB88-134341/AS).

NCEER-87-0003 "Experimentation Using the Earthquake Simulation Facilities at University at Buffalo," by A.M. Reinhorn and R.L. Ketter, to be published.

NCEER-87-0004 "The System Characteristics and Performance of a Shaking Table," by J.S. Hwang, K.C. Chang and G.C. Lee, 6/1/87, (PB88-134259/AS).

NCEER-87-0005 "A Finite Element Formulation for Nonlinear Viscoplastic Material Using a Q Model," by O. Gyebi and G. Dasgupta, 11/2/87, (PB88-213764/AS).

NCEER-87-0006 "Symbolic Manipulation Program (SMP) - Algebraic Codes for Two and Three Dimensional Finite Element Formulations," by X. Lee and G. Dasgupta, 11/9/87, (PB88-219522/AS).

NCEER-87-0007 "Instantaneous Optimal Control Laws for Tall Buildings Under Seismic Excitations," by J.N. Yang, A. Akbarpour and P. Ghaemmaghami, 6/10/87, (PB88-134333/AS).

NCEER-87-0008 "IDARC: Inelastic Damage Analysis of Reinforced Concrete Frame - Shear-Wall Structures," by Y.J. Park, A.M. Reinhorn and S.K. Kunnath, 7/20/87, (PB88-134325/AS).

NCEER-87-0009 "Liquefaction Potential for New York State: A Preliminary Report on Sites in Manhattan and Buffalo," by M. Budhu, V. Vijayakumar, R.F. Giese and L. Baumgras, 8/31/87, (PB88-163704/AS). This report is available only through NTIS (see address given above).

NCEER-87-0010 "Vertical and Torsional Vibration of Foundations in Inhomogeneous Media," by A.S. Veletsos and K.W. Dotson, 6/1/87, (PB88-134291/AS).

NCEER-87-0011 "Seismic Probabilistic Risk Assessment and Seismic Margins Studies for Nuclear Power Plants," by Howard H.M. Hwang, 6/15/87, (PB88-134267/AS). This report is available only through NTIS (see address given above).

NCEER-87-0012 "Parametric Studies of Frequency Response of Secondary Systems Under Ground-Acceleration Excitations," by Y. Yong and Y.K. Lin, 6/10/87, (PB88-134309/AS).

NCEER-87-0013 "Frequency Response of Secondary Systems Under Seismic Excitation," by J.A. HoLung, J. Cai and Y.K. Lin, 7/31/87, (PB88-134317/AS).

NCEER-87-0014 "Modelling Earthquake Ground Motions in Seismically Active Regions Using Parametric Time Series Methods," by G.W. Ellis and A.S. Cakmak, 8/25/87, (PB88-134283/AS).

NCEER-87-0015 "Detection and Assessment of Seismic Structural Damage," by E. DiPasquale and A.S. Cakmak, 8/25/87, (PB88-163712/AS).

NCEER-87-0016 "Pipeline Experiment at Parkfield, California," by J. Isenberg and E. Richardson, 9/15/87, (PB88-163720/AS).

NCEER-87-0017 "Digital Simulation of Seismic Ground Motion," by M. Shinozuka, G. Deodatis and T. Harada, 8/31/87, (PB88-155197/AS). This report is available only through NTIS (see address given above).

NCEER-87-0018 "Practical Considerations for Structural Control: System Uncertainty, System Time Delay and Truncation of Small Control Forces," J.N. Yang and A. Akbarpour, 8/10/87, (PB88-163738/AS).

NCEER-87-0019 "Modal Analysis of Nonclassically Damped Structural Systems Using Canonical Transformation," by J.N. Yang, S. Sarkani and F.X. Long, 9/27/87, (PB88-187851/AS).

NCEER-87-0020 "A Nonstationary Solution in Random Vibration Theory," by J.R. Red-Horse and P.D. Spanos, 11/3/87, (PB88-163746/AS).

NCEER-87-0021 "Horizontal Impedances for Radially Inhomogeneous Viscoelastic Soil Layers," by A.S. Veletsos and K.W. Dotson, 10/15/87, (PB88-150859/AS).

NCEER-87-0022 "Seismic Damage Assessment of Reinforced Concrete Members," by Y.S. Chung, C. Meyer and M. Shinozuka, 10/9/87, (PB88-150867/AS). This report is available only through NTIS (see address given above).

NCEER-87-0023 "Active Structural Control in Civil Engineering," by T.T. Soong, 11/11/87, (PB88-187778/AS).

NCEER-87-0024 Vertical and Torsional Impedances for Radially Inhomogeneous Viscoelastic Soil Layers," by K.W. Dotson and A.S. Veletsos, 12/87, (PB88-187786/AS).

NCEER-87-0025 "Proceedings from the Symposium on Seismic Hazards, Ground Motions, Soil-Liquefaction and Engineering Practice in Eastern North America," October 20-22, 1987, edited by K.H. Jacob, 12/87, (PB88-188115/AS).

NCEER-87-0026 "Report on the Whittier-Narrows, California, Earthquake of October 1, 1987," by J. Pantelic and A. Reinhorn, 11/87, (PB88-187752/AS). This report is available only through NTIS (see address given above).

NCEER-87-0027 "Design of a Modular Program for Transient Nonlinear Analysis of Large 3-D Building Structures," by S. Srivastav and J.F. Abel, 12/30/87, (PB88-187950/AS).

NCEER-87-0028 "Second-Year Program in Research, Education and Technology Transfer," 3/8/88, (PB88-219480/AS).

NCEER-88-0001 "Workshop on Seismic Computer Analysis and Design of Buildings With Interactive Graphics," by W. McGuire, J.F. Abel and C.H. Conley, 1/18/88, (PB88-187760/AS).

NCEER-88-0002 "Optimal Control of Nonlinear Flexible Structures," by J.N. Yang, F.X. Long and D. Wong, 1/22/88, (PB88-213772/AS).

NCEER-88-0003 "Substructuring Techniques in the Time Domain for Primary-Secondary Structural Systems," by G.D. Manolis and G. Juhn, 2/10/88, (PB88-213780/AS).

NCEER-88-0004 "Iterative Seismic Analysis of Primary-Secondary Systems," by A. Singhal, L.D. Lutes and P.D. Spanos, 2/23/88, (PB88-213798/AS).

NCEER-88-0005 "Stochastic Finite Element Expansion for Random Media," by P.D. Spanos and R. Ghanem, 3/14/88, (PB88-213806/AS).

NCEER-88-0006 "Combining Structural Optimization and Structural Control," by F.Y. Cheng and C.P. Pantelides, 1/10/88, (PB88-213814/AS).

NCEER-88-0007 "Seismic Performance Assessment of Code-Designed Structures," by H.H-M. Hwang, J-W. Jaw and H-J. Shau, 3/20/88, (PB88-219423/AS).

NCEER-88-0008 "Reliability Analysis of Code-Designed Structures Under Natural Hazards," by H.H-M. Hwang, H. Ushiba and M. Shinozuka, 2/29/88, (PB88-229471/AS).

NCEER-88-0009 "Seismic Fragility Analysis of Shear Wall Structures," by J-W Jaw and H.H-M. Hwang, 4/30/88, (PB89-102867/AS).

NCEER-88-0010 "Base Isolation of a Multi-Story Building Under a Harmonic Ground Motion - A Comparison of Performances of Various Systems," by F-G Fan, G. Ahmadi and I.G. Tadjbakhsh, 5/18/88, (PB89-122238/AS).

NCEER-88-0011 "Seismic Floor Response Spectra for a Combined System by Green's Functions," by F.M. Lavelle, L.A. Bergman and P.D. Spanos, 5/1/88, (PB89-102875/AS).

NCEER-88-0012 "A New Solution Technique for Randomly Excited Hysteretic Structures," by G.Q. Cai and Y.K. Lin, 5/16/88, (PB89-102883/AS).

NCEER-88-0013 "A Study of Radiation Damping and Soil-Structure Interaction Effects in the Centrifuge," by K. Weissman, supervised by J.H. Prevost, 5/24/88, (PB89-144703/AS).

NCEER-88-0014 "Parameter Identification and Implementation of a Kinematic Plasticity Model for Frictional Soils," by J.H. Prevost and D.V. Griffiths, to be published.

NCEER-88-0015 "Two- and Three- Dimensional Dynamic Finite Element Analyses of the Long Valley Dam," by D.V. Griffiths and J.H. Prevost, 6/17/88, (PB89-144711/AS).

NCEER-88-0016 "Damage Assessment of Reinforced Concrete Structures in Eastern United States," by A.M. Reinhorn, M.J. Seidel, S.K. Kunnath and Y.J. Park, 6/15/88, (PB89-122220/AS).

NCEER-88-0017 "Dynamic Compliance of Vertically Loaded Strip Foundations in Multilayered Viscoelastic Soils," by S. Ahmad and A.S.M. Israil, 6/17/88, (PB89-102891/AS).

NCEER-88-0018 "An Experimental Study of Seismic Structural Response With Added Viscoelastic Dampers," by R.C. Lin, Z. Liang, T.T. Soong and R.H. Zhang, 6/30/88, (PB89-122212/AS).

NCEER-88-0019 "Experimental Investigation of Primary - Secondary System Interaction," by G.D. Manolis, G. Juhn and A.M. Reinhorn, 5/27/88, (PB89-122204/AS).

NCEER-88-0020 "A Response Spectrum Approach For Analysis of Nonclassically Damped Structures," by J.N. Yang, S. Sarkani and F.X. Long, 4/22/88, (PB89-102909/AS).

NCEER-88-0021 "Seismic Interaction of Structures and Soils: Stochastic Approach," by A.S. Veletsos and A.M. Prasad, 7/21/88, (PB89-122196/AS).

NCEER-88-0022 "Identification of the Serviceability Limit State and Detection of Seismic Structural Damage," by E. DiPasquale and A.S. Cakmak, 6/15/88, (PB89-122188/AS).

NCEER-88-0023 "Multi-Hazard Risk Analysis: Case of a Simple Offshore Structure," by B.K. Bhartia and E.H. Vanmarcke, 7/21/88, (PB89-145213/AS).

NCEER-88-0024 "Automated Seismic Design of Reinforced Concrete Buildings," by Y.S. Chung, C. Meyer and M. Shinozuka, 7/5/88, (PB89-122170/AS).

NCEER-88-0025 "Experimental Study of Active Control of MDOF Structures Under Seismic Excitations," by L.L. Chung, R.C. Lin, T.T. Soong and A.M. Reinhorn, 7/10/88, (PB89-122600/AS).

NCEER-88-0026 "Earthquake Simulation Tests of a Low-Rise Metal Structure," by J.S. Hwang, K.C. Chang, G.C. Lee and R.L. Ketter, 8/1/88, (PB89-102917/AS).

NCEER-88-0027 "Systems Study of Urban Response and Reconstruction Due to Catastrophic Earthquakes," by F. Kozin and H.K. Zhou, 9/22/88, to be published.

NCEER-88-0028 "Seismic Fragility Analysis of Plane Frame Structures," by H.H-M. Hwang and Y.K. Low, 7/31/88, (PB89-131445/AS).

NCEER-88-0029 "Response Analysis of Stochastic Structures," by A. Kardara, C. Bucher and M. Shinozuka, 9/22/88, (PB89-174429/AS).

NCEER-88-0030 "Nonnormal Accelerations Due to Yielding in a Primary Structure," by D.C.K. Chen and L.D. Lutes, 9/19/88, (PB89-131437/AS).

NCEER-88-0031 "Design Approaches for Soil-Structure Interaction," by A.S. Veletsos, A.M. Prasad and Y. Tang, 12/30/88, (PB89-174437/AS).

NCEER-88-0032 "A Re-evaluation of Design Spectra for Seismic Damage Control," by C.J. Turkstra and A.G. Tallin, 11/7/88, (PB89-145221/AS).

NCEER-88-0033 "The Behavior and Design of Noncontact Lap Splices Subjected to Repeated Inelastic Tensile Loading," by V.E. Sagan, P. Gergely and R.N. White, 12/8/88, (PB89-163737/AS).

NCEER-88-0034 "Seismic Response of Pile Foundations," by S.M. Mamoon, P.K. Banerjee and S. Ahmad, 11/1/88, (PB89-145239/AS).

NCEER-88-0035 "Modeling of R/C Building Structures With Flexible Floor Diaphragms (IDARC2)," by A.M. Reinhorn, S.K. Kunnath and N. Panahshahi, 9/7/88, (PB89-207153/AS).

NCEER-88-0036 "Solution of the Dam-Reservoir Interaction Problem Using a Combination of FEM, BEM with Particular Integrals, Modal Analysis, and Substructuring," by C-S. Tsai, G.C. Lee and R.L. Ketter, 12/31/88, (PB89-207146/AS).

NCEER-88-0037 "Optimal Placement of Actuators for Structural Control," by F.Y. Cheng and C.P. Pantelides, 8/15/88, (PB89-162846/AS).

NCEER-88-0038 "Teflon Bearings in Aseismic Base Isolation: Experimental Studies and Mathematical Modeling," by A. Mokha, M.C. Constantinou and A.M. Reinhorn, 12/5/88, (PB89-218457/AS).

NCEER-88-0039 "Seismic Behavior of Flat Slab High-Rise Buildings in the New York City Area," by P. Weidlinger and M. Ettouney, 10/15/88, to be published.

NCEER-88-0040 "Evaluation of the Earthquake Resistance of Existing Buildings in New York City," by P. Weidlinger and M. Ettouney, 10/15/88, to be published.

NCEER-88-0041 "Small-Scale Modeling Techniques for Reinforced Concrete Structures Subjected to Seismic Loads," by W. Kim, A. El-Attar and R.N. White, 11/22/88, (PB89-189625/AS).

NCEER-88-0042 "Modeling Strong Ground Motion from Multiple Event Earthquakes," by G.W. Ellis and A.S. Cakmak, 10/15/88, (PB89-174445/AS).

NCEER-88-0043 "Nonstationary Models of Seismic Ground Acceleration," by M. Grigoriu, S.E. Ruiz and E. Rosenblueth, 7/15/88, (PB89-189617/AS).

NCEER-88-0044 "SARCF User's Guide: Seismic Analysis of Reinforced Concrete Frames," by Y.S. Chung, C. Meyer and M. Shinozuka, 11/9/88, (PB89-174452/AS).

NCEER-88-0045 "First Expert Panel Meeting on Disaster Research and Planning," edited by J. Pantelic and J. Stoyle, 9/15/88, (PB89-174460/AS).

NCEER-88-0046 "Preliminary Studies of the Effect of Degrading Infill Walls on the Nonlinear Seismic Response of Steel Frames," by C.Z. Chrysostomou, P. Gergely and J.F. Abel, 12/19/88, (PB89-208383/AS).

NCEER-88-0047 "Reinforced Concrete Frame Component Testing Facility - Design, Construction, Instrumentation and Operation," by S.P. Pessiki, C. Conley, T. Bond, P. Gergely and R.N. White, 12/16/88, (PB89-174478/AS).

NCEER-89-0001 "Effects of Protective Cushion and Soil Compliancy on the Response of Equipment Within a Seismically Excited Building," by J.A. HoLung, 2/16/89, (PB89-207179/AS).

NCEER-89-0002 "Statistical Evaluation of Response Modification Factors for Reinforced Concrete Structures," by H.H-M. Hwang and J-W. Jaw, 2/17/89, (PB89-207187/AS).

NCEER-89-0003 "Hysteretic Columns Under Random Excitation," by G-Q. Cai and Y.K. Lin, 1/9/89, (PB89-196513/AS).

NCEER-89-0004 "Experimental Study of 'Elephant Foot Bulge' Instability of Thin-Walled Metal Tanks," by Z-H. Jia and R.L. Ketter, 2/22/89, (PB89-207195/AS).

NCEER-89-0005 "Experiment on Performance of Buried Pipelines Across San Andreas Fault," by J. Isenberg, E. Richardson and T.D. O'Rourke, 3/10/89, (PB89-218440/AS).

NCEER-89-0006 "A Knowledge-Based Approach to Structural Design of Earthquake-Resistant Buildings," by M. Subramani, P. Gergely, C.H. Conley, J.F. Abel and A.H. Zaghw, 1/15/89, (PB89-218465/AS).

NCEER-89-0007 "Liquefaction Hazards and Their Effects on Buried Pipelines," by T.D. O'Rourke and P.A. Lane, 2/1/89, (PB89-218481).

NCEER-89-0008 "Fundamentals of System Identification in Structural Dynamics," by H. Imai, C-B. Yun, O. Maruyama and M. Shinozuka, 1/26/89, (PB89-207211/AS).

NCEER-89-0009 "Effects of the 1985 Michoacan Earthquake on Water Systems and Other Buried Lifelines in Mexico," by A.G. Ayala and M.J. O'Rourke, 3/8/89, (PB89-207229/AS).

NCEER-89-0010 "NCEER Bibliography of Earthquake Education Materials," by K.E.K. Ross, 3/10/89, (PB89-218473/AS).

NCEER-89-0011 "Inelastic Three-Dimensional Response Analysis of Reinforced Concrete Building Structures (IDARC-3D), Part I - Modeling," by S.K. Kunnath and A.M. Reinhorn, 4/17/89.

NCEER-89-0012 "Recommended Modifications to ATC-14," by C.D. Poland and J.O. Malley, 4/12/89.

NCEER-89-0013 "Repair and Strengthening of Beam-to-Column Connections Subjected to Earthquake Loading," by M. Corazao and A.J. Durrani, 2/28/89.

NCEER-89-0014 "Program EXKAL2 for Identification of Structural Dynamic Systems," by O. Maruyama, C-B. Yun, M. Hoshiya and M. Shinozuka, 5/19/89.

NCEER-89-0015 "Response of Frames With Bolted Semi-Rigid Connections, Part I - Experimental Study and Analytical Predictions," by P.J. DiCorso, A.M. Reinhorn, J.R. Dickerson, J.B. Radziminski and W.L. Harper, 6/1/89, to be published.

NCEER-89-0016 "ARMA Monte Carlo Simulation in Probabilistic Structural Analysis," by P.D. Spanos and M.P. Mignolet, 7/10/89.

NCEER-89-0017 "Preliminary Proceedings of the Conference on Disaster Preparedness - The Place of Earthquake Education in Our Schools, July 9-11, 1989," 6/23/89.

NCEER-89-0018 "Multidimensional Models of Hysteretic Material Behavior for Vibration Analysis of Shape Memory Energy Absorbing Devices, by E.J. Graesser and F.A. Cozzarelli, 6/7/89.

NCEER-89-0019 "Nonlinear Dynamic Analysis of Three-Dimensional Base Isolated Structures (3D-BASIS)," by S. Nagarajaiah, A.M. Reinhorn and M.C. Constantinou, 8/3/89.

NCEER-89-0020 "Structural Control Considering Time-Rate of Control Forces and Control Rate Constraints," by F.Y. Cheng and C.P. Pantelides, 8/3/89.

NCEER-89-0021 "Subsurface Conditions of Memphis and Shelby County," by K.W. Ng, T-S. Chang and H-H.M. Hwang, 7/26/89.

NCEER-89-0022 "Seismic Wave Propagation Effects on Straight Jointed Buried Pipelines," by K. Elhmadi and M.J. O'Rourke, 8/24/89.

NCEER-89-0023 "Workshop on Serviceability Analysis of Water Delivery Systems," edited by M. Grigoriu, 3/6/89.

NCEER-89-0024 "Shaking Table Study of a 1/5 Scale Steel Frame Composed of Tapered Members," by K.C. Chang, J.S. Hwang and G.C. Lee, 9/18/89.

NCEER-89-0025 "DYNA1D: A Computer Program for Nonlinear Seismic Site Response Analysis - Technical Documentation," by Jean H. Prevost, 9/14/89.

NCEER-89-0026 "1:4 Scale Model Studies of Active Tendon Systems and Active Mass Dampers for Aseismic Protection," by A.M. Reinhorn, T.T. Soong, R.C. Lin, Y.P. Yang, Y. Fukao, H. Abe and M. Nakai, 9/15/89, to be published.

NCEER-89-0027 "Scattering of Waves by Inclusions in a Nonhomogeneous Elastic Half Space Solved by Boundary Element Methods," by P.K. Hadley, A. Askar and A.S. Cakmak, 6/15/89.